A Humanized Yeast Phenomic Model of Deoxycytidine Kinase to Predict Genetic Buffering of Nucleoside Analog Cytotoxicity

Sean M. Santos [1] , **Mert Icyuz** [1], **Ilya Pound** [1], **Doreen William** [2], **Jingyu Guo** [1] ,
Brett A. McKinney [3], **Michael Niederweis** [2], **John Rodgers** [1] **and John L. Hartman IV**[1,*]

[1] Department of Genetics, University of Alabama at Birmingham, Birmingham, AL 35294, USA;
seansantos18@gmail.com (S.M.S); icyuz@uab.edu (M.I.); poundilya@yahoo.com (I.P.);
guo.jingyu@gmail.com (J.G.); jwrodger@uab.edu (J.R.)

[2] Department of Microbiology, University of Alabama at Birmingham, Birmingham, AL 35294, USA;
doreen.william@nct-dresden.de (D.W.); mnieder@uab.edu (M.N.)

[3] Tandy School of Computer Science and Department of Mathematics, The University of Tulsa, Tulsa,
OK 74104, USA; brett.mckinney@gmail.com

* Correspondence: jhartman@uab.edu

Abstract: Knowledge about synthetic lethality can be applied to enhance the efficacy of anticancer therapies in individual patients harboring genetic alterations in their cancer that specifically render it vulnerable. We investigated the potential for high-resolution phenomic analysis in yeast to predict such genetic vulnerabilities by systematic, comprehensive, and quantitative assessment of drug–gene interaction for gemcitabine and cytarabine, substrates of deoxycytidine kinase that have similar molecular structures yet distinct antitumor efficacy. Human deoxycytidine kinase (dCK) was conditionally expressed in the *Saccharomyces cerevisiae* genomic library of knockout and knockdown (YKO/KD) strains, to globally and quantitatively characterize differential drug–gene interaction for gemcitabine and cytarabine. Pathway enrichment analysis revealed that autophagy, histone modification, chromatin remodeling, and apoptosis-related processes influence gemcitabine specifically, while drug–gene interaction specific to cytarabine was less enriched in gene ontology. Processes having influence over both drugs were DNA repair and integrity checkpoints and vesicle transport and fusion. Non-gene ontology (GO)-enriched genes were also informative. Yeast phenomic and cancer cell line pharmacogenomics data were integrated to identify yeast–human homologs with correlated differential gene expression and drug efficacy, thus providing a unique resource to predict whether differential gene expression observed in cancer genetic profiles are causal in tumor-specific responses to cytotoxic agents.

Keywords: yeast phenomics; gene–drug interaction; genetic buffering; quantitative high throughput cell array phenotyping (Q-HTCP); cell proliferation parameters (CPPs); gemcitabine; cytarabine; recursive expectation-maximization clustering (REMc); pharmacogenomics

---

1. Introduction

Genomics has enabled targeted therapy aimed at cancer driver genes and oncogenic addiction [1], yet traditional cytotoxic chemotherapeutic agents remain among the most widely used and efficacious anticancer therapies [2]. Changes in the genetic network underlying cancer can produce vulnerabilities to cytotoxic chemotherapy that further influence the therapeutic window and provide additional insight into their mechanisms of action [3,4]. A potential advantage of so-called synthetic lethality-based treatment strategies is that they could have efficacy against passenger gene mutation or compensatory

gene expression, while classic targeted therapies are directed primarily at driver genes (Figure 1A). Quantitative high throughput cell array phenotyping of the yeast knockout and knockdown libraries provides a phenomic means for systems level, high-resolution modeling of gene interaction [5–9], which is applied here to predict cancer-relevant drug–gene interaction through integration with cancer pharmacogenomics resources (Figure 1B).

Nucleoside analogs include a diverse group of compounds with anticancer, antiviral, and immunosuppressive efficacy [10]. The anticancer agents have tissue-specific efficacy ranging from solid tumors to leukemias, yet details about how these agents confer differential activity are unknown [10,11]. Gemcitabine (2′,2′-difluoro 2′-deoxycytidine, dFdC) and cytarabine (Ara-C) are deoxycytidine analogs that undergo the first step of conversion to their active triphosphate forms by deoxycytidine kinase (dCK) (Figure 1C). The nucleoside triphosphate analogs can be incorporated into DNA and inhibit the functions of polymerases and other enzymes involved in DNA metabolism. For example, gemcitabine inhibits ribonucleotide reductase (RNR), which limits the production of deoxyribonucleotides (dNTPs) that are needed for DNA synthesis and repair [11]. Gemcitabine has been used as a single agent in the treatment of some cancers, such as pancreatic, and in combination with platinum-based drugs in non-small-cell lung, breast, and ovarian cancers [12–15]. Cytarabine, on the other hand, has been an important agent in treatments for acute myeloid leukemia and acute lymphoblastic leukemia [16].

Deoxycytidine kinase (dCK) phosphorylates deoxycytidine to deoxycytidine monophosphate (dCMP), similarly phosphorylating gemcitabine and cytarabine to dFdCMP and AraCMP, respectively. UMP/CMP kinase and the nucleoside diphosphate kinase are subsequently involved in conversion to the triphosphate form (Figure 1C). Reduced expression of dCK or high expression of RNR subunits *RRM1* and *RRM2* is associated with increased gemcitabine resistance [10,12,17–21]. Genomic analyses have suggested genetic influences on the efficacy of gemcitabine or cytarabine [22–26], which we model here at a systems level by surveying gene–drug interaction to elucidate biology underlying differential anticancer efficacies of the respective drugs, and thereby aid in predicting treatment outcomes based on individual patient cancer genetic profiles.

Saccharomyces cerevisiae does not have a dCK homolog and is thus naturally resistant to gemcitabine and cytarabine. To examine the gene–drug interaction networks for gemcitabine and cytarabine in yeast, we introduced human dCK into the yeast knockout and knockdown (YKO/KD) library by the synthetic genetic array (SGA) method [27–29] and conducted phenomic analysis on the resulting double mutant library by quantitative high-throughput cell array phenotyping (Q-HTCP) [6–9] using multiple growth inhibitory concentrations of gemcitabine or cytarabine (Figure 1B). Cell proliferation parameters (CPPs) obtained by Q-HTCP were used to quantify and compare drug–gene interaction for gemcitabine vs. cytarabine. The unbiased results provide a systems-level resource of genetic and biological information about the cytotoxicity of these drugs, incorporating knowledge about genes that either buffer or promote their effects [3,5].

Recent advances in cancer pharmacogenomics have provided gene expression and drug sensitivity data from hundreds of cancer cell lines, establishing associations between gene expression and anticancer efficacy for many compounds, including gemcitabine and cytarabine [30–32]. We investigated the potential utility of a yeast phenomic model of chemotherapy sensitivity and resistance for predicting causality in correlations between differential gene expression and drug sensitivity by generating a network-level drug–gene interaction resource. The resource integrates cancer pharmacogenomic and yeast phenomic data, using the results to query the cancer genetics literature in order to obtain systems-level biological insights about how yeast phenomic models help predict cytotoxic chemotherapy efficacy based on unique genetic alterations specific to each individual patient's cancer (Figure 1A).
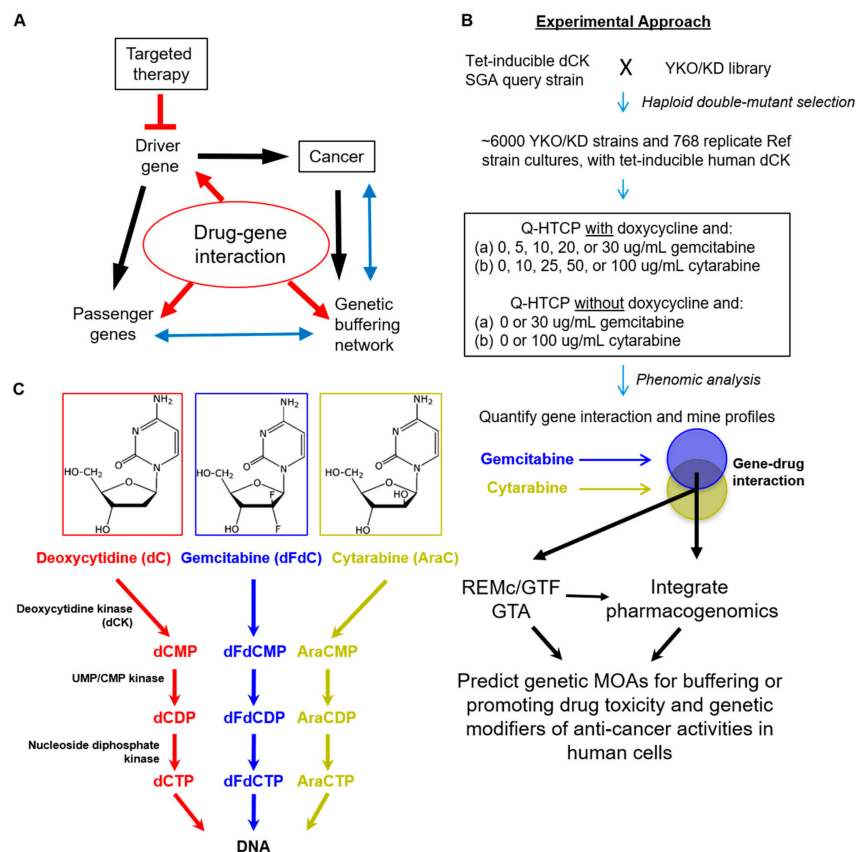
Figure 1. Experimental model of gemcitabine and cytarabine drug–gene interaction networks. (**A**) The strategy of cytotoxic anticancer drug–gene interaction is illustrated in the context of driver gene-mediated oncogenesis. Driver genes promote cancer and influence the expression of passenger genes (black arrows), which also leads to genomic instability and alterations in the genetic buffering network. The genetic buffering network (blue arrows) maintains cellular homeostasis and is altered in cancer cells by genomic instability, thereby creating the potential for drug–gene interaction that increases the therapeutic window of anticancer agents (red arrows). Drug–gene interaction can either involve driver or passenger genes directly, or the compromised genetic buffering network, which are systematically characterized by the quantitative yeast phenomic model. (**B**) The synthetic genetic array (SGA) method was used to introduce tet-inducible human deoxycytidine kinase (dCK) expression in the yeast knockout and knockdown (YKO/KD) collection. The phenomic model incorporates treatment of individually grown cultures of the YKO/KD collection, and 768 replicate reference (Ref) strain cultures, with increasing gemcitabine (0, 5, 10, 20, and 30 μg/mL) or cytarabine (0, 10, 25, 50, and 100 μg/mL) in a dextrose (HLD) media, with dCK induced by addition of doxycycline. Drug–gene interaction profiles were analyzed by recursive expectation-maximization clustering (REMc) and gene ontology (GO) term analysis to characterize phenomic modules with respect to drug–gene interaction for gemcitabine or cytarabine, and integrated with pharmacogenomics data to predict evolutionarily conserved drug–gene interactions relevant to precision oncology. (**C**) Structures and metabolism of deoxycytidine analogs.

2. Materials and Methods

2.1. Strains, Media, and Drugs

We obtained the yeast gene knockout strain library (YKO) from Research Genetics (Huntsville, AL, USA) and the knockdown (KD) collection, also referred to as the decreased abundance of mRNA production (DAmP) library, from Open Biosystems (Huntsville, AL, USA). The YKO library is in the genetic background of BY4741 (S288C MATa *ura3-Δ0 his3-Δ1 leu2-Δ0 met17-Δ0*). Additional information and strains can be obtained at https://dharmacon.horizondiscovery.com/cdnas-and-orfs/

non-mammalian-cdnas-and-orfs/yeast/#all. Some mutants appear multiple times in the library and they are treated independently in our analysis. HLD is a modified synthetic complete medium [8] and was used with 2% dextrose (HLD) as the carbon source. Doxycycline hydrochloride (BP26535) was obtained from Fisher Scientific. Gemcitabine (Gemzar) was obtained from Eli Lilly and Company (0002-7502-01). Cytarabine was obtained from Bedford Laboratories (55390-131-10).

A tet-inducible dCK query allele was constructed in the SGA background in the following way: An integrating plasmid for doxycycline-inducible gene expression was constructed by subcloning 3'UTR and 5'ORF targeting sequences from the LYP1 locus into pJH023 [33], creating pJH023_UO_lyp1, and the reverse VP16 transactivator (Tet-ON), obtained by PCR from pCM176 [34], was fused to the *ACT1* promoter by overlap PCR and subcloned into pJH023_UO_lyp1, replacing the VP16 transactivator (Tet-OFF) and creating the "Tet-ON" construct, pML1055 [35]. pML1055 was digested with NOT1 and transformed into strain 15578-1.2b_LYP1 (*MATα his3Δ1 leu2Δ0 ura3Δ0 can1Δ0::P$_{GAL1}$-T$_{ADH1}$-P$_{MFA1}$-his5$^+$$_{sp}$ hmrΔ0::URA3ca*), which was derived by backcrossing 15578-1.2b (*MATα his3Δ1 leu2Δ0 ura3Δ0 can1Δ0::P$_{GAL1}$-T$_{ADH1}$-P$_{MFA1}$-his5$^+$$_{sp}$ lyp1Δ0 hmrΔ0::URA3ca*) to restore the *LYP1* locus. The resulting chromosomal integration of pML1055 between the promoter and ORF at the *LYP1* locus was selected with nourseothricin, giving rise to DWY1 (*MATα his3Δ1 leu2Δ0 ura3Δ0 can1Δ0::P$_{GAL1}$-T$_{ADH1}$-P$_{MFA1}$-his5$^+$$_{sp}$ hmrΔ0::URA3ca Pact1-revTetR-VP16-natMX-PtetO7-LYP1*). Tet-inducible *LYP1* in DWY1 was verified phenotypically by doxycycline-dependent SAEC sensitivity [35]. Overlap PCR was performed to fuse deoxycytidine kinase (from a plasmid, gift of Bo Xu and William Parker, Southern Research) and the HPH gene (from pFA6a-HBH-hphMX4) [36], introducing flanking sequences for replacement of the *LYP1* ORF (see Additional File 1, Table S1 for primers). The PCR product was transformed into DWY1 (Additional File 2, Figure S1) and transformants selected on hygromycin were confirmed by doxycycline-induced sensitivity to gemcitabine and cytarabine, yielding MIY16 (*MATα his3Δ1 leu2Δ0 ura3Δ0 can1Δ0::P$_{GAL1}$-T$_{ADH1}$-P$_{MFA1}$-his5$^+$$_{sp}$ hmrΔ0::URA3ca lyp1-Δ0::Pact1-revTetR-VP16-natMX-PtetO7-DCK*).

The synthetic genetic array (SGA) method, a way to introduce an allele of interest into the YKO/KD library and recover haploid double mutants [28,29], was used to derive a haploid YKO/KD collection with doxycycline-inducible dCK expression.

2.2. Quantitative High Throughput Cell Array Phenotyping (Q-HTCP)

Q-HTCP, an automated method of collecting growth curve phenotypes for the YKO/KD library arrayed onto agar media, was used to obtain phenomic data [37]. A Caliper Sciclone 3000 liquid handling robot was used for cell array printing, integrated with a custom imaging robot (Hartman laboratory) and Cytomat 6001 (Thermo Fisher Scientific, Asheville, NC, USA) incubator. Images of the 384-culture arrays were obtained approximately every 2–3 hours and analyzed as previously described [9,37]. To obtain CPPs, image analysis was performed in Matlab and data were fit to the logistic equation, $G(t) = K/(1 + e^{-r(t-l)})$, assuming $G(0) < K$, where $G(t)$ is the image intensity of a spotted culture vs. time, K is the carrying capacity, r is the maximum specific growth rate, and l is the moment of maximal absolute growth rate, occurring when $G(t) = K/2$ (the time to reach half of carrying capacity) [7]. The CPPs, primarily K and L, were used as phenotypes to measure drug–gene interaction.

2.3. Quantification of Drug–Gene Interaction

Gene interaction was defined as departure of the corresponding YKO/KD strain from its expected phenotypic response to gemcitabine or cytarabine [6,9,38]. The expected phenotype depends, in part, on the difference in cell proliferation phenotypes between the mutant and reference strain without gemcitabine or cytarabine, which we have termed shift. This difference is applied to the entire data series (hence the term, 'shift'), when assessing differential response in cell proliferation phenotypes between the mutant and reference strain in the presence of escalating concentrations of gemcitabine or cytarabine [5,6,9,33]. The concentrations of gemcitabine or cytarabine (μg/mL) were chosen based on phenotypic responses being functionally discriminating in the parental strain. Gemcitabine, cytarabine,

or doxycycline, alone, did not alter cell proliferation (Figure 2C–F; Additional File 2, Figure S2A–D). Thus, shift was calculated in the presence of 5 µg/mL doxycycline without nucleoside analog.

Interaction scores were calculated as previously described [9,39], with slight modifications, as summarized below. All media conditions used for interaction score calculation had 5 µg/mL doxycycline to express dCK. Variables were defined as:

D_i = concentration (dose) of gemcitabine or cytarabine;

R_i = observed mean growth parameter for parental reference strain at D_i;

Y_i = observed growth parameter for the YKO/KD mutant strain at D_i;

$K_i = Y_i - R_i$, the difference in growth parameter between the YKO/KD mutant (Y_i) and reference (R_i) at D_i;

$K_0 = Y_0 - R_0$, the effect of gene KO/KD on the observed phenotype in the absence of gemcitabine or cytarabine—this value is annotated as 'shift' and is subtracted from all K_i to obtain L_i;

$L_i = K_i - K_0$, the interaction between (specific influence of) the KO/KD mutation on gemcitabine or cytarabine response, at D_i;

For cultures not generating a growth curve, $Y_i = 0$ for K and r. Note, however, that for cultures with extremely low growth, the L parameter asymptote is infinity and thus it was assigned Y_i max, defined as the maximum observed Y_i among all cultures exhibiting a minimum carrying capacity (K) within 2 standard deviation (SD) of the parental reference strain mean at D_i. Y_i max was also assigned to outlier values (i.e., if $Y_i > Y_i$ max).

Interaction Was Calculated by the Following Steps:

(1) Compute the average value of the 768 reference cultures (R_i) at each dose (D_i):
(2) Assign Y_i max (defined above) if growth curve is observed at D_0, but not at D_i, or if observed Y_i is greater than Y_i max.
(3) Calculate $K_i = Y_i - R_i$.
(4) Calculate $L_i = K_i - K_0$
(5) Fit data by linear regression (least squares): $L_i = A + B*D_i$
(6) Compute the interaction value 'INT' at the max dose: $INT = L_i\text{-max} = A + B*D_{max}$
(7) Calculate the mean and standard deviation of interaction scores for reference strains, $mean(REF_{INT})$ and $SD(REF_{INT})$; $mean(REF_{INT})$ is expected to be approximately zero, with $SD(REF_{INT})$ primarily useful for standardizing against variance (Additional File 1, Tables S2–S5; Additional Files 3–4).
(8) Calculate interaction z-scores:

$$\text{z-score}(YKO_{INT}) = (YKO_{INT} - mean(REF_{INT}))/SD(REF_{INT})$$

z-score(YKO_{INT}) > 2 for L or < −2 for K are referred to as gene deletion enhancers of gemcitabine or cytarabine cytotoxicity, and conversely, L interaction score < −2 or K interaction scores >2 are considered gene deletion suppressors. Due to the fact that the CPP distributions for KD strains were different from the reference strain, we used the mean and standard deviation from the KD plates only as a conservative measure of variance where z-score(KD_{INT}) = (KD_{INT} − $mean(KD_{INT})$)/$SD(KD_{INT})$.

2.4. Recursive Expectation-Maximization Clustering (REMc) and Heatmap Generation

REMc is a probability-based clustering method and was performed as previously described [40]. Clusters obtained by Weka 3.5, an EM-optimized Gaussian mixture-clustering module, were subjected to hierarchical clustering in R (http://www.r-project.org/) to further aid visualization with heatmaps. REMc was performed using L and K interaction z-scores (Figure 3A). The effect of gene deletion on the CPP (in the absence of drug), termed 'shift' (K_0), was not used for REMc, but was included for visualization in the final hierarchical clustering. Additional File 5, Files A–B contain REMc results in text files with associated data also displayed as heatmaps. In cases where a culture did not grow in the

absence of drug, 0.0001 was assigned as the interaction score, so that associated data ('NA') could be easily indicated by red coloring in the shift columns of the heatmaps.

2.5. Gene Ontology Term Finder (GTF)

A python script was used to format REMc clusters for analysis with the command line version of the GO Term Finder (GTF) tool downloaded from http://search.cpan.org/dist/GO-TermFinder/ [41]. GTF reports on enrichment of gene ontology (GO) terms by comparing the ratio of genes assigned to a term within a cluster to the respective ratio involving all genes tested. Additional File 5, File C contains GTF analysis of all REMc clusters. GO-enriched terms from REMc were investigated with respect to genes representing the term and literature underlying their annotations [42].

2.6. Gene Ontology Term Averaging (GTA) Analysis

In addition to using GTF to survey functional enrichment in REMc clusters, we developed GTA as a complementary workflow, using the GO information on SGD at https://downloads.yeastgenome.org/curation/literature/ to perform the following analysis:

1. Calculate the average and SD for interaction values of all genes in a GO term.
2. Filter results to obtain terms having GTA value greater than 2 or less than −2.
3. Obtain GTA scores defined as |GTA value| - gtaSD; filter for GTA score > 2.

The GTA analysis is contained in Additional File 6 as tables and interactive plots created using the R plotly package https://CRAN.R-project.org/package=plotly. GTA results were analyzed using both the L and K interaction scores and are included in Additional File 6 (Files A–C).

2.7. Prediction of Human Homologs that Influence Tumor Response to Gemcitabine or Cytarabine

PharmacoDB holds pharmacogenomics data from cancer cell lines, including transcriptomics and drug sensitivity [32]. The PharmacoGx R/Bioconductor package [43] was used to analyze the GDSC1000 (https://pharmacodb.pmgenomics.ca/datasets/5) and gCSI (https://pharmacodb.pmgenomics.ca/datasets/4) datasets, which contained transcriptomic and drug sensitivity results. A *p*-value < 0.05 was used for differential gene expression and drug sensitivity. For gene expression, the sign of the standardized coefficient denotes increased (+) or decreased (−) expression. The biomaRt R package [44,45] was used with the Ensembl database [46] to match yeast and human homologs from the phenomic and transcriptomic data, classifying yeast–human homology as one to one, one to many, and many to many. The Princeton Protein Orthology Database (PPOD) was also used to manually review homology in further consideration of whether or not to include particular genes in the results sections and whether or not cancer literature searches related to the homologs would be worthwhile [47].

3. Results

3.1. Quantitative Phenomic Characterization of Differential Gene–Drug Interaction

The Q-HTCP workflow incorporates high-throughput kinetic imaging and analysis of proliferating 384-culture cell arrays plated on agar media to obtain CPPs for measuring gene–drug interaction, as previously described [7,9,37]. To apply it for analysis of dCK substrates, a tetracycline-inducible human dCK allele was introduced into the complete YKO/KD library by the synthetic genetic array method [29,48] (Figure 1B). The dependence of gemcitabine and cytarabine toxicity on dCK expression was demonstrated for the reference strain (Figure 2A–F), as the two nucleosides exerted cytotoxicity only if dCK was induced by the addition of doxycycline. Induction of dCK had no effect on proliferation in the absence of gemcitabine or cytarabine (Figure 2C–F).
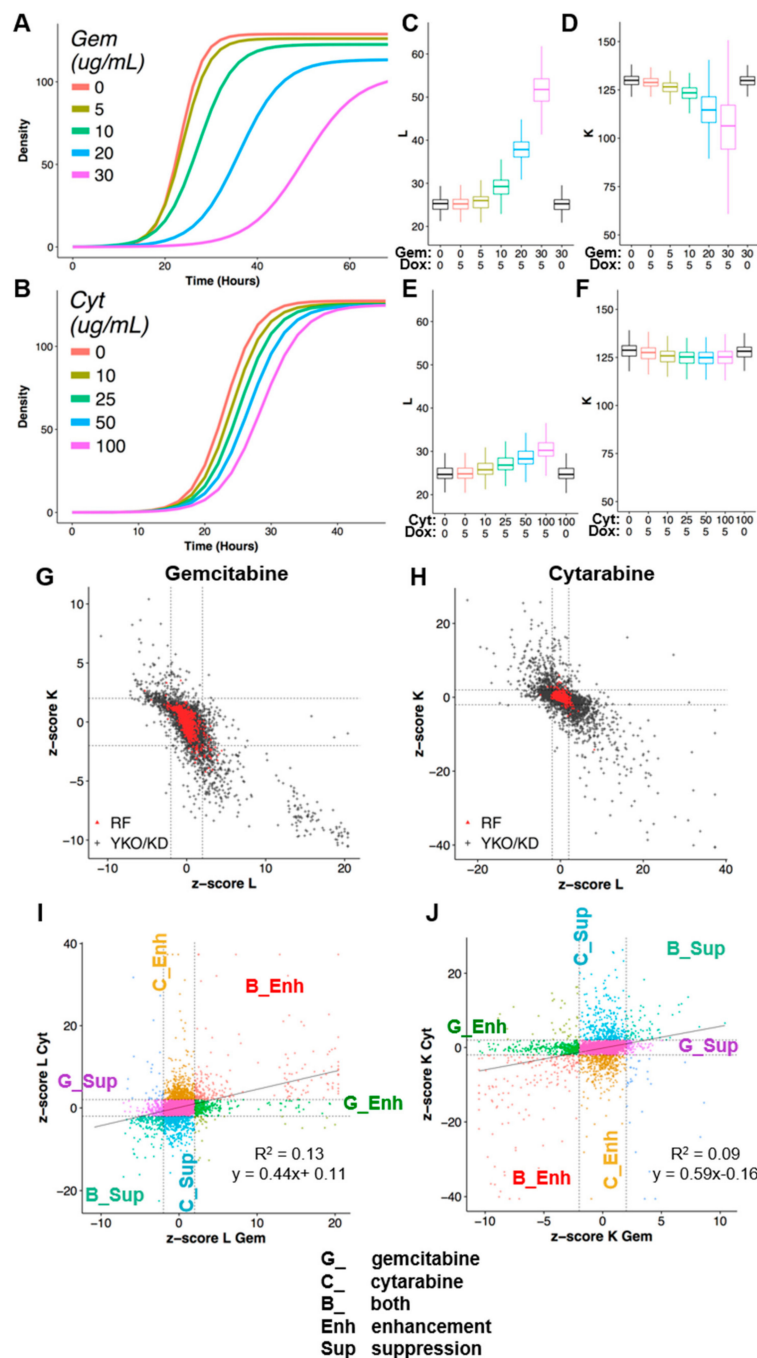
Figure 2. Phenomic analysis of drug–gene interaction for gemcitabine and cytarabine. Average growth curves (from fitting pixel intensity data of 768 replicate cultures to a logistic function) for the reference (RF) strain, treated with the indicated concentrations of (**A**) gemcitabine or (**B**) cytarabine. (**C–F**) Cell proliferation parameter (CPP) distributions from data depicted in panels A and B, also with and without induction of deoxycytidine kinase (0 or 5 µg/mL doxycycline respectively), for (**C–D**) gemcitabine and (**E–F**) cytarabine in µg/mL for (**C,E**) L and (**D,F**) K. (**G,H**) Comparison of drug–gene interaction scores calculated for L vs. K for (**G**) gemcitabine and (**H**) cytarabine, where score distributions of yeast knockout/knockdown (YKO/KD, black) and non-mutant parental (Ref, red) strain cultures are indicated along with thresholds for deletion enhancement and suppression (dashed lines at +/− 2). (**I–J**) Differential drug–gene interaction using L (**I**) or K (**J**) as the CPP for gemcitabine vs. cytarabine, classified by specificity of gene-drug interaction, where 'G', 'C', and 'B' indicate gemcitabine, cytarabine, or both, respectively. Deletion enhancement or suppression is indicated by '_Enh' or '_Sup'.

Interaction scores were calculated by departure of the observed CPP for each YKO/KD strain from that expected based on the observed phenotypes for the reference strain treated and untreated with drugs and the YKO/KD strain in the absence of drugs, incorporating multiple drug concentrations, 768 replicate reference strain control cultures, and summarized by linear regression as z-scores [6–9,33,37]. Gene interaction scores with absolute value greater than two were selected for global analysis and termed deletion enhancers (z-score_L $\geq$ 2 or z-score_K $\leq$ −2) or deletion suppressors (z-score_L $\leq$ −2 or z-score_K $\geq$ 2) of drug cytotoxicity, revealing functions that buffer or promote drug cytotoxicity, respectively [39] (Figure 2).

Growth inhibition was greater for gemcitabine than for cytarabine (Figure 2A–F), however, the phenotypic variance was also less for cytarabine, such that interactions of smaller effect size were detectable and the range of scores was greater (Additional File 1, Table S6). The CPP, 'L', (the time at which half carrying capacity is reached), is most sensitive to growth inhibitory perturbation, while 'K' (carrying capacity) reports on more extreme growth differences (Figure 2A–H). Low correlation between the gene–drug interaction profiles suggested differential buffering of these two drugs, consistent with their distinct antitumor efficacies (Figure 2I,J).

3.2. Functional Analysis of Gene Interaction Modules

Recursive expectation-maximization clustering (REMc) was used to identify modules of genes that shared similar profiles of buffering or promoting nucleoside toxicity of gemcitabine or cytarabine [40] (see Figure 3A–F; Table 1; Additional File 5). As described previously, REMc results were assessed with GO Term Finder for gene ontology functional enrichment [41] and heatmaps generated by first adding data regarding the main effect of the gene knockout or knockdown (i.e., no drug) on cell proliferation, termed 'shift' (see methods), followed by hierarchical clustering [40,41]. GO term average (GTA) scores, which are based on the average and standard deviation of drug–gene interaction for all genes of each GO term [39], were used as a complement to REMc/GTF for identifying functions that buffer or promote drug effects (Table 2, Figure 4, and Additional File 6, Files A–C). Yeast–human homologs were judged, regarding causality of differential gene expression associated with sensitivity to gemcitabine or cytarabine, by the correspondence of yeast phenomic and cancer pharmacogenomics results, thus establishing a model resource to test the utility of yeast phenomics to inform cancer genetic profiling for predicting drug-specific, antitumor efficacy (Figure 3G–H).
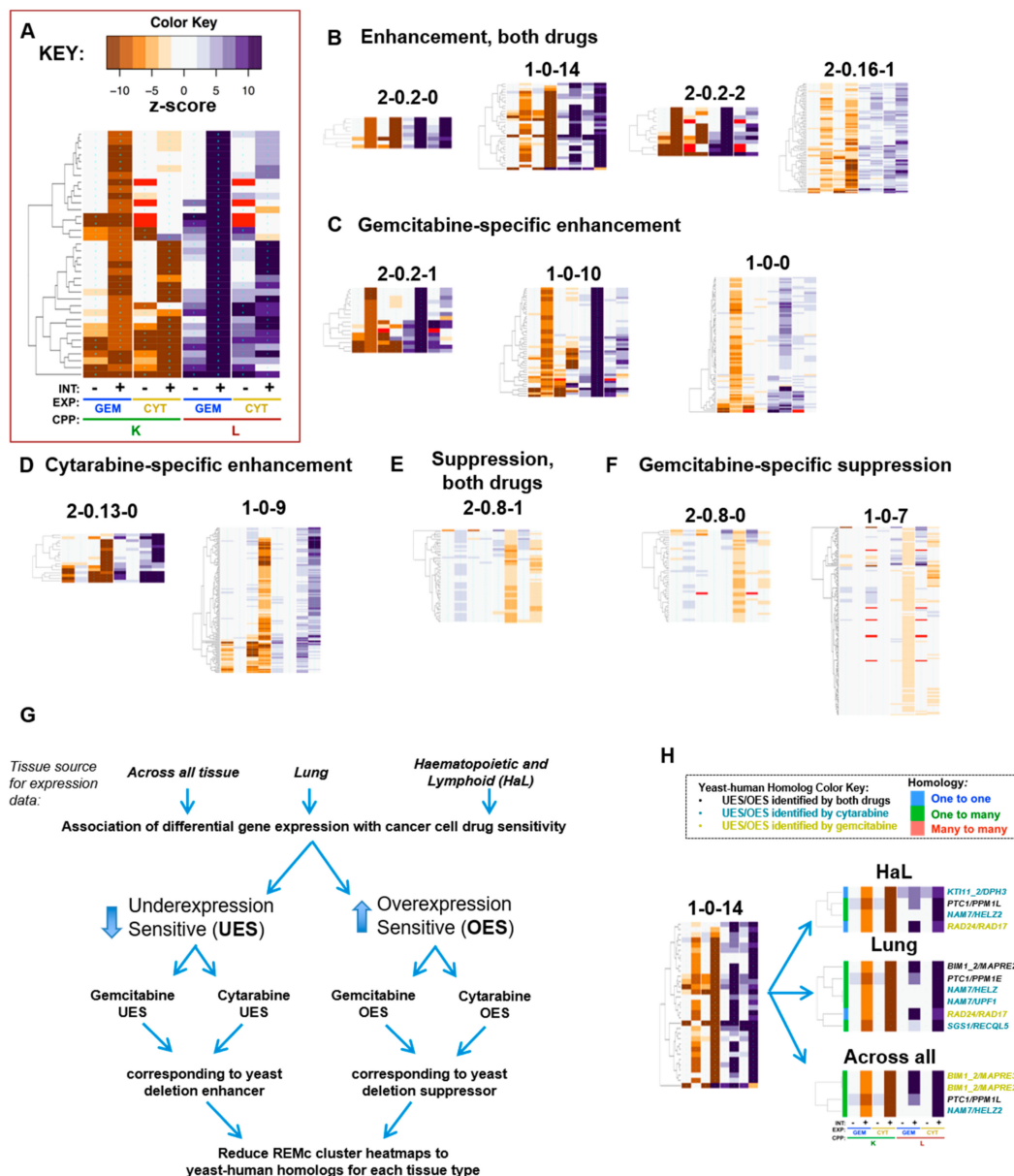
Figure 3. Prediction of drug–gene interaction in cancer cells by integration of yeast phenomic and human pharmacogenomic data. Recursive expectation-maximization clustering results were classified visually by their associated gene interaction profiles (see methods). (**A**) The order of data columns, which is consistent for all heatmaps, is indicated. K-derived interactions are in columns 2 and 4, with L-derived interactions in columns 6 and 8, for gemcitabine and cytarabine, respectively. To the left of each interaction value (indicated by '+'), is the corresponding 'shift' value (indicated by '−'), referring to the ΔCPP for the respective YKO/KD culture relative to the reference culture average in the absence of gemcitabine or cytarabine (i.e., the effect of the YKO/KD on cell proliferation independent of drug treatment; see methods). (**B–F**) Within each panel, clusters in the respective categories are displayed, left to right, in descending order, by relative strength of drug–gene interaction effects evident by the heatmaps. (**B**) Enhancing gene–drug interactions for both drugs. (**C**) Gemcitabine-specific enhancement. (**D**) Cytarabine-specific enhancement. (**E**) Suppressing gene–drug interactions for both drugs. (**F**) Gemcitabine-specific suppression. (**G**) The algorithm for integrating yeast phenomic and cancer pharmacogenomics data: For all cell lines from the Genomics of Drug Sensitivity in Cancer (GDSC) database (either lung, hematopoietic and lymphoid, or across all tissues) with increased drug sensitivity, underexpressed (UES) genes were highlighted by yeast homologs that were deletion

enhancing, while overexpressed (OES) genes were highlighted by yeast homologs that were deletion suppressing. (**H**) Yeast–human homologs identified as described in G. The category of homology from *BiomaRt* is indicated in the left column of each heatmap (see homology color key) shown at right. The gene label color (at far right) indicates whether the human homolog was found in PharmacoDB for both drugs (black), cytarabine (teal), or gemcitabine (gold). Additional Files 5 (File B) and 8 (Files B–D) contain all REMc heatmaps of the types indicated to the left and right, respectively, in panel H. Additional File 8 includes information for all yeast–human homologs from each category suggested by the study to exhibit functionally conserved gene–drug interaction.
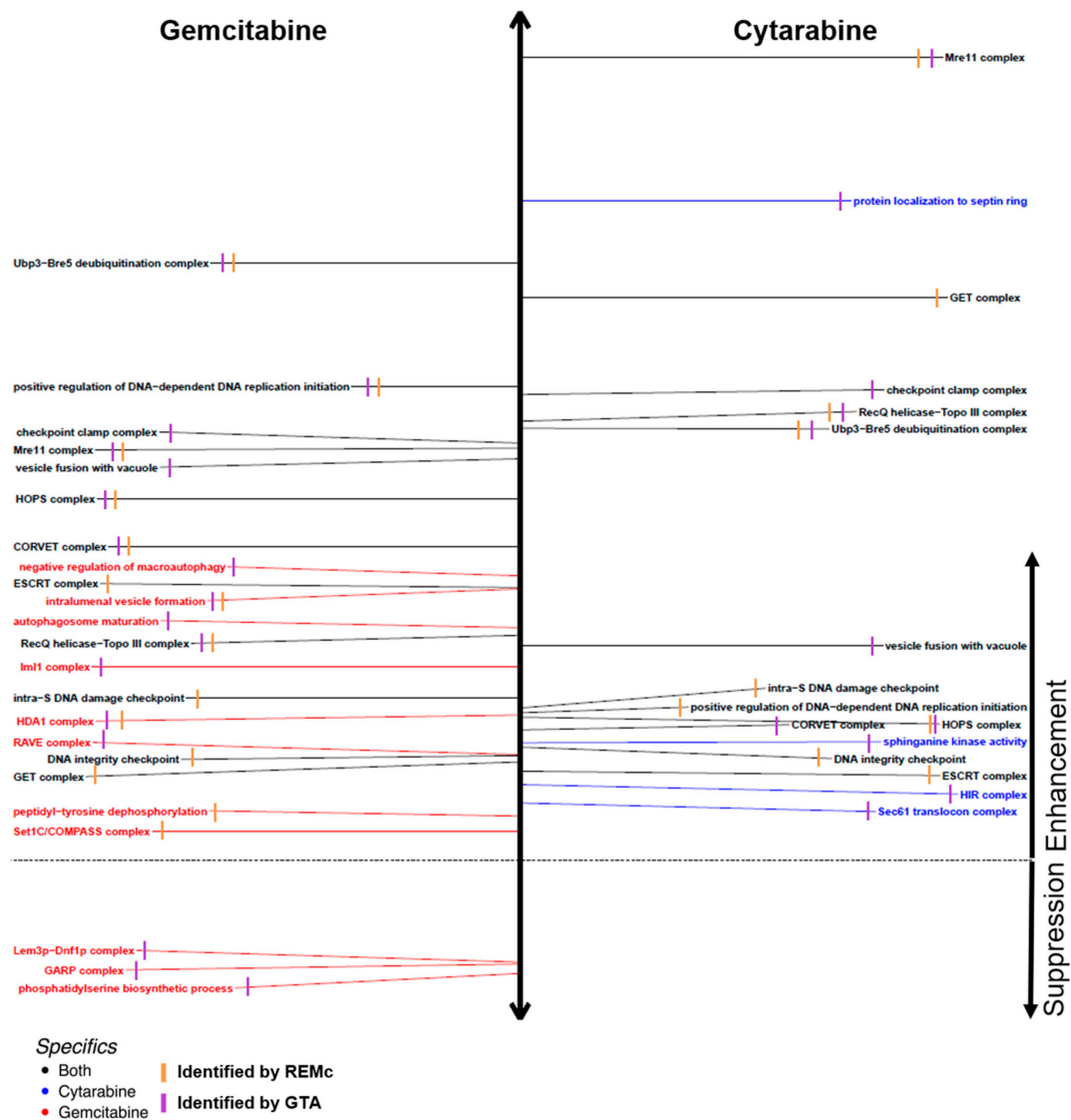
Figure 4. GO annotations associated with deletion enhancement or suppression of gemcitabine and/or cytarabine cytotoxicity. Representative GO terms are listed, which were identified by REMc/GTF (orange), GTA (purple), or both methods, for enhancement (above dashed line) or suppression (below dashed line) of gemcitabine (left, red), cytarabine (right, blue), or both media types (black). Term-specific heatmaps were manually reviewed to decide which terms should be included. Distance above or below the horizontal dashed line reflects the average interaction score for genes identified by REMc/GTF or the GTA score (see methods). See Additional Files 5 and 6 for all REMc/GTF and GTA results, and Additional File 7 for GO term-specific heatmaps.

Table 1. GO terms enriched in REMc clusters.

GO Term	Drug	INT	O	Cluster	Genes in Term	p-Value	Genes	Fig.	GTA Gem L	GTA Cyt L
Ubp3-Bre5 deubiquitination complex	Both	Enh	C	2-0.2-0	2/2	2.57×10^{-5}	UBP3:BRE5	Figure 5D	19.8	14.32
positive regulation of DNA-dependent DNA replication initiation	Both	Enh	P	1-0-2	3/4	2.09×10^{-4}	RFM1:FKH2:SUM1	Figure 5B	15.7	4.9
Mre11 complex	Both	Enh	C	2-0.14-1	2/3	5.66×10^{-4}	RAD50:XRS2	Figure 5B	13.7	26.6
HOPS complex	Both	Enh	C	2-0.14-1	2/7	3.94×10^{-3}	PEP3:VPS33	Figure 5D	12.0	4.8
CORVET complex	Both	Enh	C	2-0.14-1	2/7	3.94×10^{-3}	PEP3:VPS33	Figure 5D	10.4	4.3
RecQ helicase-Topo III complex	Both	Enh	C	1-0-14	2/3	3.31×10^{-3}	SGS1:RMI1	Figure 5B	7.5	14.6
GET complex	Both	Enh	C	2-0.14-0	2/3	4.68×10^{-4}	GET1:GET2	Figure 5D	3.3	18.6
DNA integrity checkpoint	Both	Enh	P	1-0-14	4/40	3.85×10^{-3}	DUN1:RAD17:RAD24:SGS1	Figure 5A	4.8	4.8
α-glucoside transmembrane transporter activity	Cyt	Enh	F	2-0.17-3	2/2	5.98×10^{-3}	MAL31:MAL11	Figure 7A	−0.7	2.2
intralumenal vesicle formation	Gem	Enh	P	1-0-10	3/7	2.90×10^{-3}	DOA4:VPS24:BRO1	Figure 6A	9.0	1.6
HDA1 complex	Gem	Enh	C	1-0-0	2/3	7.08×10^{-2}	HDA1:HDA3	Figure 6B	4.8	0.3
Swr1 complex	Gem	Enh	C	1-0-11	3/12	3.46×10^{-2}	SWC3:VPS71:SWR1	Figure 6B	2.9	−1.6
peptidyl-tyrosine dephosphorylation	Gem	Enh	P	1-0-0	5/20	2.18×10^{-3}	OCA2:SIW14:OCA1:OCA4:OCA6	Figure 6C	1.5	0.5
Set1C/COMPASS complex	Gem	Enh	C	1-0-0	3/6	5.74×10^{-3}	SDC1:SWD3:BRE2	Figure 6B	1.0	0.6
phospholipid-translocating ATPase activity	Gem	Sup	F	1-0-8	3/7	9.70×10^{-3}	DRS2:LEM3:DNF2	Figure 6D	−1.6	−0.9

For each GO term, the table indicates which drugs interact with it, the interaction type (enhancing or suppressing), the ontology ('O') it derives from (cellular process or component, or molecular function), the REMc cluster ID from which the term was most specific, the fraction of the genes in the term that were observed in the cluster, and the *p*-value for enrichment of the genes. Relevant figures and associated GTA data are also given.

Table 2. GO terms identified by gene ontology term averaging (GTA).

Term	Drug	INT_Type	Ont	Cluster	*p*-Value	Genes	Fig.	Gem GTA_K	Gem GTA_L	Cyt GTA_K	Cyt GTA_L
checkpoint clamp complex	Both	Enh L/K	C	NA	NA	RAD17 | MEC3	Figure 5B	−7.3	13.8	−23.5	15.4
HOPS complex	Both	Enh L/K	C	2-0.14-1	3.94×10^{-3}	VPS16 | VPS8 | PEP3 | VPS41 | VPS33 | PEP5	Figure 5D	−6.3	12.0	−11.4	4.8
Mre11 complex	Both	Enh L/K	C	2-0.14-1	5.66×10^{-4}	MRE11 | RAD50 | XRS2	Figure 5B	−8.8	13.7	−39.3	26.6
RecQ helicase-Topo III complex	Both	Enh L/K	C	1-0-14	3.31×10^{-3}	RMI1 | SGS1 | TOP3	Figure 5B	−7.7	7.5	−24.7	14.6
Ubp3-Bre5 deubiquitination complex	Both	Enh L/K	C	2-0.2-0	2.57×10^{-5}	UBP3 | BRE5	Figure 5D	−9.2	19.8	−16.9	14.3
vesicle fusion with vacuole	Both	Enh L/K	P	NA	NA	VAM3 | VPS33	Figure 5D	−7.4	13.3	−11.4	7.1
Sec61 translocon complex	Cyt	Enh K	C	NA	NA	SEC61 | SBH2	Figure 7A	−0.4	1.1	−5.1	1.9
HIR complex	Cyt	Enh L	C	NA	NA	HIR1 | HIR2 | HPC2 | HIR3	Figure 7A	−1.0	1.0	−0.6	2.5
sphinganine kinase activity	Cyt	Enh L	F	NA	NA	LCB4 | LCB5	Figure 7A	−0.1	0.3	−1.2	3.9
protein localization to septin ring	Cyt	Enh L/K	P	NA	NA	ELM1 | HSL1	Figure 7A	−1.3	2.5	−17.8	21.9
autophagosome maturation	Gem	Enh K	P	NA	NA	VAM3 | CCZ1	Figure 6A	−5.6	7.7	−1.6	2.5
Elongator holoenzyme complex	Gem	Enh K	C	NA	NA	TUP1 | ELP4 | ELP2 | IKI3 | IKI1 | ELP3 | ELP6	Figure S4C	−3.6	3.4	−2.6	2.5
ESCRT I complex	Gem	Enh K	C	NA	NA	STP22 | VPS28 | SRN2 | MVB12	Figure 5D	−6.9	9.1	−0.8	2.5
negative regulation of macroautophagy	Gem	Enh K	P	NA	NA	PHO85 | PHO80 | KSP1 | PCL5 | SIC1	Figure 6A	−5.8	9.4	−4.1	1.8
protein urmylation	Gem	Enh K	P	NA	NA	ELP2 | UBA4 | NCS2 | URM1 | URE2 | ELP6	Figure S4C	−3.7	1.5	1.0	1.2
CORVET complex	Gem	Enh L/K	C	2-0.14-1	3.94×10^{-3}	VPS16 | VPS8 | PEP3 | VPS41 | VPS33 | VPS3 | PEP5	Figure 5D	−6.6	10.4	−10.4	4.3
ESCRT-0 complex	Gem	Enh L/K	C	NA	NA	VPS27 | HSE1	Figure 5D	−5.7	10.4	−3.9	2.6
HDA1 complex	Gem	Enh L/K	C	1-0-0	7.08×10^{-2}	HDA3 | HDA1 | HDA2	Figure 6B	−4.8	4.8	−0.6	0.3
GATOR (Iml1) complex	Gem	Enh L/K	C	NA	NA	NPR2 | NPR3	Figure 6A	−4.4	6.4	1.0	2.2
intralumenal vesicle formation	Gem	Enh L/K	P	1-0-10	2.90×10^{-3}	VPS20 | VPS24 | BRO1 | DOA4 | VPS4 | SNF7	Figure 6A	−5.7	9.0	−1.8	1.6
positive regulation of DNA-dependent DNA replication initiation	Gem	Enh L/K	P	1-0-2	2.09×10^{-4}	SUM1 | FKH2 | RFM1 | FKH1	Figure 5B	−8.1	15.7	−2.4	4.9
RAVE complex	Gem	Enh L/K	C	NA	NA	RAV1 | RAV2	Figure 6A	−4.2	3.5	0.6	−0.2
GARP complex	Gem	Sup L	C	NA	NA	VPS51 | VPS53 | VPS54 | VPS52	Figure 6D	1.7	−3.4	1.5	−1.0
Lem3p-Dnf1p complex	Gem	Sup L	C	NA	NA	DNF1 | LEM3	Figure 6D	1.6	−3.4	−0.1	0.2
phosphatidylserine biosynthetic process	Gem	Sup L	C	NA	NA	DEP1 | CHO1 | UME6	Figure 6D	2.6	−3.7	0.8	−0.3

See Table 1 for data descriptions. 'NA' indicates terms identified by GTA only (i.e., not identified by REMc/GTF).

Heatmaps were also produced systematically to visualize drug–gene interaction profiles for all genes assigned to GO terms identified by REMc/GTF or GTA; these are referred to as term-specific heatmaps and are grouped by GO term parent–child relationships (Additional File 7).

Cancer pharmacogenomics data in PharmacoDB were mined using *PharmacoGx* [43] and *biomaRt* [44,45] with the Genomics of Drug Sensitivity in Cancer (GDSC) [30,49] or Genentech Cell Line Screening Initiative (gCSI) [31,50] datasets to match yeast drug–gene interaction by homology to differential gene expression in gemcitabine or cytarabine sensitive cancer cell lines (Figure 3G–H; Additional File 8). Yeast gene deletion enhancers identified human homologs underexpressed in gemcitabine- or cytarabine-sensitive cells, termed UES, while yeast gene deletion suppressors identified human homologs overexpressed in drug-sensitive cells, termed OES (Figure 3G).

The analysis was focused on the GDSC database, because it had expression data available for both gemcitabine and cytarabine; however, analysis of the gCSI data was also conducted for gemcitabine (Additional File 8, File A). Differential expression was analyzed: (1) across all tissue types, to consider interactions that might be applicable in novel treatment settings; (2) in hematopoietic and lymphoid tissue (HaL); and (3) in lung tissue, as cytarabine and gemcitabine are used to treat HaL and lung cancers, respectively. Gemcitabine is also used for pancreatic cancer; however, the number of cell lines tested (30) was lower than for lung (156) or HaL (152). Thus, yeast genes that were deletion enhancing or suppressing were catalogued with human homologs that were UES or OES in PharmacoDB (Figure 3G,H, Tables 3–5, and Additional File 8, File A).

In summary REMc, GTF, and GTA revealed functional genetic modules that alternatively buffer (deletion enhancing) or promote (deletion suppressing) drug cytotoxicity [5,40,51] and illustrated whether the effects were shared or differential between gemcitabine and cytarabine (Figure 4). Yeast phenomic information was integrated with pharmacogenomics data results according to yeast–human gene homology to identify correlated differential gene expression associated with drug sensitivity in cancer cell lines (Figures 5–7). This approach serves to generate hypotheses regarding whether differential expression of a particular gene is causal for increased drug sensitivity [52] and ultimately whether yeast phenomic models can improve the predictive value of cancer pharmacogenomics data in the context of precision oncology [53–58].

4. Functions that Respond to Gemcitabine and Cytarabine Similarly

4.1. Genetic Modules that Buffer Cytotoxicity of Both Gemcitabine and Cytarabine

To characterize gemcitabine and cytarabine, which have similar molecular structures and mechanisms of action, yet different spectra of antitumor efficacy, we first surveyed for buffering genes shared in common. Examples of genes with deletion-enhancing interactions for both drugs are displayed in clusters 2-0.2-0, 1-0-14, 2-0.2-2, and 2-0.16-1 (Figure 3B). GO enrichment was observed in these clusters for the DNA integrity checkpoint; positive regulation of DNA replication; and the Mre11, RecQ helicase-Topo III, CORVET, HOPS, GET, and Ubp3-Bre5 deubiquitination complexes (Figure 4, Table 1). GTA identified many of the same functions and additionally revealed the terms vesicle fusion with vacuole and checkpoint clamp complex (Table 2). We mapped yeast gene–drug interactions to respective human homologs in PharmacoDB to find evidence for evolutionary conservation of gene–drug interaction (Figure 5C,D, Additional File 8, Files B–D) and buffering mechanisms.

4.2. DNA Integrity Checkpoint and Repair-Related Complexes

As gemcitabine and cytarabine triphosphate analogs are incorporated into DNA, we anticipated shared interactions with genes functioning in DNA metabolism and repair. Overlap was observed, however there were differential effects between genes assigned to the same gene ontology terms, such that GO TermFinder enrichment in REMc clusters was less than might have been expected. For example, deletion-enhancing gene–drug interaction for the GO term, DNA integrity checkpoint, was enriched in cluster 1-0-14, which displayed deletion enhancement for both gemcitabine and cytarabine (Table 1,

Figures 3 and 5A). However, its child term, intra-S DNA damage checkpoint, was not GO-enriched because of differential clustering among drug–gene interactions associated with the term (Additional File 5, File C). Similarly, intra-S DNA damage checkpoint was not identified by GTA due to variation in interaction between genes assigned to the term, highlighting the utility in displaying the phenomic data for each GO term for manual review (Figure 5A).
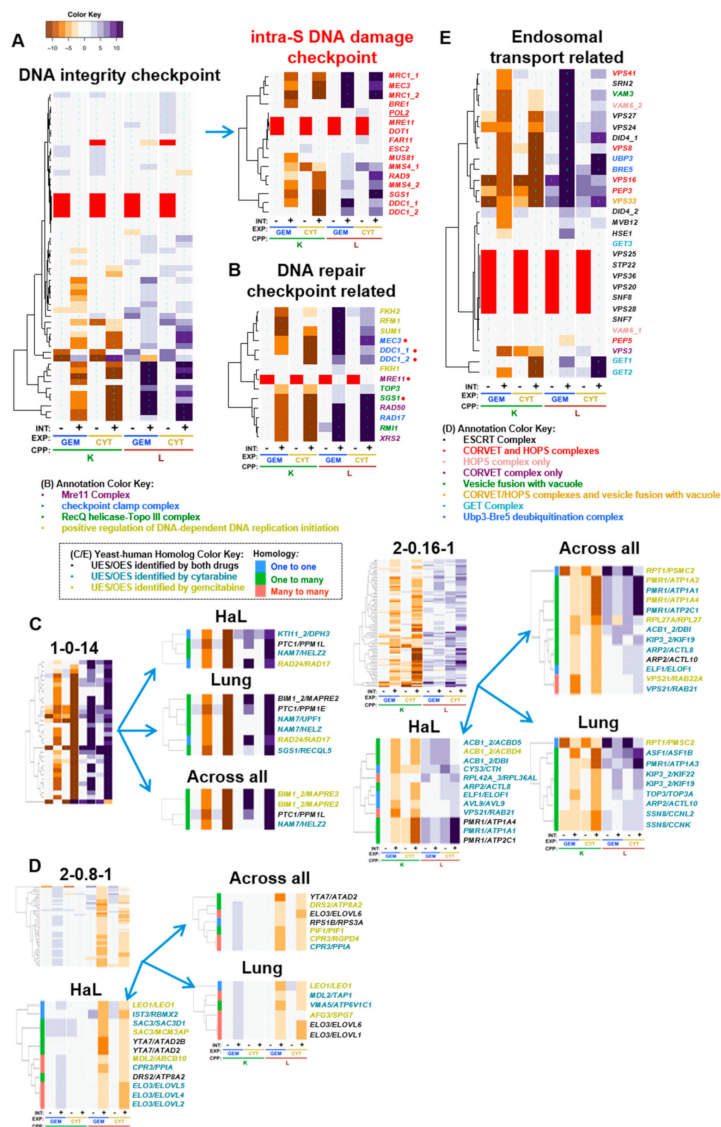

Figure 5. Drug–gene interaction common to gemcitabine and cytarabine. Genes that similarly influence the cytotoxicity of both gemcitabine and cytarabine suggest common pathways that buffer or promote toxicity, as illustrated by: (**A**) GO term-specific heatmaps for DNA integrity checkpoint and its child term intra-S DNA damage checkpoint, which buffer gemcitabine and cytarabine, along with (**B**) genes comprising other DNA checkpoint/repair-related GO terms, such as positive regulation of DNA-dependent DNA replication initiation, and the Mre11, checkpoint clamp and RecQ helicase-Topo III complexes; (**C,D**) REMc clusters filtered for PharmacoDB results for yeast-human homologs that exhibited (C) deletion enhancement and UES or (D) deletion suppression and OES; and (**E**) deletion enhancing endosomal transport-related GO terms, including vesicle fusion with vacuole, and the CORVET/HOPS, ESCRT, GET, and Ubp3-Bre5 deubiquitination complexes. Gene labels are color-coordinated with legends in panels B and E, and as described in Figure 3H for panels C and D. Genes in the YKD collection are underlined.

Enriched complexes functionally related to the DNA integrity checkpoint function included the RecQ helicase-Topo III, the checkpoint clamp, and the Mre11 complexes (Figure 5B). Rmi1, Top3, and Sgs1 form the RecQ helicase Topo III complex, which is involved in Rad53 checkpoint activation and maintenance of genome integrity [59], and together with replication protein A function in DNA decatenation and disentangling of chromosomes [60]. *RMI1* and *SGS1* deletion-enhancement clustered together in 1-0-14, while *TOP3* had a similar, but slightly weaker interaction pattern in cluster 1-0-16 (Additional File 5, File B). The human homolog of *SGS1*, *RECQL5*, was UES for cytarabine in lung cancer cells (Figure 5C; see 1-0-14 in 5C, all cluster heatmaps available in Additional File 5, File B). *RECQL5* preserves genome stability during transcription elongation, and deletion of *RECQL5* increases cancer susceptibility [61,62]. Human *TOP3A* was also UES for cytarabine in lung tissue (Figure 5C; 2-0.16-1). *TOP3A* is underexpressed in ovarian cancer, and mutations in *TOP3A* are associated with increased risk for acute myeloid leukemia and myelodysplastic syndromes, suggesting potential cancer vulnerabilities if somatic, but they can also occur in the germline, which would lead to enhanced host toxicity [63–65].
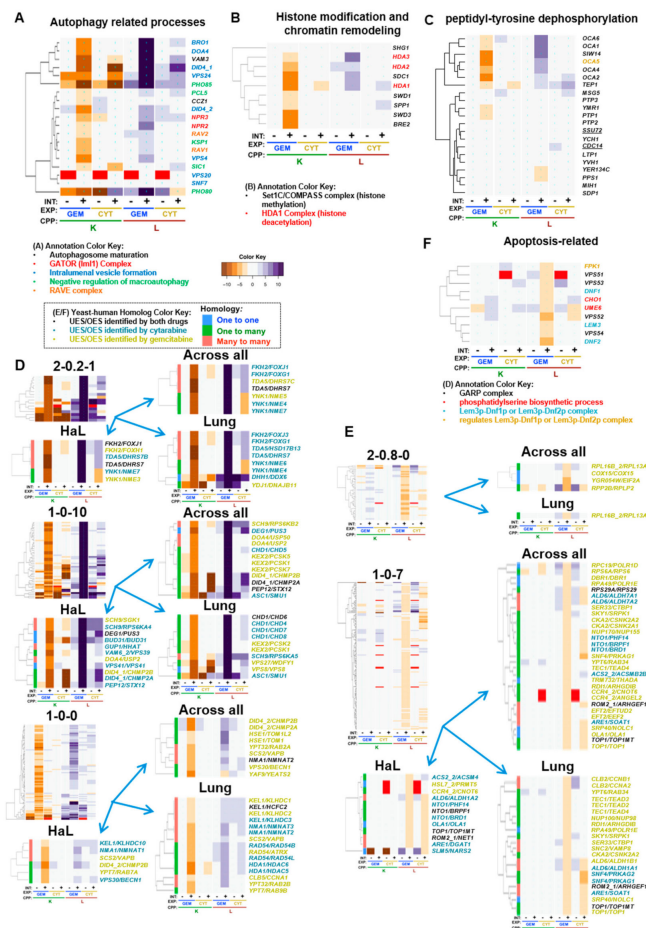

Figure 6. Gemcitabine-specific gene interaction. (**A–C**) Cellular processes that buffer gemcitabine to a greater extent than cytarabine included: (**A**) autophagy-related processes; (**B**) histone modification and chromatin remodeling (particularly for K interaction); and (**C**) peptidyl-tyrosine dephosphorylation, representing the genes *OCA (1–6)* (*OCA5* was manually added to the panel (see text); *OCA3/SIW14* are aliases). (**D,E**) When comparing gene-drug interactions of homologs across cancer pharmacogenomic and yeast phenomic experiments, human genes are predicted to (**D**) buffer gemcitabine toxicity if they are UES and deletion enhancing, or to (**E**) promote gemcitabine toxicity if they are OES and deletion suppressing. (**F**) Apoptosis-related genes and complexes were observed to promote toxicity of gemcitabine more than toxicity of cytarabine. Gene labels are color-coordinated with legends in panels A, B, and F, and as described in Figure 3H for panels D and E.

Table 3. Yeast–human homologs predicted to similarly buffer or promote both gemcitabine and cytarabine toxicity.

yGene	hGene	H	Drug	Cluster	Tissue	Gem K	Cyt K	Gem L	Cyt L	Ref	Description (Human)
NAM7	HELZ	2	Cyt	1-0-14	L	−6.5	−16.7	1.1	13.6	[66–69]	helicase with zinc finger
NAM7	HELZ2	2	Cyt	1-0-14	A, H	−6.5	−16.7	1.1	13.6		helicase with zinc finger 2
NAM7	UPF1	2	Cyt	1-0-14	L	−6.5	−16.7	1.1	13.6	[70–72]	UPF1, RNA helicase and ATPase
PTC1	PPM1E	2	Both	1-0-14	L	−8.8	−12.7	7.9	15.7	[73]	protein phosphatase, Mg2+/Mn2+ dependent 1E
PTC1	PPM1L	2	Both	1-0-14	A, H	−8.8	−12.7	7.9	15.7	[74]	protein phosphatase, Mg2+/Mn2+ dependent 1L
RAD24	RAD17	1	Gem	1-0-14	H, L	−7.4	−27.6	14.2	8.3	[75–79]	RAD17 checkpoint clamp loader component
SGS1	RECQL5	2	Cyt	1-0-14	L	−8.4	−33.4	3.4	19.3	[61,62]	RecQ like helicase 5
KTI11_2	DPH3	1	Cyt	1-0-14	H	−7.7	−10.3	6.5	9.1	[80–82]	diphthamide biosynthesis 3
BIM1_2	MAPRE2	2	Gem	1-0-14	A	−7.7	−15.4	16.0	20.0	[83]	microtubule associated protein RP/EB family member 2
BIM1_2	MAPRE2	2	Both	1-0-14	L	−7.7	−15.4	16.0	20.0	[83]	microtubule associated protein RP/EB family member 2
BIM1_2	MAPRE3	2	Gem	1-0-14	A	−7.7	−15.4	16.0	20.0	[84]	microtubule associated protein RP/EB family member 3
ASF1	ASF1B	2	Cyt	2-0.16-1	L	−6.1	−9.5	4.1	8.3	[85]	anti-silencing function 1B histone chaperone
AVL9	AVL9	1	Cyt	2-0.16-1	H	−4.3	−2.5	0.2	2.9	[86–88]	AVL9 cell migration associated
PMR1	ATP1A1	2	Cyt	2-0.16-1	A, H	−3.8	−9.8	3.6	10.1	[89]	ATPase Na+/K+ transporting subunit α 1
PMR1	ATP1A2	2	Gem	2-0.16-1	A	−3.8	−9.8	3.6	10.1	[90]	ATPase Na+/K+ transporting subunit α 2
PMR1	ATP1A3	2	Cyt	2-0.16-1	L	−3.8	−9.8	3.6	10.1		ATPase Na+/K+ transporting subunit α 3
PMR1	ATP1A4	2	Gem	2-0.16-1	A	−3.8	−9.8	3.6	10.1		ATPase Na+/K+ transporting subunit α 4
PMR1	ATP1A4	2	Both	2-0.16-1	H	−3.8	−9.8	3.6	10.1		ATPase Na+/K+ transporting subunit α 4
PMR1	ATP2C1	2	Cyt	2-0.16-1	A	−3.8	−9.8	3.6	10.1	[91,92]	ATPase secretory pathway Ca2+ transporting 1
PMR1	ATP2C1	2	Both	2-0.16-1	H	−3.8	−9.8	3.6	10.1	[91,92]	ATPase secretory pathway Ca2+ transporting 1
TOP3	TOP3A	2	Cyt	2-0.16-1	L	−5.2	−4.0	3.3	3.4	[63–65]	DNA topoisomerase III α
VPS21	RAB21	3	Cyt	2-0.16-1	A, H	−7.2	−4.1	−0.4	2.4	[93,94]	RAB21, member RAS oncogene family
VPS21	RAB22A	3	Gem	2-0.16-1	A	−7.2	−4.1	−0.4	2.4	[95–97]	RAB22A, member RAS oncogene family
ACB1_2	ACBD4	2	Gem	2-0.16-1	H	−5.4	−4.8	4.5	0.6	[98,99]	acyl-CoA binding domain containing 4
ACB1_2	ACBD5	2	Cyt	2-0.16-1	H	−5.4	−4.8	4.5	0.6	[100]	acyl-CoA binding domain containing 5
ACB1_2	DBI	2	Cyt	2-0.16-1	A, H	−5.4	−4.8	4.5	0.6	[101–103]	diazepam binding inhibitor, acyl-CoA binding protein
CPR3	PPIA	3	Cyt	2-0.8-1	A, H	2.1	1.6	−4.1	−2.8	[104–106]	peptidylprolyl isomerase A
CPR3	RGPD4	3	Gem	2-0.8-1	A	2.1	1.6	−4.1	−2.8		RANBP2-like and GRIP domain containing 4
ELO3	ELOVL1	3	Both	2-0.8-1	L	2.2	1.3	−3.4	−4.0	[107,108]	ELOVL fatty acid elongase 1
ELO3	ELOVL2	3	Cyt	2-0.8-1	H	2.2	1.3	−3.4	−4.0	[109]	ELOVL fatty acid elongase 2
ELO3	ELOVL4	3	Cyt	2-0.8-1	H	2.2	1.3	−3.4	−4.0		ELOVL fatty acid elongase 4
ELO3	ELOVL5	3	Cyt	2-0.8-1	H	2.2	1.3	−3.4	−4.0		ELOVL fatty acid elongase 5
ELO3	ELOVL6	3	Both	2-0.8-1	A, L	2.2	1.3	−3.4	−4.0	[110,111]	ELOVL fatty acid elongase 6
MDL2	ABCB10	3	Gem	2-0.8-1	H	2.5	1.5	−3.0	−3.0	[112]	ATP binding cassette subfamily B member 10
MDL2	TAP1	3	Cyt	2-0.8-1	L	2.5	1.5	−3.0	−3.0		transporter 1, ATP binding cassette subfamily B member
PIF1	PIF1	2	Gem	2-0.8-1	A	2.2	1.5	−4.5	−3.4	[113]	PIF1 5′-to-3′ DNA helicase
RPS1B	RPS3A	1	Both	2-0.8-1	A	2.3	0.9	−3.9	−2.3	[114,115]	ribosomal protein S3A
SAC3	MCM3AP	2	Gem	2-0.8-1	H	2.2	1.5	−5.2	−3.8	[116]	minichromosome maintenance complex component 3 associated protein
SAC3	SAC3D1	2	Cyt	2-0.8-1	H	2.2	1.5	−5.2	−3.8	[117,118]	SAC3 domain containing 1
YTA7	ATAD2	2	Both	2-0.8-1	A, H	1.8	1.0	−6.0	−3.6	[119–125]	ATPase family, AAA domain containing 2
YTA7	ATAD2B	2	Both	2-0.8-1	H	1.8	1.0	−6.0	−3.6		ATPase family, AAA domain containing 2B

Genes selected for discussion in the results were included in the table. The homology types (H) are one to one (1), one to many (2), and many to many (3). Drugs (Gem, Cyt, or Both) with which the genes interacted in a UES or OES manner in the GDSC database are indicated. The REMc clusters 1-0-14 and 2-0.16-1 are deletion enhancing and 2-0.8-1 is deletion suppressing (see Figure 5C,D). Tissue types from which genes were UES or OES in the PharmacoDB data are indicated for across all tissue (A), lung (L), and hematopoietic (H). Related references cited (Ref), and gene descriptions are given. Additional File 8 contains other tables of this type.

Figure 7. Cytarabine-specific gene interaction. (**A**) GO terms identified by GTA that revealed deletion enhancement to be greater for cytarabine than gemcitabine. (**B**) Human homologs of cytarabine-specific yeast gene deletion enhancers found to exhibit underexpression sensitivity for cytarabine in cancer cell lines.

The checkpoint clamp in yeast is comprised of Rad17/hRad1, Ddc1, and Mec3, which function downstream of Rad24/hRad17 in the DNA damage checkpoint pathway [75–77] to recruit yDpb11/hTopB1 to stalled replication forks and activate the yMec1/hATR protein kinase activity, initiating the DNA damage response [78]. The human homolog of yeast *RAD24*, *RAD17*, was UES for gemcitabine in both lung and hematopoietic and lymphoid tissue (Figure 5C; 1-0-14), representing a synthetic lethal relationship of potential therapeutic relevance. Consistent with this finding in yeast, depletion of *hRAD17* can sensitize pancreatic cancer cells to gemcitabine [79].

Mre11, Xrs2, and Rad50 constitute the Mre11 complex, which participates in the formation and processing of double-strand DNA breaks involved in recombination and repair [126], and clustered together in 1-0-14 (Figure 5B,C). Deficiency in the Mre1 complex is known to sensitize human cells to nucleoside analog toxicity [127], as also seen in cancer cell lines deficient for other checkpoint-signaling genes, such as Rad9, Chk1, or ATR, [128]. Single nucleotide polymorphisms in DNA damage response (*ATM* and *CHEK1*) have been associated with overall survival in pancreatic cancer patients treated with gemcitabine and radiation therapy [129]. Taken together, the results highlight evolutionarily conserved genes that function in DNA replication and recombination-based repair and are required to buffer the cytotoxic effects of both cytarabine and gemcitabine.

4.3. Positive Regulation of DNA-Dependent DNA Replication Initiation

The term, positive regulation of DNA-dependent DNA replication initiation, was identified by REMc/GTF and GTA for buffering interactions with both drugs, though stronger for gemcitabine (Tables 1 and 2). Genes representing this term were *FKH2, RFM1,* and *SUM1* (Figure 5B). The origin binding protein, Sum1, is required for efficient replication initiation [130] and forms a complex with Rfm1 and the histone deacetylase, Hst1, which is recruited to replication origins to deacetylate H4K5 for initiation [131]. *HST1* was also a strong deletion enhancer but was observed only for the L parameter and clustered in 2-0.2-2. The forkhead box proteins, Fkh1 and Fkh2, contribute to proper replication

origin timing and long range clustering of origins in G1 phase [132] and appear to buffer the cytotoxicity of gemcitabine more so than cytarabine, with *FKH2* deletion showing a stronger effect than its paralog (Figure 5B). Multiple human forkhead box protein homologs (*yFKH2/hFOXJ1/FOXG1/FOXJ3/FOXH1*) (Figure 6D) were observed as UES in PharmacoDB, of which *FOXJ1* underexpression is a marker of poor prognosis in gastric cancer [133], reduced expression of *FOXG1* is correlated with worse prognosis in breast cancer [134], *FOXJ3* is inhibited by miR-517a and associated with lung and colorectal cancer cell proliferation and invasion [135,136], and *FOXH1* is overexpressed in breast cancer and *FOXH1* inhibition reduces proliferation in breast cancer cell lines [137]. Although not UES in PharmacoDB, inhibition of the *HST1* homolog, *SIRT1,* by Tenovin-6 inhibits the growth of acute lymphoblastic leukemia cells and enhances cytarabine cytotoxicity [138], enhances gemcitabine efficacy in pancreatic cancer cell lines, and improves survival in a pancreatic cancer mouse model [139]. Thus, loss of this gene module that positively regulates DNA replication initiation appears to be robustly involved in oncogenesis and is also synthetic lethal with gemcitabine and cytarabine.

4.4. Endosomal Transport and Related Processes

GO annotated processes, enriched by REMc/GTF and GTA, and having deletion enhancement profiles related to endosome transport included vesicle fusion with vacuole (*VAM3* and *VPS33*), the CORVET/HOPS (*VPS41, VPS8, VPS16, PEP3, VPS33, VAM6,* and *VPS3*), ESCRT (*VPS27, VPS24, DID4, MVB12; HSE1* and *SRN2* were gemcitabine specific), GET complex (*GET1, GET2*; 2-0.14-0), and Ubp3-Bre5 deubiquitination (*UBP3* and *BRE5*) complexes (Tables 1 and 2, Figure 5E). The CORVET and HOPS tethering complexes function in protein and lipid transport between endosomes and lysosomes/vacuoles, are required for vacuolar fusion, recognize SNARE complexes, help determine endomembrane identity, and interact with the ESCRT complex [140,141]. The ESCRT complex recognizes ubiquitinated endosomal proteins to mediate degradation through the multivesicular body pathway [142,143]. The Ubp3-Bre5 deubiquitination complex maintains Sec23, a subunit of COPII vesicles required for transport between the ER and Golgi, by cleaving its ubiquitinated form [144]. The GET complex (*GET1-3*) mediates insertion of tail-anchored proteins into the ER membrane, a critical process within the secretory pathway for vesicular trafficking [145–147]. Thus, these complexes, which function in processes related to endosomal transport, appear to be critical for buffering the toxicity of nucleoside analogs.

Several deletion-enhancing endosomal genes had human homologs associated with UES in cancer cell lines and/or reported roles in cancer biology (Figures 5E and 6D), including: (1) *VPS41/VPS41*, in which a single nucleotide polymorphism is associated with familial melanoma [148]; (2) *VPS27/WDFY1*, which is regulated by *NPR2* to maintain the metastatic phenotype of cancer cells [149,150]; (3) human homologs of yeast *HSE1, TOM1,* and *TOM1L2, TOM1L2* hypomorphic mice having increased tumor incidence associated with alterations in endosomal trafficking [151]; (4) *VPS8/VPS8* and *VAM6/VPS39*, which are predicted to be homologous members of the CORVET complex [152]; and (5) *VPS21/RAB21/RAB22A*, where *RAB21* promotes carcinoma-associated fibroblast invasion and knockdown inhibits glioma cell proliferation [93,94], and *RAB22A* promotes oncogenesis in lung, breast, and ovarian cancer [95–97]. Thus, it seems tumors arising in the context of deficiencies in certain endosomal trafficking genes could be vulnerable to gemcitabine and/or cytarabine.

4.5. 'Non-GO-enriched' Homolog Pairs with Corresponding UES and Deletion Enhancement

We next explored yeast–human homologs exhibiting yeast deletion enhancement and underexpression sensitivity in cancer, systematically and regardless of whether their functions were enriched within gene ontology (Table 3, Figure 5C). 'Non-enriched' interaction can be explained by a small total number of genes performing the function, only select genes annotated to a term impacting the phenotype, by genes contributing to a function without yet being annotated to it, by novel functions, and other possibilities.

With regard to the above, human homologs of the yeast type 2C protein phosphatase, *PTC1*, included *PPM1L* and *PPM1E* (Figure 5C; 1-0-14). *PPM1L* has reduced expression in familial adenomatous polyposis [74], while *PPM1E* upregulation has been associated with cell proliferation in gastric cancer [73]. Such differential interactions of paralogs could result from tissue specific expression and functional differentiation of regulatory proteins. Previously, we reported *ptc1-Δ0* to buffer transcriptional repression of *RNR1* [33], which is upregulated as part of the DNA damage response to increase dNTP pools [153].

The microtubule binding proteins, *yBIM1/hMAPRE2/hMAPRE3*, were deletion enhancing in yeast and UES in cancer for gemcitabine (Figure 5C; 1-0-14), of which frameshift mutations were reported in *MAPRE3* for gastric and colorectal cancers [84], however, *MAPRE2* is upregulated in invasive pancreatic cancer cells [83], demonstrating that the yeast phenomic model could help distinguish causal influence in cases of paralogous gene expression having what appear to be opposing effects on phenotypic response of cancer cells to cytotoxic chemotherapy.

NAM7 is a yeast RNA helicase that was deletion-enhancing for both drugs, though slightly stronger for cytarabine, while its human homologs *HELZ, HELZ2*, and *UPF1*, were UES only with cytarabine (Figure 5C; 1-0-14). *HELZ* has differential influence in cancer, acting as a tumor suppressor or oncogene [66–69]. *UPF1* downregulation is associated with poor prognosis in gastric cancer and hepatocellular carcinoma, and mutations often occur in pancreatic adenosquamous carcinoma [70–72]. Thus, it is possible cytarabine could have efficacy for patients with mutational loss of function in members of this helicase family.

ASF1/ASF1B (Figure 5C; 2-0.16-1) functions in nucleosome assembly as an anti-silencing factor and is one of the most overexpressed histone chaperones in cancer [85]. The yeast phenomic data suggest that anticancer approaches that target ASF1 as a driver [154] could be augmented by combination with gemcitabine or cytarabine.

AVL9/AVL9 (Figure 5C; 2-0.16-1) functions in exocytic transport from the Golgi [86]. *AVL9* knockdown resulted in abnormal mitoses associated with defective protein trafficking and increased cell migration with development of cysts [87], but also reduced cell proliferation and migration in other studies [88]. Regardless, the yeast phenomic model together with pharmacogenomics data would predict that functional loss of AVL9 renders cells vulnerable to cytarabine.

PMR1 is a P-type ATPase that transports Mn++ and Ca++ into the Golgi. Several of its human homologs, *ATP1A1, ATP1A2, ATP1A3, ATP1A4, ATP2C1*, were UES, either for gemcitabine or cytarabine, in the PharmacoDB analysis (Figure 5C; 2-0.16-1). Reduced expression of *ATP1A1* can promote development of renal cell carcinoma [89], reduced expression of *ATP1A2* is associated with breast cancer [90], and mutations in *ATP2C1* impair the DNA damage response and increase the incidence of squamous cell tumors in mice [91,92]. Like with *FKH2* (described above), *PMR1* deletion-enhancement points to multiple human homologs that are both implicated in the cancer literature to promote cancer when underexpressed, yet are also UES in the pharmacogenomics data, suggesting a potentially clinically useful synthetic lethal vulnerability.

KTI11/DPH3 (Figure 5C; 1-0-14), is a multi-functional protein involved in the biosynthesis of dipthamide and tRNA modifications important for regulation of translation, development and stress response [80,81], and has promoter mutations associated with skin cancer [82]. It was observed to be UES only for cytarabine and in hematopoietic and lymphoid cancer (the context cytarabine is used clinically).

ACB1 binds acyl-CoA esters and transports them to acyl-CoA-consuming processes, which is upregulated in response to DNA replication stress [155]. Human homologs of *ACB1* exhibiting UES (Figure 5C; 2-0.16-1) included: (1) *DBI*, which is upregulated in hepatocellular carcinoma and lung cancer, and its expression is negatively associated with multidrug resistance in breast cancer [101–103]; (2) *ACBD4*, which promotes ER-peroxisome associations [98] and is upregulated by a histone deacetylase inhibitor, valproic acid, in a panel of cancer cell lines [99]; and (3) *ACBD5*, which also promotes ER-peroxisome associations, but its link to cancer is unclear [100]. Thus, it appears

this gene family may influence epigenetic processes that buffer the cytotoxic effects of gemcitabine and cytarabine.

4.6. Deletion Suppression of Toxicity for Both Nucleosides

As opposed to deletion-enhancing interactions, which represent functions that buffer the cytotoxic effects of the drugs, deletion suppression identifies genes that promote toxicity, thus predicting overexpression sensitivity (OES) in pharmacogenomics data that represent causal tumor vulnerabilities. REMc/GTF identified as deletion-suppressing the GO terms glutaminyl-tRNA(Gln) biosynthesis (1-0-3), the nucleoplasmic THO (2-0.8-1), RNA cap binding (1-0-3), and the NuA3b histone acetyltransferase complexes (1-0-7) (Additional File 5, File C), while GTA identified mitochondrial translational elongation and the nuclear cap binding complex (Additional File 6, File A). However, the respective term-specific heatmaps revealed weak effects and high shift for many of the genes (Additional File 2, Figure S3), highlighting the utility of this phenomic visualization tool for prioritizing findings and leading us to shift our focus to individual yeast–human homologs identified in gene deletion suppressing clusters that were OES in the pharmacogenomics analysis, as detailed below.

In cluster 2-0.8-1, yeast-human homologs with correlated gene deletion suppression and OES for both gemcitabine and cytarabine (Figure 5D; Table 3) included: (1) *YTA7/ATAD2/ATAD2B*, which localizes to chromatin and regulates histone gene expression. *ATAD2* overexpression portends poor prognosis in gastric, colorectal, cervical, hepatocellular carcinoma, lung, and breast cancer, and thus overexpression sensitivity could represent the potential to target a driver gene [119–125]; (2) *PIF1/PIF1*, a DNA helicase, which is involved in telomere regulation and is required during oncogenic stress [113]; (3) *RPS1B/RPS3A*, which is a small subunit ribosomal protein that is overexpressed in hepatitis B-associated hepatocellular carcinoma and non-small-cell lung cancer [114,115]; (4) *LEO1/LEO1*, which associates with the RNA polymerase II and acts as an oncogene in acute myelogenous leukemia [156]; (5) *ELO3/ELOVL1/ELOVL2/ELOVL4/ELOVL6*, which constitutes a family of fatty acid elongases that function in sphingolipid biosynthesis, among which *ELOVL1* is overexpressed in breast and colorectal cancer tissue [107,108], *ELOVL2* is upregulated in hepatocellular carcinoma [109], and *ELOVL6* is overexpressed and associated with poor prognosis in liver and breast cancer [110,111]; (6) *MDL2/ABCB10*, which is a mitochondrial inner membrane ATP-binding cassette protein and is upregulated in breast cancer [112]; (7) *CPR3/PPIA*, which is a mitochondrial cyclophilin that is upregulated in lung cancer, esophageal, and pancreatic cancer [104–106]; and (8) *SAC3/MCM3AP/SAC3D1*, which is a nuclear pore-associated protein functioning in transcription and mRNA export, with *MCM3AP* being upregulated in glioma cells [116], while *SAC3D1* is upregulated in cervical cancer and hepatocellular carcinoma [117,118]. Yeast gene deletion suppression, together with overexpression sensitivity of human homologs in cancer, reveals potential therapeutic vulnerabilities that can be further explored in both systems.

5. Gemcitabine-Specific Gene Interaction Modules

5.1. Gemcitabine-Specific Gene Deletion Enhancement

Gemcitabine-specific deletion enhancement indicates genes for which loss of function increases vulnerability to gemcitabine to a greater extent than cytarabine. Therefore, these genes provide insight into cytotoxic mechanisms that are unique between the two deoxycytidine analogs. Representative clusters were GO-enriched for intralumenal vesicle formation (1-0-10), peptidyl-tyrosine dephosphorylation (1-0-0), and the Set1C/COMPASS and HDA1 complexes (Figure 3C, Figure 6A–C, Table 1). GTA identified negative regulation of macroautophagy; protein urmylation; and the RAVE, GATOR (Iml1), and Elongator holoenzyme complexes (Figure 6A, Table 2). Pharmacogenomics integration is highlighted for clusters 2-0.2-1, 1-0-10, and 1-0-0 (Figure 6D; see also, Additional File 8). Taken together, the results suggest that autophagy-related processes and perhaps others less well-characterized by GO buffer cytotoxicity of gemcitabine to a greater extent than cytarabine.

Table 4. Yeast–human homologs predicted to buffer or promote gemcitabine to greater degree than cytarabine.

yGene	hGene	H	Drug	Cluster	Tissue	Gem_K	Cyt_K	Gem_L	Cyt_L	Ref	Description_Human
CLB5	CCNA1	3	Gem	1-0-0	L	−3.5	1.4	5.4	−0.1	[157]	cyclin A1
HDA1	HDAC5	2	Cyt	1-0-0	L	−6.4	−2.6	5.0	2.2	[158]	histone deacetylase 5
HDA1	HDAC6	2	Cyt	1-0-0	L	−6.4	−2.6	5.0	2.2	[99,159–165]	histone deacetylase 6
HSE1	TOM1	2	Gem	1-0-0	A	−3.3	1.2	6.5	0.0		target of myb1 membrane trafficking protein
HSE1	TOM1L2	2	Gem	1-0-0	A	−3.3	1.2	6.5	0.0	[151]	target of myb1 like 2 membrane trafficking protein
NMA1	NMNAT1	3	Cyt	1-0-0	H	−4.6	−2.0	4.2	2.5	[166]	nicotinamide nucleotide adenylyltransferase 1
NMA1	NMNAT2	3	Both	1-0-0	A	−4.6	−2.0	4.2	2.5	[167]	nicotinamide nucleotide adenylyltransferase 2
NMA1	NMNAT2	3	Cyt	1-0-0	L	−4.6	−2.0	4.2	2.5	[167]	nicotinamide nucleotide adenylyltransferase 2
NMA1	NMNAT3	3	Cyt	1-0-0	L	−4.6	−2.0	4.2	2.5		nicotinamide nucleotide adenylyltransferase 3
RAD54	ATRX	2	Gem	1-0-0	L	−4.9	−0.9	4.5	3.9	[168]	ATRX, chromatin remodeler
RAD54	RAD54B	2	Cyt	1-0-0	L	−4.9	−0.9	4.5	3.9		RAD54 homolog B
RAD54	RAD54L	2	Cyt	1-0-0	L	−4.9	−0.9	4.5	3.9		RAD54 like
SCS2	VAPB	3	Gem	1-0-0	A, H, L	−4.3	−0.2	3.8	1.4	[100,169]	VAMP associated protein B and C
VPS30	BECN1	2	Gem	1-0-0	A	−5.9	−2.0	2.4	2.6	[170]	beclin 1
VPS30	BECN1	2	Cyt	1-0-0	H	−5.9	−2.0	2.4	2.6	[170]	beclin 1
DID4_2	CHMP2A	2	Gem	1-0-0	A	−6.1	−1.2	5.2	1.8	[171]	charged multivesicular body protein 2A
DID4_2	CHMP2B	2	Gem	1-0-0	A, H	−6.1	−1.2	5.2	1.8	[172,173]	charged multivesicular body protein 2B
YPT32	RAB2A	3	Gem	1-0-0	A	−4.4	0.3	5.0	−1.8	[174]	RAB2A, member RAS oncogene family
YPT32	RAB2B	3	Gem	1-0-0	L	−4.4	0.3	5.0	−1.8	[175]	RAB2B, member RAS oncogene family
KEX2	PCSK1	2	Gem	1-0-10	A, L	−7.8	−0.3	15.4	−0.9	[176]	proprotein convertase subtilisin/kexin type 1
KEX2	PCSK2	2	Gem	1-0-10	L	−7.8	−0.3	15.4	−0.9	[177]	proprotein convertase subtilisin/kexin type 2
KEX2	PCSK5	2	Gem	1-0-10	A	−7.8	−0.3	15.4	−0.9	[177,178]	proprotein convertase subtilisin/kexin type 5
KEX2	PCSK7	2	Gem	1-0-10	A	−7.8	−0.3	15.4	−0.9	[177,179]	proprotein convertase subtilisin/kexin type 7
PEP12	STX12	2	Both	1-0-10	A	−8.0	−16.1	13.6	5.3	[180,181]	syntaxin 12
PEP12	STX12	2	Cyt	1-0-10	H	−8.0	−16.1	13.6	5.3	[180,181]	syntaxin 12
VPS27	WDFY1	2	Gem	1-0-10	L	−8.1	−9.1	14.3	5.2	[149,150]	WD repeat and FYVE domain containing 1
VPS41	VPS41	1	Cyt	1-0-10	H	−6.5	−0.9	14.0	4.0	[148]	VPS41, HOPS complex subunit
VPS8	VPS8	1	Gem	1-0-10	L	−8.5	−12.3	14.4	3.5	[152]	VPS8, CORVET complex subunit
VAM6_2	VPS39	2	Cyt	1-0-10	H	−8.0	−2.8	13.9	4.0	[152]	VPS39, HOPS complex subunit
DID4_1	CHMP2A	2	Both	1-0-10	A	−8.0	−12.3	14.5	8.2	[171]	charged multivesicular body protein 2A
DID4_1	CHMP2A	2	Cyt	1-0-10	H	−8.0	−12.3	14.5	8.2	[171]	charged multivesicular body protein 2A
DID4_1	CHMP2B	2	Gem	1-0-10	A, H	−8.0	−12.3	14.5	8.2	[172,173]	charged multivesicular body protein 2B
FKH2	FOXG1	3	Cyt	2-0.2-1	A, L	−9.7	−2.1	19.7	5.1	[134]	forkhead box G1
FKH2	FOXH1	3	Gem	2-0.2-1	H	−9.7	−2.1	19.7	5.1	[137]	forkhead box H1
FKH2	FOXJ1	3	Cyt	2-0.2-1	A, H	−9.7	−2.1	19.7	5.1	[133]	forkhead box J1
FKH2	FOXJ3	3	Cyt	2-0.2-1	L	−9.7	−2.1	19.7	5.1	[135,136]	forkhead box J3
YNK1	NME3	2	Gem	2-0.2-1	H	−9.3	1.0	20.0	−4.0		NME/NM23 nucleoside diphosphate kinase 3
YNK1	NME4	2	Cyt	2-0.2-1	A, L	−9.3	1.0	20.0	−4.0		NME/NM23 nucleoside diphosphate kinase 4
YNK1	NME5	2	Gem	2-0.2-1	A	−9.3	1.0	20.0	−4.0	[182]	NME/NM23 family member 5

Table 4. *Cont.*

yGene	hGene	H	Drug	Cluster	Tissue	Gem_K	Cyt_K	Gem_L	Cyt_L	Ref	Description_Human
YNK1	NME6	2	Cyt	2-0.2-1	L	−9.3	1.0	20.0	−4.0		NME/NM23 nucleoside diphosphate kinase 6
YNK1	NME7	2	Cyt	2-0.2-1	A, H	−9.3	1.0	20.0	−4.0		NME/NM23 family member 7
ALD6	ALDH1A1	3	Cyt	1-0-7	L	1.3	1.7	−2.4	−3.5	[183–185]	aldehyde dehydrogenase 1 family member A1
ALD6	ALDH1A2	3	Cyt	1-0-7	A, H	1.3	1.7	−2.4	−3.5		aldehyde dehydrogenase 1 family member A2
ALD6	ALDH1B1	3	Gem	1-0-7	L	1.3	1.7	−2.4	−3.5	[185]	aldehyde dehydrogenase 1 family member B1
ALD6	ALDH7A1	3	Cyt	1-0-7	A	1.3	1.7	−2.4	−3.5	[185]	aldehyde dehydrogenase 7 family member A1
CKA2	CSNK2A1	2	Gem	1-0-7	A	1.2	−0.2	−2.5	−1.5	[186–193]	casein kinase 2 α 1
CKA2	CSNK2A2	2	Gem	1-0-7	A, L	1.2	−0.2	−2.5	−1.5	[186–193]	casein kinase 2 α 2
CLB2	CCNA2	3	Gem	1-0-7	L	2.0	0.4	−2.2	0.6	[194–197]	cyclin A2
CLB2	CCNB1	3	Gem	1-0-7	L	2.0	0.4	−2.2	0.6	[194–197]	cyclin B1
EFT2	EEF2	3	Gem	1-0-7	A	0.9	0.8	−2.4	−1.8	[198]	eukaryotic translation elongation factor 2
EFT2	EFTUD2	3	Gem	1-0-7	A	0.9	0.8	−2.4	−1.8	[199]	elongation factor Tu GTP binding domain containing 2
OLA1	OLA1	1	Gem	1-0-7	A	1.0	0.8	−2.6	−3.0	[200–202]	Obg like ATPase 1
OLA1	OLA1	1	Cyt	1-0-7	H	1.0	0.8	−2.6	−3.0	[200–202]	Obg like ATPase 1
RPA49	POLR1E	1	Gem	1-0-7	A, L	1.8	−0.9	−2.6	0.6	[203–206]	RNA polymerase I subunit E
SKY1	SRPK1	2	Gem	1-0-7	A, L	0.8	−0.6	−2.1	−1.3	[207]	SRSF protein kinase 1
SNC2	VAMP8	3	Gem	1-0-7	L	1.4	0.1	−2.3	−0.6	[208,209]	vesicle associated membrane protein 8
TOP1	TOP1	2	Gem	1-0-7	A, L	1.3	0.3	−3.1	−3.9	[210]	DNA topoisomerase I
TOP1	TOP1MT	2	Both	1-0-7	A, H, L	1.3	0.3	−3.1	−3.9		DNA topoisomerase I mitochondrial
YPT6	RAB34	2	Gem	1-0-7	A, L	1.4	1.1	−2.1	1.7	[211–213]	RAB34, member RAS oncogene family
RPP2B	RPLP2	2	Gem	2-0.8-0	A	1.7	0.2	−5.3	−2.8	[214]	ribosomal protein lateral stalk subunit P2
YGR054W	EIF2A	1	Gem	2-0.8-0	A	1.8	0.2	−4.1	−1.0	[215]	eukaryotic translation initiation factor 2A

Data headers are the same as described above for Table 3. The REMc clusters 1-0-0, 1-0-0, and 2-0.2-1 are deletion enhancing, while 1-0-7 and 2-0.8-0 are deletion suppressing (see Figure 6D,E).

5.2. Autophagy Related Processes

Autophagy-related processes and complexes consisted of intralumenal vesicle formation (1-0-0; BRO1, DOA4, DID4, VPS24, VPS4), the GATOR/SEACIT/Iml1 complex (NPR2, NPR3), autophagosome maturation (VAM3, CCZ1), negative regulation of macroautophagy (PHO85, PCL5, KSP1, SIC1, PHO80), and the RAVE complex (RAV1, RAV2) (Figure 6A).

Of the autophagy-related complexes, Npr2 and Npr3 form an evolutionarily conserved heterodimer involved in mediating induction of autophagy by inhibition of TORC1 signaling in response to amino acid starvation [216], also promoting non-nitrogen starvation-induced autophagy [217] (Figure 6A). The RAVE complex (*RAV1/2*) promotes assembly of the vacuolar ATPase [218,219], which is required for vacuolar acidification and efficient autophagy [220]. Gene deletion strains in the term negative regulation of macroautophagy (*PHO85, PHO80,* and *SIC1*) [221], which seemed from the automated assessment to suggest an opposing effect, were less compelling following detailed visualization of the data, due to the associated high shift and cytarabine deletion-enhancing interaction (Figure 6A).

Regarding the term intralumenal vesicle formation, Vps24 and Did4 are components of the ESCRT-III complex (see Figures 5E and 6A), which functions at endosomes, and the ATPase Vps4 is required for disassembly of the complex [222]. Doa4 interacts with Vps20 of ESCRT-III to promote intralumenal vesicle formation, which also requires *BRO1* [223]. Pharmacogenomics correlation revealed UES in cancer cell lines for *DID4/CHMP2A/CHMP2B* (Figure 6D; 1-0-10). During autophagy, *CHMP2A* translocates to the phagophore to regulate separation of the inner and outer autophagosomal membranes to form double-membrane autophagosomes [171]. *CHMP2B* is a member of the ESCRT-III complex required for efficient autophagy and has reduced expression in melanoma [172,173], raising the hypothesis that gemcitabine could have efficacy in that context.

Other genes involved in autophagy-related processes that had human homologs UES in cancer cell lines included: (1) *PEP12/STX12* (Figure 6D; 1-0-10), a t-SNARE required for mitophagy [180], for which underexpression is associated with risk of recurrence [181]; and (2) *VPS30/BECN1,* knockdown of which enhances gemcitabine cytotoxicity in pancreatic cancer stem cells [170]. Furthermore, gemcitabine treatment has been found to upregulate autophagy in pancreatic or breast cancer, which buffers drug cytotoxicity as inferred by the combination of gemcitabine with autophagy inhibitors' increased killing of cancer cells [224–226]. Thus, autophagy-related findings from the yeast model appear consistent with, and to build upon, previous cancer cell models.

5.3. Histone Modification and Chromatin Remodeling

GTF/REMc identified the Hda1 and Set1C/COMPASS (1-0-0) complexes as gemcitabine-specific deletion enhancing, which was confirmed by term-specific heatmaps (Figure 6B). The Set1C complex has been characterized to have a role in cell cycle coordination [227], which may be reflected by greater deletion enhancing interaction for the K than for the L CPP. The Set1C/COMPASS complex catalyzes mono-, di-, and tri- methylation of histone H3K4, which can differentially influence gene transcription depending on the number of methyl groups added [228–231], and was implicated by *BRE2*, *SWD1*, *SWD3*, *SDC1*, *SPP1*, and *SHG1* (Figure 6B). The SWD1 ortholog, *RBBP5*, which was UES with gemcitabine in lung tissue (Additional File 8, File C; 1-0-4), is upregulated in self-renewing cancer stem cells in glioblastoma and necessary for their self-renewal, is involved in the epithelial-mesenchymal transition in prostate cancer cells via its role in H3K4 trimethylation, and is upregulated in hepatocellular carcinoma [232–235]. Furthermore, gemcitabine sensitivity of pancreatic cancer cell lines was enhanced by H3K4me3 inhibition with verticillin A [233].

Histone deacetylases also influence cell cycle regulation [236], and the three genes that make up the yeast Hda1 deacetylase complex (homologous to mammalian class II Hda1-like proteins [237,238]) were gemcitabine deletion enhancers (Figure 6B). Similar effects in cancer cells include *HDAC6* knockdown in pediatric acute myeloid leukemia cells, which enhances cytarabine-induced apoptosis [158–160] and the use of histone deacetylase inhibitors in combination with gemcitabine, which augments killing of pancreatic cancer cell lines [161–165] and HeLa cells [99].

5.4. Peptidyl–Tyrosine Dephosphorylation

REMc/GTF identified peptidyl-tyrosine dephosphorylation (1-0-0), for which the term-specific heatmap (Additional File 7) revealed six genes previously characterized for their requirement in oxidant-induced cell cycle arrest and RNA virus replication [239,240], OCA1-6. Two additional tyrosine phosphatases, *YMR1* and *PTP1*, had similar interaction profiles (Figure 6C). *OCA1-3* deletions enhance growth defects associated with reactive oxygen species or caffeine treatment [239,240], and *OCA1-4* and *OCA6* are deletion suppressors of the cdc13-1 mutation [241]. Although it does not have a tyrosine phosphatase motif, Oca5 deletion also displayed gemcitabine-specific enhancement, consistent with the other genes annotated to this module (Figure 6C). However, due to the regulatory nature and limited evolutionary conservation of tyrosine phosphorylation, it is not obvious how to predict functionally homologous genetic modules in cancer cells.

5.5. Elongator Holoenzyme Complex and Protein Urmylation

By GTA, K interactions revealed protein urmylation (*NCS6*, *NCS2*, *UBA4*, *ELP6*, *ELP2*, *URM1*, and *URE2*) and the elongator holoenzyme complex (*IKI1, IKI3, ELP2, ELP3, ELP4,* and *ELP6*) (Additional File 2, Figure S4). Protein urmylation involves the covalent modification of lysine residues with the ubiquitin-related modifier, Urm1 [242]. The elongator holoenzyme complex has function in tRNA wobble position uridine thiolation (Additional File 2, Figure S4), which occurs using Ure1 as a sulfur carrier [243–245]. The two processes share the *ELP2* and *ELP6* genes and may be distinct modules buffering gemcitabine cytotoxicity. However, several genes involved in tRNA wobble uridine modification have roles in cancer development and deficiency in this pathway enhances targeted therapy in melanoma [246,247], implicating this module as potentially important for personalized anticancer efficacy of gemcitabine.

5.6. Gemcitabine-Buffering by Non-GO-Enriched Yeast-Human Homologs

Homologs with correlated gemcitabine-specific yeast gene deletion enhancement and cancer cell UES (clusters 2-0.2-1, 1-0-10, and 1-0-0) included the family of nucleoside diphosphate kinases (NDKs) (Figure 6D; Table 4). A single member of the NDK family, *YNK1*, exists in yeast, while the human genome encodes several paralogs (*NME* genes) (Additional File 8, File A). The NDKs transfer the γ phosphate of ATP to nucleoside diphosphate as the final step of purine and pyrimidine nucleoside and deoxynucleoside triphosphate biosynthesis and salvage [248,249]. Thus, NDK appears to modulate gemcitabine toxicity by differential activity for endogenous substrates vs. nucleoside analog drugs. In yeast, deletion enhancement by YNK1 was selective for gemcitabine, however the effects in cancer cells are potentially more complex due to multiple NDK genes. In PharmacoDB, *NME3* and *5* were UES for gemcitabine, while *NME4*, *6*, and *7* were OES for cytarabine, implicating differential specificity of *NME* genes for natural and/or medicinal nucleosides as well as possible influences of other kinases, which have, for example, been shown to act on gemcitabine diphosphate [250]. *NME5* overexpression was previously associated with gemcitabine-resistant cancer, and its knockdown can increase gemcitabine efficacy [182]. Thus, the anticancer efficacy of gemcitabine could be influenced by differential expression and activity of NDK isoforms across tissues [251], such that NME gene expression could be predictive of response to nucleoside analogs, or perhaps targeted for synergistic antitumor activity.

KEX2 is the yeast member of the calcium-dependent proprotein convertase subtilisin/kexin type serine proteases, which functions in the secretory pathway. Four of the seven human homologs of KEX2 were UES in the pharmacogenomics analysis (Figure 6D; 1-0-10), including: (1) *PCSK1*, which can be downregulated by pancreatic cancer derived exosomes [176], (2) *PCSK2*, which has reduced expression in lung cancer [177], (3) *PCSK5*, which is also reduced in lung cancer and, furthermore, when reduced in triple negative breast cancer, leads to loss of the Gdf11 tumor suppressor [177,178], and (4) *PCSK7*, which has been reported both to have reduced expression in lung cancer and increased expression

in gemcitabine-resistant cells [177,179]. Thus, loss of this gene family may create cancer-specific vulnerabilities to gemcitabine cytotoxicity.

NMA1 and its human homologs *NMNAT1, NMNAT2,* and *NMNAT3* are nicotinic acid mononucleotide adenylyltransferases involved in NAD biosynthesis and homeostasis, which were found to be UES for both gemcitabine and cytarabine (Figure 6D, 1-0-0). Loss of function mutations and underexpression of *NMNAT1* are associated with increased rRNA expression and sensitivity to DNA damage in lung cancer cell lines [166], consistent with the hypothesis that they could have deletion-enhancing therapeutic benefit in cancers treated with gemcitabine or cytarabine.

RAD54 is a DNA-dependent ATPase that stimulates strand exchange in recombinational DNA repair, which is a known vulnerability of cancer [252]. The human homolog of *RAD54, ATRX,* was UES by PharmacoDB analysis (Figure 6D, 1-0-0), and loss of *ATRX* has been associated with improved response to gemcitabine plus radiation therapy in glioma patients with *IDH1* mutations [168].

SCS2/VAPB is an integral ER membrane protein that was deletion-enhancing and UES for gemcitabine (Figure 6D, 1-0-0). *VAPB* regulates phospholipid metabolism and interacts with *ACBD5* (also described above) to promote ER-peroxisome tethering [100] and promotes proliferation in breast cancer via *AKT1* [169].

YPT32/RAB2A/RAB2B (Figure 6D, 1-0-0) is a Rab family GTPase involved in the trans-Golgi exocytic pathway, which accumulates during replication stress in yeast [155]. *RAB2A* overexpression promotes breast cancer stem cell expansion and tumorigenesis [174], and downregulation of *RAB2B* by miR-448 promotes cell cycle arrest and apoptosis in pancreatic cancer cells [175].

CLB5, a B-type cyclin, is involved in initiation of DNA replication and G1-S progression, for which promoter hypermethylation of the human homolog, *CCNA1*, is associated with multiple cancers [157], and which was found to be UES with gemcitabine (Figure 6D, 1-0-0).

5.7. Gemcitabine-Specific Gene Deletion Suppression

Representing this class of gene interaction, pharmacogenomics integration is highlighted for clusters 2-0.8-0 and 1-0-7 (Figure 6E). Although there was limited gene ontology enrichment, the term phosphatidylserine biosynthetic process (*UME6* and *CHO1*) and the GARP (*VPS51-54*) and Lem3p-Dnf1p complexes were identified (Figure 6F, Table 2). Ume6 is involved in both positive and negative regulation of the phosphatidylserine synthase, Cho1 [253,254]. Phosphatidylserine exposure to the plasma membrane is a marker of yeast and mammalian apoptosis [255], the latter of which is induced by gemcitabine [256]. In pancreatic cancer cells, addition of the sphingolipid, sphingomyelin, enhances gemcitabine cytotoxicity through increased apoptosis [256,257]. Moreover, GARP complex deficiency leads to reduction of sphingomyelin [258] and accumulation of sphingolipid intermediates, consistent with the hypothesis that reduced sphingolipid metabolism alleviates gemcitabine-mediated apoptosis. Lem3 complexes with Dnf1 or Dnf2 to form phospholipid flippases at the plasma and early endosome/trans-Golgi network membranes and regulate phosphatidylethanolamine and phosphatidylserine membrane content [259,260], potentially further influencing the apoptotic response. The Lem3-Dnf1 and Lem3-Dnf2 flippases are regulated by the serine/threonine kinase Fpk1 [261], which is also a gemcitabine-specific deletion suppressor (Figure 6F).

5.8. Correlation of Gemcitabine-Specific Gene Deletion Suppression with OES in Cancer Cells

Although yeast genes associated with GO-enriched terms from gemcitabine-specific deletion suppression (2-0.8-0 and 1-0-7) did not have human homologs that were OES in GDSC, several homologs of 'non-GO-enriched' genes were OES (Figure 6E; Table 4). These included: (1) *YGR054W/EIF2A*, a eukaryotic initiation factor orthologous between yeast and human that has been implicated in translation of upstream ORFs as part of tumor initiation [215]. Thus, gemcitabine treatment in the context of EIF2A overexpression may increase efficacy. (2) *EFT2/EEF2/EFTUD2* (eukaryotic translation elongation factor 2), which further implicates translational regulation as a gemcitabine-targetable cancer driver. *EEF2* is overexpressed in numerous cancer types [198] and *EFTUD2* knockdown induces

apoptosis in breast cancer cells [199]. (3) *RPP2B/RPLP2*, a component of the 60S ribosomal subunit stalk that is overexpressed in gynecologic cancer [214], again suggesting dysregulated translation promotes gemcitabine toxicity. (4) *RPA49/POLR1E*, a component of Pol1 [203–205] that has higher expression in bladder cancer and has been recently proposed as a novel target for anticancer therapy [206]. (5) *OLA1/OLA1* is a GTPase that is conserved from human to bacteria [200]. It is implicated in regulation of ribosomal translation [201] and has increased expression associated with poorer survival in lung cancer patients [202]. The interactions described above suggest gemcitabine may be more effective in the context of "oncogenic ribosomes" [262]. (6) *CKA2*, the α catalytic subunit of casein kinase 2, has two human homologs, *CSNK2A1* and CSNK2A2, which were OES with gemcitabine. They can be upregulated in cancer [186–191] and are considered targets for treatment [193]. (7) *CLB2/CCNA2/CCNB1*, a B-type cyclin involved in cell cycle progression, of which both *CCNA2* and *CCNB1* are overexpressed in breast and colorectal cancer [194–197]. Moreover, the observation that *CLB2* deletion (suppressing effect) opposes that of *CLB5* (deletion enhancing; see above Figure 6D, 1-0-0) has been previously described in the context of loss of the S-phase checkpoint [263]. (8) *SKY1/SRPK1* (serine–arginine-rich serine–threonine kinase), which is overexpressed in glioma and prostate, breast, and lung cancer [207]. (9) *SNC2/VAMP8*, which functions in fusion of Golgi-derived vesicles with the plasma membrane and is overexpressed in glioma and breast cancer [208,209]. (10) *YPT6/RAB34*, which functions in fusion of endosome-derived vesicles with the late Golgi and is overexpressed in glioma, breast cancer, and hepatocellular carcinoma [211–213]. (11) *TOP1/TOP1/TOP1MT*, Topoisomerase I, which has increased copy number in pancreatic and bile duct cancer [210]. (12) *ALD6*, which encodes cytosolic aldehyde dehydrogenase and was a deletion suppressor for both gemcitabine and cytarabine, having multiple homologs that were OES (*ALDH1A1*, *ALDH1A2*, *ALDH1B1*, and *ALDH7A1. ALDH1B1*). Overexpression of ALDH genes is observed in colorectal and pancreatic cancer [183,184] and is a prognostic marker of cancer stem cells [185].

6. Cytarabine-Specific Gene Interaction Modules

6.1. Cytarabine-Specific Gene Deletion Enhancement

Cytarabine-specific deletion enhancement suggests functions that buffer cytotoxic effects of cytarabine to a greater extent than gemcitabine, potentially informing on differential activities of the drugs. There was no notable GO enrichment by REMc/GTF, but four functions of potential relevance were revealed by GTA (Figure 7A, Table 2). Two of them, the HIR complex (*HIR1-3,* HPC2) and sphinganine kinase activity (*LCB4, LCB5*) were relatively weak, being deletion-enhancing only for the L CPP (Figure 7A). *LCB4/5* homologs that were UES in PharmacoDB included: (1) *CERKL* (Additional File 8, Files B–C; 1-0-6), a ceramide kinase-like gene that regulates autophagy by stabilizing *SIRT1* [264], a gene mentioned above for its inhibition being synergistic with cytarabine against acute lymphoblastic leukemia cells [138], and (2) *AGK*, which is overexpressed in hepatocellular carcinoma, glioma, breast, and cervical squamous cell cancers [265–268]. Two stronger interaction modules, evidenced by deletion enhancement for both the K and L CPPs, were protein localization to septin ring (*HSL1* and *ELM1*) and the *Sec61* translocon complex (*SBH1, SBH2,* and *SEC61*) (Figure 7A, Table 2). In yeast, Hsl1 and Elm1 are annotated as "bud sensors" to recruit Hsl7 to the septin ring at the bud site to degrade the mitotic inhibitor, Swe1 [269]. The *HSL1* homologs, *BRSK1* and *BRSK2*, were UES in the cancer data. *BRSK1* is mutated in gastric and colorectal carcinoma [270] and its decreased expression is associated with breast cancer [271], but *BRSK2* is overexpressed in pancreatic cancer, where it is AKT-activating [272]. PharmacoDB also identified the *SEC61* homolog, *SEC61A1*, which is upregulated in colon adenocarcinoma tissue [273].

Table 5. Yeast–human homologs predicted to buffer cytarabine to greater degree than gemcitabine.

yGene	hGene	H	Drug	Cluster	Tissue	Gem_K	Cyt_K	Gem_L	Cyt_L	Ref	Description_Human
CCH1	CACNA1A	2	Cyt	1-0-9	A, L	0.2	−4.5	0.5	5.5	[274]	calcium voltage-gated channel subunit alpha1 A
CCH1	CACNA1B	2	Cyt	1-0-9	A, L	0.2	−4.5	0.5	5.5	[274]	calcium voltage-gated channel subunit alpha1 B
CCH1	CACNA1C	2	Cyt	1-0-9	A, H, L	0.2	−4.5	0.5	5.5	[274]	calcium voltage-gated channel subunit alpha1 C
CCH1	CACNA1E	2	Cyt	1-0-9	A, L	0.2	−4.5	0.5	5.5	[274]	calcium voltage-gated channel subunit alpha1 E
CCH1	CACNA1F	2	Cyt	1-0-9	A	0.2	−4.5	0.5	5.5	[274]	calcium voltage-gated channel subunit alpha1 F
CCH1	NALCN	2	Cyt	1-0-9	H	0.2	−4.5	0.5	5.5		sodium leak channel, non-selective
FAT1	SLC27A2	2	Cyt	1-0-9	L	0.7	−8.5	−0.9	8.9	[275]	solute carrier family 27 member 2
FAT1	SLC27A3	2	Cyt	1-0-9	L	0.7	−8.5	−0.9	8.9	[276]	solute carrier family 27 member 3
FOL2	GCH1	1	Cyt	1-0-9	L	−0.9	−9.4	0.7	7.1	[277]	GTP cyclohydrolase 1
HSL1	BRSK1	3	Cyt	1-0-9	A, L	0.9	−10.4	0.1	11.6	[270,271]	BR serine/threonine kinase 1
HSL1	BRSK2	3	Cyt	1-0-9	A, L	0.9	−10.4	0.1	11.6	[272]	BR serine/threonine kinase 2
IZH1	ADIPOR1	3	Cyt	1-0-9	H	1.1	−5.8	−0.4	7.6	[278,279]	adiponectin receptor 1
IZH1	PAQR4	3	Cyt	1-0-9	A, L	1.1	−5.8	−0.4	7.6		progestin and adipoQ receptor family member 4
NAP1	NAP1L3	2	Cyt	1-0-9	A, L	1.0	−4.7	−1.5	5.6	[280]	nucleosome assembly protein 1 like 3
NAP1	NAP1L4	2	Cyt	1-0-9	L	1.0	−4.7	−1.5	5.6		nucleosome assembly protein 1 like 4
PTM1	TMEM87B	3	Cyt	1-0-9	A, H	−0.7	−3.8	−0.2	5.7	[281]	transmembrane protein 87B

The data descriptions are the same as for Table 3.

6.2. Human Genes that have Deletion Enhancing Yeast Homologs and Confer Cytarabine UES

We identified human genes that were UES to cytarabine and homologous to yeast genes in REMc clusters (1-0-9 and 2-0.13-0) displaying a pattern of cytarabine-specific deletion enhancement (Figure 7B; Table 5). Cancer-relevant examples include:

(1) Ptm1, which is a protein of unknown function that copurifies with late Golgi vesicles containing the v-SNARE, Tlg2p, but interestingly, its human homologs, *TMEM87A* and *TMEM87B*, were UES for cytarabine and identified in a study focused on cytarabine efficacy in acute myelogenous leukemia [281].

(2) *NAP1/NAP1L3/NAP1L4*, which is a nucleosome assembly protein involved in nuclear transport and exchange of histones H2A and H2B and also interacts with Clb2, is phosphorylated by CK2, and has protein abundance that increases in response to DNA replication stress [155]. *NAP1L3* is overexpressed in breast cancer [280].

(3) *CCH1*, which is a voltage-gated high-affinity calcium channel with several homologs that were UES, including: *CACNA1A*, underexpressed in breast, colorectal, esophageal, gastric, and brain cancers; *CACNA1B*, underexpressed in breast and brain cancers; *CACNA1C*, underexpressed in brain, bladder, lung, lymphoma, prostate, and renal cancers; *CACNA1E*, underexpressed in breast, brain, gastric, leukemia, lung, and prostate cancers; and *CACNA1F*, underexpressed in lymphoma [274].

(4) *IZH1*, a yeast membrane protein involved in zinc ion homeostasis, having a human homolog, *PAQR1/ADIPOR1* that encodes the adiponectin receptor protein 1, which is differentially regulated in breast cancers [278,279].

(5) *FAT1*, a yeast fatty acid transporter and very long-chain fatty acyl-CoA synthetase that corresponds to *SLC27A2* (very long-chain acyl Co-A synthetase), which is underexpressed in lung cancer [275], and *SLC27A3* (long-chain fatty acid transport), which is hypermethylated in melanoma [276].

(6) *FOL2/GCH1*, a GTP-cyclohydrolase that catalyzes the first step in folic acid biosynthesis. Downregulation of *GCH1* occurs in esophageal squamous cell carcinoma [277].

7. Discussion

Informative phenomic models have been developed for multiple human diseases, including cystic fibrosis, neurodegenerative disorders, and cancer [9,282–284]. Molecular models include mutations in conserved residues of yeast homologs of a disease gene and introduction of human alleles into yeast. Complementation of gene functions by human homologs, and vice versa, has demonstrated evolutionary conservation of gene functions [285–287]. Like their basic functions, gene interactions are conserved [288,289] and yeast is unique in its capability to address complex genetic interactions experimentally [290]. Here, we model how yeast phenomic assessment of gene–drug interaction could be employed as part of a precision oncology paradigm to predict efficacy of cytotoxic chemotherapy based on the unique cancer genetic profiles of individual patients.

To model the networks that buffer deoxyribonucleoside analogs, we humanized yeast by introducing deoxycytidine kinase into the YKO/KD strain collection, as yeast do not encode dCK in their genomes, and thus cannot activate the unphosphorylated drugs. We hypothesized that gemcitabine and cytarabine would have different buffering profiles, despite their similar mechanisms of action, due to their distinct anticancer efficacies. Results of the unbiased yeast phenomic experiments confirmed this expectation, revealing distinct, though partially overlapping, gene interaction networks. Differential interaction predominated despite the similarity of the molecules, illustrating that distinct mechanisms for buffering anticancer cytotoxic drug responses can be inferred from yeast phenomics and thus applied to predict how an individual's cancer genome could influence responses to treatment [3,5].

Deletion enhancement of both gemcitabine and cytarabine suggested processes that function to buffer nucleoside analog cytotoxicity in common (Figure 5), in contrast to buffering mechanisms that acted differentially in response to the drugs. Functionally enriched processes that buffered

both drugs to a similar extent included the intra-S DNA damage checkpoint; positive regulation of DNA-dependent DNA replication initiation; vesicle fusion with vacuole; and the Mre11, checkpoint clamp, RecQ helicase-Topo III, CORVET, HOPS, ESCRT, GET, Ubp3-Bre5 deubiquitination complexes.

Among the drug-specific deletion enhancing interactions, autophagy, histone modification, chromatin remodeling, and peptidyl-tyrosine dephosphorylation buffered gemcitabine more so than cytarabine (Figure 6). There were only a few cytarabine-specific deletion enhancing GO-enriched terms, but there were many individual genes with human homologs having cancer relevance that buffered cytarabine relatively specifically (Figure 7). On the other hand, genes that preferentially promote cytotoxicity were observed primarily for gemcitabine, and enriched functions were related to apoptosis, including phosphatidylserine biosynthesis, and the GARP and Lem2/3 complexes (Figure 6).

The model we constructed incorporates the powerful pharmacogenomics datasets and analysis tools from PharmacoDB, mining them by integration of yeast phenomic drug–gene interaction experiments. We integrated yeast phenomic and PharmacoDB data to identify, across the respective datasets, correlations between deletion enhancement and underexpression sensitivity or deletion suppression and overexpression sensitivity. Deletion enhancement indicates genes that are biomarkers and synergistic targets to augment drug efficacy and expand the therapeutic window, whereas deletion suppression identifies genes that promote drug cytotoxicity, and thus confer sensitivity when hyper-functional and resistance when deficient. A particularly attractive class of drug–gene interaction is overexpression sensitivity involving driver genes, however, anticancer efficacy could also be conferred by lethal drug–gene interactions involving passenger genes, tumor suppressor genes, or components of genetic buffering networks that become altered due to genomic instability (Figure 1A). The cancer literature revealed many deletion enhancing/UES and deletion suppressing/OES genes to have roles in cancer, suggesting that integration of yeast phenomic models and pharmacogenomics data could have clinical utility for choosing cytotoxic treatments based on gene expression profiles of individual cancers. While predictions sometimes involved GO-enriched processes, often the genes were identified individually. Assessment of conserved buffering genes (number of yeast deletion enhancers with human homologs exhibiting underexpression sensitivity) was estimated to be around 50% (Additional File 8, File A—see 'Conservation_buffering_homologs').

We focused discussion of conserved homologs with cancer relevance based on the integration of yeast and human data, the extent of homology, the annotated functions, and the existing cancer literature. We note that although genes specifically buffering cytarabine were less well annotated and less conserved overall, they were equally relevant in the model, with about half of all buffering gene interactions in yeast evidenced in the PharmacoDB functional genomic data (Additional File 8, File A.—'Conservation_buffering_homologs' worksheet). Thus, the supplemental materials serve as a resource for future analyses of genes that remain to be annotated (Additional File 8, Files A–D).

As shown by Birrell et al., differential gene expression is a poor predictor of which genes are required for response to a drug [52]. Thus, yeast phenomic models (i.e., Q-HTCP of the YKO/KD library) may help clarify the milieu of potentially causal associations between differential gene expression and drug sensitivity observed in cancer cells by individually testing in yeast the influences on cell proliferation of evolutionarily related protein products. As far as we know, this work represents the first application of this fundamental observation from yeast to systems level experimental data from human cells. Literature-based validations of the yeast phenomic model of nucleoside analogs in human cancer cell lines and other cancer models are exemplified in Table 6. These examples illustrate that integrative, systems level drug–gene interaction modeling employing the experimental power of *S. cerevisiae* phenomics could be applicable to cancer genomic profiling for systems level, precision oncology.

Table 6. Disease relevance of buffering interactions from the yeast phenomic model evidenced by the cancer biology literature.

Gene (Yeast/Human)	Process/Complex	Description (Human)	Ref	Nucleoside Analog Relevance
RAD24/RAD17	DNA damage checkpoint	RAD17 checkpoint clamp loader component	[79]	Depletion of RAD17 sensitizes pancreatic cancer cells to gemcitabine
RAD50/RAD50	Mre11 complex	RAD50 double strand break repair protein	[127]	Depletion of human Rad50 sensitizes Ataxia-telangiectasia (AT) fibroblasts to gemcitabine
HDA1/HDAC6	Hda1 complex; histone deacetylation	histone deacetylase 6	[160,165]	HDAC inhibitors enhance sensitivity to gemcitabine in pancreatic cancer cells and are associated with reduction of HDAC6; HDAC6 inhibition induces apoptosis in cytarabine treated AML cells
RAD54/ATRX	Chromatin remodeling	ATRX, chromatin remodeler	[168]	Glioma patients with IDH1 mutations and loss of ATRX had improved response to gemcitabine plus radiation therapy
KEX2/PCSK7	serine-type endopeptidase activity	proprotein convertase subtilisin/kexin type 7	[179]	Overexpressed in gemcitabine resistant pancreatic cancer cell lines
YNK1/NME5	Nucleoside diphosphate phosphorylation	NME/NM23 family member 5	[182]	Depletion of NME5 sensitizes gemcitabine-resistant cancer cell lines to gemcitabine
VPS30/BECN1	Autophagy	beclin 1	[170]	Depletion of *BECN1* sensitizes pancreatic cancer stem cells to gemcitabine
LCB4/5/CERKL	sphinganine kinase activity	ceramide kinase like	[138,264]	CERKL stabilizes SIRT1, SIRT1 chemical inhibition sensitizes acute myeloid leukemia cells to cytarabine

Deletion-enhancing/UES drug–gene interactions are highlighted; most exemplify loss of buffering functions that lead to increased drug sensitivity; however, there is one instance (KEX2/PCSK7) of overexpression of the buffering gene that increases drug resistance.

In summary, the yeast phenomic model of nucleoside analog toxicity appears to serve as a valuable resource for interpreting cancer pharmacogenomics data regarding gene–drug interaction that could be predictive of patient-specific chemotherapeutic efficacy. Since it's not possible to collect comparable phenomic information from human populations or cancerous tissue alone [5], systems-level yeast phenomic models can help expand and integrate relevant (i.e., evolutionarily conserved) aspects of the extensive cancer literature with regard to cancer-specific vulnerabilities to cytotoxic therapies. A deeper understanding of how genomic instability influences the genetic network that buffers chemotherapeutic agents like nucleoside analogs could guide future research to personalize anticancer therapies based on cancer genomic profiles unique to individual patients. Thus, a future direction for this work should include development of algorithms that prospectively predict chemotherapy response in individual patient cancer cells, which could be tested as part of a prognostic evaluation. In this initial study, we focused on expression data from PharmacoDB, rather than mutation data, because differential gene expression in cancer cells is more analogous to the quantitative changes in gene expression resulting from gene KO/KD than qualitative or indeterminate effects resulting from point mutations, for example. However, an interesting future direction could be to analyze mutation data in conjunction with gene expression and yeast phenomic data, for example to identify eQTLs associated with UES or OES genes [291]. With regard to the number of interactions observed in the yeast model, we note this depends on the inclusiveness of homology. *S. cerevisiae*, as a single cell organism and evolutionarily distant relative of humans, is informative about gene interactions across many different human cell types. Thus, yeast genetic interactions are merely hypothesis-generating and require appropriate future testing of human homologs and in human cell types. While yeast phenomic models of human disease are powerful engines of discovery, findings can only be truly prioritized and focused at this time in models more directly relevant to the human conditions of interest.

8. Conclusions

A humanized yeast phenomic model of deoxycytidine kinase was developed to map drug–gene interactions modulating antiproliferative effects of nucleoside analogs in a eukaryotic cell and to investigate the relevance of the resulting networks for precision oncology by integration with cancer pharmacogenomics-derived associations between gene expression and cancer cell line drug sensitivity. The yeast phenomic model revealed gene–drug interaction for the two deoxycytidine analogs, gemcitabine and cytarabine, to be largely different, consistent with the distinct types of cancer for which they are used clinically. The model overall suggested evolutionary conservation of drug–gene interaction that could be used as a resource to predict anticancer therapeutic efficacy based on genetic information specific to individual patients' tumors. Yeast phenomics affords a scalable, high-resolution approach to model, at a systems level, the genetic requirements for sensitivity and resistance to cytotoxic agents and, thus, the potential to resolve complex influences of genetic variation on drug response more accurately. Global and quantitative models of the distinct genetic buffering networks required to maintain cellular homeostasis after exposure to chemotherapeutic agents could aid precision oncology paradigms aimed at identifying composite genomic derangements that create enhanced cancer cell-specific vulnerabilities to particular anticancer drugs. Further in this regard, cytotoxic chemotherapeutic agents are used in combination, so another direction for yeast phenomic analysis of anticancer agents would be to characterize clinically relevant drug combinations.

Supplementary Materials: The following are available online at http://www.mdpi.com/2073-4425/10/10/770/s1, Additional File 1: Supplemental tables: Tables S1–S6. Table S1: Primers used in construction of the synthetic genetic array (SGA) 'query' strain (MIY16) for doxycycline-inducible deoxycytidine kinase expression (see Figure S1), Table S2: Drug–gene interaction data from genome-wide experiments for gemcitabine YKO/KD strains, Table S3: Drug–gene interaction data from genome-wide experiments for gemcitabine reference strains, Table S4: Drug–gene interaction data from genome-wide experiments for cytarabine YKO/KD strains. Table S5: Drug–gene interaction data from genome-wide experiments for cytarabine reference strains, Table S6: Summary statistics of interaction z-scores for the YKO/YKD and reference cultures from the phenomic analyses of gemcitabine and cytarabine drug–gene interaction, including the ranges, averages, standard deviations, and representative interaction z-scores in the tails of the distributions. Additional File 2: Supplemental figures. Figure S1: Construction of tet-inducible dCK allele, Figure S2: Reference strain distributions for rate (r) and area under curve (AUC) with gemcitabine or cytarabine treatment, Figure S3: Gene deletion suppression modules exhibiting high shift or variable interaction, Figure S4: Elongator holoenzyme complex, protein urmylation, and tRNA wobble position uridine thiolation gene modules exhibit variable shift and deletion enhancing interaction profiles. Additional File 3: Gene–gemcitabine interaction plots for (A) YKO, (B) KD, and (C) reference strains. Additional File 4: Gene–cytarabine interaction plots for (A) YKO, (B) KD, and (C) reference strains. The first two pages in Additional Files 3 and 4 display the reference distributions used to calculate gene–drug interactions. Summary data comparing them are in Additional File 1, Table S6. Additional File 5: REMc results: File A is a table providing REMc results and associated gene interaction and shift data. File B is the heatmap representation of each REMc cluster after incorporating shift values and hierarchical clustering. Gene label colors for YKO and YKD are black and red, respectively. File C contains tables of GTF results from the process, function, and component ontologies for each REMc cluster. Additional File 6. Gene ontology term averaging (GTA) results and interactive plots. File A contains all GTA values, cross-referenced with REMc-enriched terms. Files B and C display GTA values associated with above-threshold GTA scores plotted for gemcitabine vs. cytarabine for L and K, respectively. They should be opened in an Internet web browser so that embedded information from Additional File 6A can be viewed by scrolling over points on the graphs. Subsets in each of the plots can be toggled off and on by clicking on the respective legend label. In the embedded information, X1 represents gemcitabine and X2 represents cytarabine information. Additional File 7: GO term-specific heatmaps for REMc/GTF-enriched modules, generated as described in methods and Figure 3. Child terms are presented in subsequent pages of the parent file name. GO terms having more than 100 children, with two or fewer genes annotated to the term, or a file size over 400 KB are not represented. All heatmaps are generated with the same layout (see Figure 3). Additional File 8: Integration of yeast phenomic drug–gene interaction data with cancer cell line pharmacogenomic data (gene expression and drug sensitivity correlations) to predict differential gene expression in cancer cells that is causally associated with enhanced gemcitabine or cytarabine cytotoxicity. File A contains three tables of all UES and OES human genes from the GDSC (gemcitabine and cytarabine) and gCSI (gemcitabine only) databases, also indicating whether deletion-enhancing or deletion-suppressing gene–drug interactions from phenomic analysis of yeast homologs predicted causal associations. Homology relationships and other associated data are coassembled. Files B–D consist of heatmaps and corresponding tables of yeast drug–gene interaction sets that predict causality for UES or OES human genes identified (File B) across all tissue, (File C) in lung, or (File D) in hematopoietic and lymphoid tissue. See Figure 3 for explanation of colors for gene labels and homology type. Note: the teal color, which represents cytarabine-specific UES/OES in the heatmaps in the main manuscript figures corresponds to darker blue in the supplemental heatmaps, while gold, representing

gemcitabine-specific UES/OES in the main manuscript corresponds to bright yellow. Black corresponds to UES or OES for both drugs).

List of Abbreviations and Glossary of Terms

AraC—cytarabine; cytosine arabinoside. CPPs—cell proliferation parameters: parameters of the logistic growth equation used to fit cell proliferation data obtained by Q-HTCP. The CPPs used to assess gene interaction in this study were K (carrying capacity) and L (time required to reach half of carrying capacity) [7–9,37]. DAmP—decreased abundance of mRNA. Production: refers to a method of making YKD alleles, where the 3′ UTR of essential genes is disrupted, reducing mRNA stability and gene dosage [292]. dCK—deoxycytidine kinase. dCMP—deoxycytidine monophosphate. DE—deletion enhancer: gene loss of function (knockout or knockdown) that results in enhancement/increase of drug sensitivity [9]. dFdC—2′,2′-difluoro 2′-deoxycytidine, gemcitabine. dNTP—deoxyribonucleotide triphosphate. DS—deletion suppressor: gene loss of function (knockout or knockdown) that results in suppression / reduction of drug sensitivity [9]. ESCRT—endosomal sorting complex required for transport. GARP complex—Golgi-associated retrograde protein complex. gCSI—the Genentech cell line screening initiative: one of two pharmacogenomics datasets used in this study (https://pharmacodb.pmgenomics.ca/datasets/4). GDSC1000–Genomics of Drug Sensitivity in Cancer: One of two pharmacogenomics datasets used in this study (https://pharmacodb.pmgenomics.ca/datasets/5). GO—gene ontology. GTF—gene ontology term finder: an algorithm to assess GO term enrichment amongst a list of genes; applied to REMc (clustering) results [41]. GTA—gene ontology term averaging: an assessment of GO term function obtained by averaging the gene interaction values for all genes of a GO term. GTA value—gene ontology term average value. gtaSD—standard deviation of GTA value. GTA score—(GTA value – gtaSD). HaL—hematopoietic and lymphoid tissue. HDAC—histone deacetylase complex. HLD—human-like media with dextrose [8]: the yeast media used in this study. INT—interaction score. NDK—nucleoside diphosphate kinase. OES—overexpression sensitivity: refers to association of increased gene expression with drug sensitivity in pharmacogenomics data [32]. PharmacoDB—the resource used for cancer pharmacogenomics analysis [32]. PPOD—Princeton protein orthology database. Q-HTCP—quantitative high-throughput cell array phenotyping: a method of imaging, image analysis, and growth curve fitting to obtain cell proliferation parameters [7,37]. Ref—reference: the genetic background from which the YKO/KD library was derived. REMc—recursive expectation maximization clustering: a probabilistic clustering algorithm that determines a discrete number of clusters from a data matrix [40]. RNR—ribonucleotide reductase. SD—standard deviation. SGA—synthetic genetic array. SGD—saccharomyces genome database. UES—underexpression sensitivity: refers to association of reduced gene expression with drug sensitivity in pharmacogenomics data [32]. YKO—yeast knockout. YKD—yeast knockdown: DAmP alleles. YKO/KD—yeast knockout or knockdown.

References

1. Torti, D.; Trusolino, L. Oncogene addiction as a foundational rationale for targeted anticancer therapy: Promises and perils. *EMBO Mol. Med.* **2011**, *3*, 623–636. [CrossRef] [PubMed]

2. Masui, K.; Gini, B.; Wykosky, J.; Zanca, C.; Mischel, P.S.; Furnari, F.B.; Cavenee, W.K. A tale of two approaches: Complementary mechanisms of cytotoxic and targeted therapy resistance may inform next-generation cancer treatments. *Carcinogenesis* **2013**, *34*, 725–738. [CrossRef]

3. Hartwell, L.H.; Szankasi, P.; Roberts, C.J.; Murray, A.W.; Friend, S.H. Integrating genetic approaches into the discovery of anticancer drugs. *Science* **1997**, *278*, 1064–1068. [CrossRef] [PubMed]

4. Srivas, R.; Shen, J.P.; Yang, C.C.; Sun, S.M.; Li, J.; Gross, A.M.; Jensen, J.; Licon, K.; Bojorquez-Gomez, A.; Klepper, K.; et al. A Network of Conserved Synthetic Lethal Interactions for Exploration of Precision Cancer Therapy. *Mol. Cell* **2016**, *63*, 514–525. [CrossRef] [PubMed]

5. Hartman, J.L., IV; Garvik, B.; Hartwell, L. Principles for the buffering of genetic variation. *Science* **2001**, *291*, 1001–1004. [CrossRef] [PubMed]

6. Hartman, J.L., IV; Tippery, N.P. Systematic quantification of gene interactions by phenotypic array analysis. *Genome Biol.* **2004**, *5*, R49. [CrossRef]

7. Shah, N.A.; Laws, R.J.; Wardman, B.; Zhao, L.P.; Hartman, J.L., IV. Accurate, precise modeling of cell proliferation kinetics from time-lapse imaging and automated image analysis of agar yeast culture arrays. *BMC Syst. Biol.* **2007**, *1*, 3. [CrossRef] [PubMed]

8. Hartman, J.L., IV; Stisher, C.; Outlaw, D.A.; Guo, J.; Shah, N.A.; Tian, D.; Santos, S.M.; Rodgers, J.W.; White, R.A. Yeast Phenomics: An Experimental Approach for Modeling Gene Interaction Networks that Buffer Disease. *Genes* **2015**, *6*, 24–45. [CrossRef]

9. Louie, R.J.; Guo, J.; Rodgers, J.W.; White, R.; Shah, N.; Pagant, S.; Kim, P.; Livstone, M.; Dolinski, K.; McKinney, B.A.; et al. A yeast phenomic model for the gene interaction network modulating CFTR-*ΔF*508 protein biogenesis. *Genome Med.* **2012**, *4*, 103. [CrossRef] [PubMed]

10. Galmarini, C.M.; Mackey, J.R.; Dumontet, C. Nucleoside analogues and nucleobases in cancer treatment. *Lancet Oncol.* **2002**, *3*, 415–424. [CrossRef]

11. Parker, W.B. Enzymology of purine and pyrimidine antimetabolites used in the treatment of cancer. *Chem. Rev.* **2009**, *109*, 2880–2893. [CrossRef] [PubMed]

12. de Sousa Cavalcante, L.; Monteiro, G. Gemcitabine: Metabolism and molecular mechanisms of action, sensitivity and chemoresistance in pancreatic cancer. *Eur. J. Pharmacol.* **2014**, *741*, 8–16. [CrossRef] [PubMed]

13. Hayashi, H.; Kurata, T.; Nakagawa, K. Gemcitabine: Efficacy in the treatment of advanced stage nonsquamous non-small cell lung cancer. *Clin. Med. Insights Oncol.* **2011**, *5*, 177–184. [CrossRef] [PubMed]

14. Raja, F.A.; Counsell, N.; Colombo, N.; Pfisterer, J.; du Bois, A.; Parmar, M.K.; Vergote, I.B.; Gonzalez-Martin, A.; Alberts, D.S.; Plante, M.; et al. Platinum versus platinum-combination chemotherapy in platinum-sensitive recurrent ovarian cancer: A meta-analysis using individual patient data. *Ann. Oncol.* **2013**, *24*, 3028–3034. [CrossRef] [PubMed]

15. Alli, E.; Sharma, V.B.; Hartman, A.R.; Lin, P.S.; McPherson, L.; Ford, J.M. Enhanced sensitivity to cisplatin and gemcitabine in Brca1-deficient murine mammary epithelial cells. *BMC Pharmacol.* **2011**, *11*, 7. [CrossRef]

16. Reese, N.D.; Schiller, G.J. High-dose cytarabine (HD araC) in the treatment of leukemias: A review. *Curr. Hematol. Malig. Rep.* **2013**, *8*, 141–148. [CrossRef] [PubMed]

17. Giovannetti, E.; Del Tacca, M.; Mey, V.; Funel, N.; Nannizzi, S.; Ricci, S.; Orlandini, C.; Boggi, U.; Campani, D.; Del Chiaro, M.; et al. Transcription analysis of human equilibrative nucleoside transporter-1 predicts survival in pancreas cancer patients treated with gemcitabine. *Cancer Res.* **2006**, *66*, 3928–3935. [CrossRef]

18. Skrypek, N.; Duchene, B.; Hebbar, M.; Leteurtre, E.; van Seuningen, I.; Jonckheere, N. The MUC4 mucin mediates gemcitabine resistance of human pancreatic cancer cells via the Concentrative Nucleoside Transporter family. *Oncogene* **2013**, *32*, 1714–1723. [CrossRef]

19. Song, J.H.; Kim, S.H.; Kweon, S.H.; Lee, T.H.; Kim, H.J.; Kim, H.J.; Kim, T.S. Defective expression of deoxycytidine kinase in cytarabine-resistant acute myeloid leukemia cells. *Int. J. Oncol.* **2009**, *34*, 1165–1171.

20. Duxbury, M.S.; Ito, H.; Zinner, M.J.; Ashley, S.W.; Whang, E.E. RNA interference targeting the M2 subunit of ribonucleotide reductase enhances pancreatic adenocarcinoma chemosensitivity to gemcitabine. *Oncogene* **2004**, *23*, 1539–1548. [CrossRef]

21. Davidson, J.D.; Ma, L.; Flagella, M.; Geeganage, S.; Gelbert, L.M.; Slapak, C.A. An increase in the expression of ribonucleotide reductase large subunit 1 is associated with gemcitabine resistance in non-small cell lung cancer cell lines. *Cancer Res.* **2004**, *64*, 3761–3766. [CrossRef] [PubMed]

22. Li, L.; Fridley, B.L.; Kalari, K.; Jenkins, G.; Batzler, A.; Weinshilboum, R.M.; Wang, L. Gemcitabine and arabinosylcytosin pharmacogenomics: Genome-wide association and drug response biomarkers. *PLoS ONE* **2009**, *4*, e7765. [CrossRef] [PubMed]

23. Innocenti, F.; Owzar, K.; Cox, N.L.; Evans, P.; Kubo, M.; Zembutsu, H.; Jiang, C.; Hollis, D.; Mushiroda, T.; Li, L.; et al. A genome-wide association study of overall survival in pancreatic cancer patients treated with gemcitabine in CALGB 80303. *Clin. Cancer Res.* **2012**, *18*, 577–584. [CrossRef] [PubMed]

24. You, L.; Chang, D.; Du, H.Z.; Zhao, Y.P. Genome-wide screen identifies PVT1 as a regulator of Gemcitabine sensitivity in human pancreatic cancer cells. *Biochem. Biophys. Res. Commun.* **2011**, *407*, 1–6. [CrossRef]

25. Bargal, S.A.; Rafiee, R.; Crews, K.R.; Wu, H.; Cao, X.; Rubnitz, J.E.; Ribeiro, R.C.; Downing, J.R.; Pounds, S.B.; Lamba, J.K. Genome-wide association analysis identifies SNPs predictive of in vitro leukemic cell sensitivity to cytarabine in pediatric AML. *Oncotarget* **2018**, *9*, 34859–34875. [CrossRef] [PubMed]

26. Gamazon, E.R.; Lamba, J.K.; Pounds, S.; Stark, A.L.; Wheeler, H.E.; Cao, X.; Im, H.K.; Mitra, A.K.; Rubnitz, J.E.; Ribeiro, R.C.; et al. Comprehensive genetic analysis of cytarabine sensitivity in a cell-based model identifies polymorphisms associated with outcome in AML patients. *Blood* **2013**, *121*, 4366–4376. [CrossRef]

27. Giaever, G.; Chu, A.M.; Ni, L.; Connelly, C.; Riles, L.; Veronneau, S.; Dow, S.; Lucau-Danila, A.; Anderson, K.; Andre, B.; et al. Functional profiling of the Saccharomyces cerevisiae genome. *Nature* **2002**, *418*, 387–391. [CrossRef]

28. Tong, A.H.; Boone, C. Synthetic genetic array analysis in Saccharomyces cerevisiae. *Methods Mol. Biol.* **2006**, *313*, 171–192.

29. Singh, I.; Pass, R.; Togay, S.O.; Rodgers, J.W.; Hartman, J.L., IV. Stringent Mating-Type-Regulated Auxotrophy Increases the Accuracy of Systematic Genetic Interaction Screens with Saccharomyces cerevisiae Mutant Arrays. *Genetics* **2009**, *181*, 289–300. [CrossRef]

30. Yang, W.; Soares, J.; Greninger, P.; Edelman, E.J.; Lightfoot, H.; Forbes, S.; Bindal, N.; Beare, D.; Smith, J.A.; Thompson, I.R.; et al. Genomics of Drug Sensitivity in Cancer (GDSC): A resource for therapeutic biomarker discovery in cancer cells. *Nucleic Acids Res.* **2013**, *41*, D955–D961. [CrossRef]

31. Klijn, C.; Durinck, S.; Stawiski, E.W.; Haverty, P.M.; Jiang, Z.; Liu, H.; Degenhardt, J.; Mayba, O.; Gnad, F.; Liu, J.; et al. A comprehensive transcriptional portrait of human cancer cell lines. *Nat. Biotechnol.* **2015**, *33*, 306–312. [CrossRef] [PubMed]

32. Smirnov, P.; Kofia, V.; Maru, A.; Freeman, M.; Ho, C.; El-Hachem, N.; Adam, G.A.; Ba-Alawi, W.; Safikhani, Z.; Haibe-Kains, B. PharmacoDB: An integrative database for mining in vitro anticancer drug screening studies. *Nucleic Acids Res.* **2018**, *46*, D994–D1002. [CrossRef] [PubMed]

33. Hartman, J.L., IV. Buffering of deoxyribonucleotide pool homeostasis by threonine metabolism. *Proc. Natl. Acad. Sci. USA* **2007**, *104*, 11700–11705. [CrossRef] [PubMed]

34. Belli, G.; Gari, E.; Piedrafita, L.; Aldea, M.; Herrero, E. An activator/repressor dual system allows tight tetracycline-regulated gene expression in budding yeast. *Nucleic Acids Res.* **1998**, *26*, 942–947. [CrossRef] [PubMed]

35. William, D. *Charakterisierung der C Terminalen Domäne von Mycobacterium Tuberculosis Protein A*; Friedrich-Alexander-Universität Erlangen-Nürnberg: Erlangen, Germany, 2012.

36. Goldstein, A.L.; McCusker, J.H. Three new dominant drug resistance cassettes for gene disruption in Saccharomyces cerevisiae. *Yeast* **1999**, *15*, 1541–1553. [CrossRef]

37. Rodgers, J.; Guo, J.; Hartman, J.L., IV. Phenomic assessment of genetic buffering by kinetic analysis of cell arrays. *Methods Mol. Biol.* **2014**, *1205*, 187–208. [CrossRef] [PubMed]

38. Mani, R.; St Onge, R.P.; Hartman, J.L., IV; Giaever, G.; Roth, F.P. Defining genetic interaction. *Proc. Natl. Acad. Sci. USA* **2008**, *105*, 3461–3466. [CrossRef] [PubMed]

39. Santos, S.M.; Hartman, J.L., IV. A yeast phenomic model for the influence of Warburg metabolism on genetic buffering of doxorubicin. *bioRxiv* **2019**, 517490. [CrossRef]

40. Guo, J.; Tian, D.; McKinney, B.A.; Hartman, J.L., IV. Recursive expectation-maximization clustering: A method for identifying buffering mechanisms composed of phenomic modules. *Chaos* **2010**, *20*, 026103. [CrossRef]

41. Boyle, E.I.; Weng, S.; Gollub, J.; Jin, H.; Botstein, D.; Cherry, J.M.; Sherlock, G. GO::TermFinder—Open source software for accessing Gene Ontology information and finding significantly enriched Gene Ontology terms associated with a list of genes. *Bioinformatics* **2004**, *20*, 3710–3715. [CrossRef] [PubMed]

42. Cherry, J.M.; Hong, E.L.; Amundsen, C.; Balakrishnan, R.; Binkley, G.; Chan, E.T.; Christie, K.R.; Costanzo, M.C.; Dwight, S.S.; Engel, S.R.; et al. Saccharomyces Genome Database: The genomics resource of budding yeast. *Nucleic Acids Res.* **2012**, *40*, D700–D705. [CrossRef] [PubMed]

43. Smirnov, P.; Safikhani, Z.; El-Hachem, N.; Wang, D.; She, A.; Olsen, C.; Freeman, M.; Selby, H.; Gendoo, D.M.; Grossmann, P.; et al. PharmacoGx: An R package for analysis of large pharmacogenomic datasets. *Bioinformatics* **2016**, *32*, 1244–1246. [CrossRef] [PubMed]

44. Durinck, S.; Moreau, Y.; Kasprzyk, A.; Davis, S.; De Moor, B.; Brazma, A.; Huber, W. BioMart and Bioconductor: A powerful link between biological databases and microarray data analysis. *Bioinformatics* **2005**, *21*, 3439–3440. [CrossRef] [PubMed]

45. Durinck, S.; Spellman, P.T.; Birney, E.; Huber, W. Mapping identifiers for the integration of genomic datasets with the R/Bioconductor package biomaRt. *Nat. Protoc.* **2009**, *4*, 1184–1191. [CrossRef] [PubMed]

46. Zerbino, D.R.; Achuthan, P.; Akanni, W.; Amode, M.R.; Barrell, D.; Bhai, J.; Billis, K.; Cummins, C.; Gall, A.; Giron, C.G.; et al. Ensembl 2018. *Nucleic Acids Res.* **2018**, *46*, D754–D761. [CrossRef]

47. Heinicke, S.; Livstone, M.S.; Lu, C.; Oughtred, R.; Kang, F.; Angiuoli, S.V.; White, O.; Botstein, D.; Dolinski, K. The Princeton Protein Orthology Database (P-POD): A comparative genomics analysis tool for biologists. *PLoS ONE* **2007**, *2*, e766. [CrossRef]

48.   Tong, A.H.; Evangelista, M.; Parsons, A.B.; Xu, H.; Bader, G.D.; Page, N.; Robinson, M.; Raghibizadeh, S.; Hogue, C.W.; Bussey, H.; et al. Systematic genetic analysis with ordered arrays of yeast deletion mutants. *Science* **2001**, *294*, 2364–2368. [CrossRef]

49.   Garnett, M.J.; Edelman, E.J.; Heidorn, S.J.; Greenman, C.D.; Dastur, A.; Lau, K.W.; Greninger, P.; Thompson, I.R.; Luo, X.; Soares, J.; et al. Systematic identification of genomic markers of drug sensitivity in cancer cells. *Nature* **2012**, *483*, 570–575. [CrossRef]

50.   Haverty, P.M.; Lin, E.; Tan, J.; Yu, Y.; Lam, B.; Lianoglou, S.; Neve, R.M.; Martin, S.; Settleman, J.; Yauch, R.L.; et al. Reproducible pharmacogenomic profiling of cancer cell line panels. *Nature* **2016**, *533*, 333–337. [CrossRef]

51.   Hartwell, L.H.; Hopfield, J.J.; Leibler, S.; Murray, A.W. From molecular to modular cell biology. *Nature* **1999**, *402*, C47–C52. [CrossRef]

52.   Birrell, G.W.; Brown, J.A.; Wu, H.I.; Giaever, G.; Chu, A.M.; Davis, R.W.; Brown, J.M. Transcriptional response of Saccharomyces cerevisiae to DNA-damaging agents does not identify the genes that protect against these agents. *Proc. Natl. Acad. Sci. USA* **2002**, *99*, 8778–8783. [CrossRef] [PubMed]

53.   O'Neil, N.J.; Bailey, M.L.; Hieter, P. Synthetic lethality and cancer. *Nat. Rev. Genet.* **2017**, *18*, 613–623. [CrossRef] [PubMed]

54.   McGary, K.L.; Park, T.J.; Woods, J.O.; Cha, H.J.; Wallingford, J.B.; Marcotte, E.M. Systematic discovery of nonobvious human disease models through orthologous phenotypes. *Proc. Natl. Acad. Sci. USA* **2010**, *107*, 6544–6549. [CrossRef] [PubMed]

55.   Shen, J.P.; Ideker, T. Synthetic Lethal Networks for Precision Oncology: Promises and Pitfalls. *J. Mol. Biol.* **2018**, *430*, 2900–2912. [CrossRef] [PubMed]

56.   Shaheen, M.; Allen, C.; Nickoloff, J.A.; Hromas, R. Synthetic lethality: Exploiting the addiction of cancer to DNA repair. *Blood* **2011**, *117*, 6074–6082. [CrossRef] [PubMed]

57.   Shin, S.H.; Bode, A.M.; Dong, Z. Precision medicine: The foundation of future cancer therapeutics. *NPJ Precis. Oncol.* **2017**, *1*, 12. [CrossRef]

58.   Shimomura, I.; Yamamoto, Y.; Ochiya, T. Synthetic Lethality in Lung Cancer-From the Perspective of Cancer Genomics. *Medicines* **2019**, *6*, 38. [CrossRef]

59.   Chang, M.; Bellaoui, M.; Zhang, C.; Desai, R.; Morozov, P.; Delgado-Cruzata, L.; Rothstein, R.; Freyer, G.A.; Boone, C.; Brown, G.W. RMI1/NCE4, a suppressor of genome instability, encodes a member of the RecQ helicase/Topo III complex. *EMBO J.* **2005**, *24*, 2024–2033. [CrossRef] [PubMed]

60.   Cejka, P.; Plank, J.L.; Dombrowski, C.C.; Kowalczykowski, S.C. Decatenation of DNA by the S. cerevisiae Sgs1-Top3-Rmi1 and RPA complex: A mechanism for disentangling chromosomes. *Mol. Cell* **2012**, *47*, 886–896. [CrossRef]

61.   Saponaro, M.; Kantidakis, T.; Mitter, R.; Kelly, G.P.; Heron, M.; Williams, H.; Soding, J.; Stewart, A.; Svejstrup, J.Q. RECQL5 controls transcript elongation and suppresses genome instability associated with transcription stress. *Cell* **2014**, *157*, 1037–1049. [CrossRef]

62.   Hu, Y.; Raynard, S.; Sehorn, M.G.; Lu, X.; Bussen, W.; Zheng, L.; Stark, J.M.; Barnes, E.L.; Chi, P.; Janscak, P.; et al. RECQL5/Recql5 helicase regulates homologous recombination and suppresses tumor formation via disruption of Rad51 presynaptic filaments. *Genes Dev.* **2007**, *21*, 3073–3084. [CrossRef] [PubMed]

63.   Martin, C.A.; Sarlos, K.; Logan, C.V.; Thakur, R.S.; Parry, D.A.; Bizard, A.H.; Leitch, A.; Cleal, L.; Ali, N.S.; Al-Owain, M.A.; et al. Mutations in TOP3A Cause a Bloom Syndrome-like Disorder. *Am. J. Hum. Genet.* **2018**, *103*, 221–231. [CrossRef] [PubMed]

64.   Bai, Y.; Li, L.D.; Li, J.; Lu, X. Targeting of topoisomerases for prognosis and drug resistance in ovarian cancer. *J. Ovarian Res.* **2016**, *9*, 35. [CrossRef] [PubMed]

65.   Broberg, K.; Huynh, E.; Schlawicke Engstrom, K.; Bjork, J.; Albin, M.; Ingvar, C.; Olsson, H.; Hoglund, M. Association between polymorphisms in RMI1, TOP3A, and BLM and risk of cancer, a case-control study. *BMC Cancer* **2009**, *9*, 140. [CrossRef] [PubMed]

66.   Nagai, H.; Yabe, A.; Mine, N.; Mikami, I.; Fujiwara, H.; Terada, Y.; Hirano, A.; Tsuneizumi, M.; Yokota, T.; Emi, M. Down-regulation in human cancers of DRHC, a novel helicase-like gene from 17q25.1 that inhibits cell growth. *Cancer Lett.* **2003**, *193*, 41–47. [CrossRef] [PubMed]

67.   Hamamoto, R.; Furukawa, Y.; Morita, M.; Iimura, Y.; Silva, F.P.; Li, M.; Yagyu, R.; Nakamura, Y. SMYD3 encodes a histone methyltransferase involved in the proliferation of cancer cells. *Nat. Cell Biol.* **2004**, *6*, 731–740. [CrossRef]

68. Hasgall, P.A.; Hoogewijs, D.; Faza, M.B.; Panse, V.G.; Wenger, R.H.; Camenisch, G. The putative RNA helicase HELZ promotes cell proliferation, translation initiation and ribosomal protein S6 phosphorylation. *PLoS ONE* **2011**, *6*, e22107. [CrossRef]

69. Schepeler, T.; Holm, A.; Halvey, P.; Nordentoft, I.; Lamy, P.; Riising, E.M.; Christensen, L.L.; Thorsen, K.; Liebler, D.C.; Helin, K.; et al. Attenuation of the β-catenin/TCF4 complex in colorectal cancer cells induces several growth-suppressive microRNAs that target cancer promoting genes. *Oncogene* **2012**, *31*, 2750–2760. [CrossRef]

70. Li, L.; Geng, Y.; Feng, R.; Zhu, Q.; Miao, B.; Cao, J.; Fei, S. The Human RNA Surveillance Factor UPF1 Modulates Gastric Cancer Progression by Targeting Long Non-Coding RNA MALAT1. *Cell. Physiol. Biochem.* **2017**, *42*, 2194–2206. [CrossRef]

71. Chang, L.; Li, C.; Guo, T.; Wang, H.; Ma, W.; Yuan, Y.; Liu, Q.; Ye, Q.; Liu, Z. The human RNA surveillance factor UPF1 regulates tumorigenesis by targeting Smad7 in hepatocellular carcinoma. *J. Exp. Clin. Cancer Res.* **2016**, *35*, 8. [CrossRef]

72. Liu, C.; Karam, R.; Zhou, Y.; Su, F.; Ji, Y.; Li, G.; Xu, G.; Lu, L.; Wang, C.; Song, M.; et al. The UPF1 RNA surveillance gene is commonly mutated in pancreatic adenosquamous carcinoma. *Nat. Med.* **2014**, *20*, 596–598. [CrossRef] [PubMed]

73. Chen, M.B.; Liu, Y.Y.; Cheng, L.B.; Lu, J.W.; Zeng, P.; Lu, P.H. AMPKalpha phosphatase Ppm1E upregulation in human gastric cancer is required for cell proliferation. *Oncotarget* **2017**, *8*, 31288–31296. [CrossRef] [PubMed]

74. Thean, L.F.; Loi, C.; Ho, K.S.; Koh, P.K.; Eu, K.W.; Cheah, P.Y. Genome-wide scan identifies a copy number variable region at 3q26 that regulates PPM1L in APC mutation-negative familial colorectal cancer patients. *Genes Chromosomes Cancer* **2010**, *49*, 99–106. [CrossRef] [PubMed]

75. Kondo, T.; Matsumoto, K.; Sugimoto, K. Role of a complex containing Rad17, Mec3, and Ddc1 in the yeast DNA damage checkpoint pathway. *Mol. Cell. Biol.* **1999**, *19*, 1136–1143. [CrossRef] [PubMed]

76. Paciotti, V.; Lucchini, G.; Plevani, P.; Longhese, M.P. Mec1p is essential for phosphorylation of the yeast DNA damage checkpoint protein Ddc1p, which physically interacts with Mec3p. *EMBO J.* **1998**, *17*, 4199–4209. [CrossRef] [PubMed]

77. Majka, J.; Burgers, P.M. Yeast Rad17/Mec3/Ddc1: A sliding clamp for the DNA damage checkpoint. *Proc. Natl. Acad. Sci. USA* **2003**, *100*, 2249–2254. [CrossRef] [PubMed]

78. Navadgi-Patil, V.M.; Burgers, P.M. The unstructured C-terminal tail of the 9-1-1 clamp subunit Ddc1 activates Mec1/ATR via two distinct mechanisms. *Mol. Cell* **2009**, *36*, 743–753. [CrossRef] [PubMed]

79. Fredebohm, J.; Wolf, J.; Hoheisel, J.D.; Boettcher, M. Depletion of RAD17 sensitizes pancreatic cancer cells to gemcitabine. *J. Cell Sci.* **2013**, *126*, 3380–3389. [CrossRef]

80. Liu, S.; Bachran, C.; Gupta, P.; Miller-Randolph, S.; Wang, H.; Crown, D.; Zhang, Y.; Wein, A.N.; Singh, R.; Fattah, R.; et al. Diphthamide modification on eukaryotic elongation factor 2 is needed to assure fidelity of mRNA translation and mouse development. *Proc. Natl. Acad. Sci. USA* **2012**, *109*, 13817–13822. [CrossRef] [PubMed]

81. Villahermosa, D.; Fleck, O. Elp3 and Dph3 of Schizosaccharomyces pombe mediate cellular stress responses through tRNA(Lys)UUU modifications. *Sci. Rep.* **2017**, *7*, 7225. [CrossRef]

82. Denisova, E.; Heidenreich, B.; Nagore, E.; Rachakonda, P.S.; Hosen, I.; Akrap, I.; Traves, V.; Garcia-Casado, Z.; Lopez-Guerrero, J.A.; Requena, C.; et al. Frequent DPH3 promoter mutations in skin cancers. *Oncotarget* **2015**, *6*, 35922–35930. [CrossRef] [PubMed]

83. Abiatari, I.; Gillen, S.; DeOliveira, T.; Klose, T.; Bo, K.; Giese, N.A.; Friess, H.; Kleeff, J. The microtubule-associated protein MAPRE2 is involved in perineural invasion of pancreatic cancer cells. *Int. J. Oncol.* **2009**, *35*, 1111–1116. [PubMed]

84. Kim, Y.R.; Kim, H.S.; An, C.H.; Kim, S.S.; Yoo, N.J.; Lee, S.H. Frameshift mutation of MAPRE3, a microtubule-related gene, in gastric and colorectal cancers with microsatellite instability. *Pathology* **2010**, *42*, 493–496. [CrossRef] [PubMed]

85. Shah, M.A.; Denton, E.L.; Arrowsmith, C.H.; Lupien, M.; Schapira, M. A global assessment of cancer genomic alterations in epigenetic mechanisms. *Epigenet. Chromatin* **2014**, *7*, 29. [CrossRef] [PubMed]

86. Harsay, E.; Schekman, R. Avl9p, a member of a novel protein superfamily, functions in the late secretory pathway. *Mol. Biol. Cell* **2007**, *18*, 1203–1219. [CrossRef] [PubMed]

87. Li, Y.; Xu, J.; Xiong, H.; Ma, Z.; Wang, Z.; Kipreos, E.T.; Dalton, S.; Zhao, S. Cancer driver candidate genes AVL9, DENND5A and NUPL1 contribute to MDCK cystogenesis. *Oncoscience* **2014**, *1*, 854–865. [CrossRef]

88. Zhang, W.; Wang, J.; Chai, R.; Zhong, G.; Zhang, C.; Cao, W.; Yan, L.; Zhang, X.; Xu, Z. Hypoxia-regulated lncRNA CRPAT4 promotes cell migration via regulating AVL9 in clear cell renal cell carcinomas. *Onco Targets Ther.* **2018**, *11*, 4537–4545. [CrossRef]

89. Zhang, D.; Zhang, P.; Yang, P.; He, Y.; Wang, X.; Yang, Y.; Zhu, H.; Xu, N.; Liang, S. Downregulation of ATP1A1 promotes cancer development in renal cell carcinoma. *Clin. Proteom.* **2017**, *14*, 15. [CrossRef]

90. Bogdanov, A.; Moiseenko, F.; Dubina, M. Abnormal expression of ATP1A1 and ATP1A2 in breast cancer. *F1000Res.* **2017**, *6*, 10. [CrossRef]

91. Cialfi, S.; Le Pera, L.; De Blasio, C.; Mariano, G.; Palermo, R.; Zonfrilli, A.; Uccelletti, D.; Palleschi, C.; Biolcati, G.; Barbieri, L.; et al. The loss of ATP2C1 impairs the DNA damage response and induces altered skin homeostasis: Consequences for epidermal biology in Hailey-Hailey disease. *Sci. Rep.* **2016**, *6*, 31567. [CrossRef]

92. Okunade, G.W.; Miller, M.L.; Azhar, M.; Andringa, A.; Sanford, L.P.; Doetschman, T.; Prasad, V.; Shull, G.E. Loss of the Atp2c1 secretory pathway Ca(2+)-ATPase (SPCA1) in mice causes Golgi stress, apoptosis, and midgestational death in homozygous embryos and squamous cell tumors in adult heterozygotes. *J. Biol. Chem.* **2007**, *282*, 26517–26527. [CrossRef] [PubMed]

93. Ge, J.; Chen, Q.; Liu, B.; Wang, L.; Zhang, S.; Ji, B. Knockdown of Rab21 inhibits proliferation and induces apoptosis in human glioma cells. *Cell. Mol. Biol. Lett.* **2017**, *22*, 30. [CrossRef]

94. Hooper, S.; Gaggioli, C.; Sahai, E. A chemical biology screen reveals a role for Rab21-mediated control of actomyosin contractility in fibroblast-driven cancer invasion. *Br. J. Cancer* **2010**, *102*, 392–402. [CrossRef] [PubMed]

95. Zhou, Y.; Wu, B.; Li, J.H.; Nan, G.; Jiang, J.L.; Chen, Z.N. Rab22a enhances CD147 recycling and is required for lung cancer cell migration and invasion. *Exp. Cell Res.* **2017**, *357*, 9–16. [CrossRef]

96. Wang, T.; Gilkes, D.M.; Takano, N.; Xiang, L.; Luo, W.; Bishop, C.J.; Chaturvedi, P.; Green, J.J.; Semenza, G.L. Hypoxia-inducible factors and RAB22A mediate formation of microvesicles that stimulate breast cancer invasion and metastasis. *Proc. Natl. Acad. Sci. USA* **2014**, *111*, E3234–E3242. [CrossRef]

97. Zhang, Y.; Zhao, F.J.; Chen, L.L.; Wang, L.Q.; Nephew, K.P.; Wu, Y.L.; Zhang, S. MiR-373 targeting of the Rab22a oncogene suppresses tumor invasion and metastasis in ovarian cancer. *Oncotarget* **2014**, *5*, 12291–12303. [CrossRef] [PubMed]

98. Costello, J.L.; Castro, I.G.; Schrader, T.A.; Islinger, M.; Schrader, M. Peroxisomal ACBD4 interacts with VAPB and promotes ER-peroxisome associations. *Cell Cycle* **2017**, *16*, 1039–1045. [CrossRef] [PubMed]

99. Chavez-Blanco, A.; Perez-Plasencia, C.; Perez-Cardenas, E.; Carrasco-Legleu, C.; Rangel-Lopez, E.; Segura-Pacheco, B.; Taja-Chayeb, L.; Trejo-Becerril, C.; Gonzalez-Fierro, A.; Candelaria, M.; et al. Antineoplastic effects of the DNA methylation inhibitor hydralazine and the histone deacetylase inhibitor valproic acid in cancer cell lines. *Cancer Cell Int.* **2006**, *6*, 2. [CrossRef]

100. Hua, R.; Cheng, D.; Coyaud, E.; Freeman, S.; Di Pietro, E.; Wang, Y.; Vissa, A.; Yip, C.M.; Fairn, G.D.; Braverman, N.; et al. VAPs and ACBD5 tether peroxisomes to the ER for peroxisome maintenance and lipid homeostasis. *J. Cell Biol.* **2017**, *216*, 367–377. [CrossRef]

101. Shen, K.; Rice, S.D.; Gingrich, D.A.; Wang, D.; Mi, Z.; Tian, C.; Ding, Z.; Brower, S.L.; Ervin, P.R., Jr.; Gabrin, M.J.; et al. Distinct genes related to drug response identified in ER positive and ER negative breast cancer cell lines. *PLoS ONE* **2012**, *7*, e40900. [CrossRef]

102. Venturini, I.; Zeneroli, M.L.; Corsi, L.; Avallone, R.; Farina, F.; Alho, H.; Baraldi, C.; Ferrarese, C.; Pecora, N.; Frigo, M.; et al. Up-regulation of peripheral benzodiazepine receptor system in hepatocellular carcinoma. *Life Sci.* **1998**, *63*, 1269–1280. [CrossRef]

103. Harris, F.T.; Rahman, S.M.; Hassanein, M.; Qian, J.; Hoeksema, M.D.; Chen, H.; Eisenberg, R.; Chaurand, P.; Caprioli, R.M.; Shiota, M.; et al. Acyl-coenzyme A-binding protein regulates β-oxidation required for growth and survival of non-small cell lung cancer. *Cancer Prev. Res. (Phila.)* **2014**, *7*, 748–757. [CrossRef] [PubMed]

104. Yang, H.; Chen, J.; Yang, J.; Qiao, S.; Zhao, S.; Yu, L. Cyclophilin A is upregulated in small cell lung cancer and activates ERK1/2 signal. *Biochem. Biophys. Res. Commun.* **2007**, *361*, 763–767. [CrossRef] [PubMed]

105. Qi, Y.J.; He, Q.Y.; Ma, Y.F.; Du, Y.W.; Liu, G.C.; Li, Y.J.; Tsao, G.S.; Ngai, S.M.; Chiu, J.F. Proteomic identification of malignant transformation-related proteins in esophageal squamous cell carcinoma. *J. Cell. Biochem.* **2008**, *104*, 1625–1635. [CrossRef] [PubMed]

106. Li, M.; Zhai, Q.; Bharadwaj, U.; Wang, H.; Li, F.; Fisher, W.E.; Chen, C.; Yao, Q. Cyclophilin A is overexpressed in human pancreatic cancer cells and stimulates cell proliferation through CD147. *Cancer* **2006**, *106*, 2284–2294. [CrossRef]

107. Yamashita, Y.; Nishiumi, S.; Kono, S.; Takao, S.; Azuma, T.; Yoshida, M. Differences in elongation of very long chain fatty acids and fatty acid metabolism between triple-negative and hormone receptor-positive breast cancer. *BMC Cancer* **2017**, *17*, 589. [CrossRef] [PubMed]

108. Mika, A.; Kobiela, J.; Czumaj, A.; Chmielewski, M.; Stepnowski, P.; Sledzinski, T. Hyper-Elongation in Colorectal Cancer Tissue—Cerotic Acid is a Potential Novel Serum Metabolic Marker of Colorectal Malignancies. *Cell. Physiol. Biochem.* **2017**, *41*, 722–730. [CrossRef]

109. Zekri, A.R.; Hassan, Z.K.; Bahnassy, A.A.; Sherif, G.M.; ELdahshan, D.; Abouelhoda, M.; Ali, A.; Hafez, M.M. Molecular prognostic profile of Egyptian HCC cases infected with hepatitis C virus. *Asian Pac. J. Cancer Prev.* **2012**, *13*, 5433–5438. [CrossRef]

110. Su, Y.C.; Feng, Y.H.; Wu, H.T.; Huang, Y.S.; Tung, C.L.; Wu, P.; Chang, C.J.; Shiau, A.L.; Wu, C.L. Elovl6 is a negative clinical predictor for liver cancer and knockdown of Elovl6 reduces murine liver cancer progression. *Sci. Rep.* **2018**, *8*, 6586. [CrossRef]

111. Feng, Y.H.; Chen, W.Y.; Kuo, Y.H.; Tung, C.L.; Tsao, C.J.; Shiau, A.L.; Wu, C.L. Elovl6 is a poor prognostic predictor in breast cancer. *Oncol. Lett.* **2016**, *12*, 207–212. [CrossRef]

112. Liang, H.F.; Zhang, X.Z.; Liu, B.G.; Jia, G.T.; Li, W.L. Circular RNA circ-ABCB10 promotes breast cancer proliferation and progression through sponging miR-1271. *Am. J. Cancer Res.* **2017**, *7*, 1566–1576. [PubMed]

113. Gagou, M.E.; Ganesh, A.; Phear, G.; Robinson, D.; Petermann, E.; Cox, A.; Meuth, M. Human PIF1 helicase supports DNA replication and cell growth under oncogenic-stress. *Oncotarget* **2014**, *5*, 11381–11398. [CrossRef] [PubMed]

114. Lim, K.H.; Kim, K.H.; Choi, S.I.; Park, E.S.; Park, S.H.; Ryu, K.; Park, Y.K.; Kwon, S.Y.; Yang, S.I.; Lee, H.C.; et al. RPS3a over-expressed in HBV-associated hepatocellular carcinoma enhances the HBx-induced NF-kappaB signaling via its novel chaperoning function. *PLoS ONE* **2011**, *6*, e22258. [CrossRef] [PubMed]

115. Slizhikova, D.K.; Vinogradova, T.V.; Sverdlov, E.D. The NOLA2 and RPS3A genes as highly informative markers for human squamous cell lung cancer. *Bioorg. Khim.* **2005**, *31*, 195–199.

116. Yang, C.; Zheng, J.; Xue, Y.; Yu, H.; Liu, X.; Ma, J.; Liu, L.; Wang, P.; Li, Z.; Cai, H.; et al. The Effect of MCM3AP-AS1/miR-211/KLF5/AGGF1 Axis Regulating Glioblastoma Angiogenesis. *Front. Mol. Neurosci.* **2017**, *10*, 437. [CrossRef] [PubMed]

117. Tang, X.; Xu, Y.; Lu, L.; Jiao, Y.; Liu, J.; Wang, L.; Zhao, H. Identification of key candidate genes and small molecule drugs in cervical cancer by bioinformatics strategy. *Cancer Manag. Res.* **2018**, *10*, 3533–3549. [CrossRef]

118. Han, M.E.; Kim, J.Y.; Kim, G.H.; Park, S.Y.; Kim, Y.H.; Oh, S.O. SAC3D1: A novel prognostic marker in hepatocellular carcinoma. *Sci. Rep.* **2018**, *8*, 15608. [CrossRef]

119. Zhang, M.; Zhang, C.; Du, W.; Yang, X.; Chen, Z. ATAD2 is overexpressed in gastric cancer and serves as an independent poor prognostic biomarker. *Clin. Transl. Oncol.* **2016**, *18*, 776–781. [CrossRef]

120. Kalashnikova, E.V.; Revenko, A.S.; Gemo, A.T.; Andrews, N.P.; Tepper, C.G.; Zou, J.X.; Cardiff, R.D.; Borowsky, A.D.; Chen, H.W. ANCCA/ATAD2 overexpression identifies breast cancer patients with poor prognosis, acting to drive proliferation and survival of triple-negative cells through control of B-Myb and EZH2. *Cancer Res.* **2010**, *70*, 9402–9412. [CrossRef]

121. Zhang, Y.; Sun, Y.; Li, Y.; Fang, Z.; Wang, R.; Pan, Y.; Hu, H.; Luo, X.; Ye, T.; Li, H.; et al. ANCCA protein expression is a novel independent poor prognostic marker in surgically resected lung adenocarcinoma. *Ann. Surg. Oncol.* **2013**, *20*, S577–S582. [CrossRef]

122. Luo, Y.; Ye, G.Y.; Qin, S.L.; Yu, M.H.; Mu, Y.F.; Zhong, M. ATAD2 Overexpression Identifies Colorectal Cancer Patients with Poor Prognosis and Drives Proliferation of Cancer Cells. *Gastroenterol. Res. Pract.* **2015**, *2015*, 936564. [CrossRef] [PubMed]

123. Hou, M.; Huang, R.; Song, Y.; Feng, D.; Jiang, Y.; Liu, M. ATAD2 overexpression is associated with progression and prognosis in colorectal cancer. *Jpn. J. Clin. Oncol.* **2016**, *46*, 222–227. [CrossRef] [PubMed]

124. Zheng, L.; Li, T.; Zhang, Y.; Guo, Y.; Yao, J.; Dou, L.; Guo, K. Oncogene ATAD2 promotes cell proliferation, invasion and migration in cervical cancer. *Oncol. Rep.* **2015**, *33*, 2337–2344. [CrossRef]

125. Hwang, H.W.; Ha, S.Y.; Bang, H.; Park, C.K. ATAD2 as a Poor Prognostic Marker for Hepatocellular Carcinoma after Curative Resection. *Cancer Res. Treat.* **2015**, *47*, 853–861. [CrossRef] [PubMed]

126. Usui, T.; Ohta, T.; Oshiumi, H.; Tomizawa, J.; Ogawa, H.; Ogawa, T. Complex formation and functional versatility of Mre11 of budding yeast in recombination. *Cell* **1998**, *95*, 705–716. [CrossRef]

127. Ewald, B.; Sampath, D.; Plunkett, W. ATM and the Mre11-Rad50-Nbs1 complex respond to nucleoside analogue-induced stalled replication forks and contribute to drug resistance. *Cancer Res.* **2008**, *68*, 7947–7955. [CrossRef] [PubMed]

128. Karnitz, L.M.; Flatten, K.S.; Wagner, J.M.; Loegering, D.; Hackbarth, J.S.; Arlander, S.J.; Vroman, B.T.; Thomas, M.B.; Baek, Y.U.; Hopkins, K.M.; et al. Gemcitabine-induced activation of checkpoint signaling pathways that affect tumor cell survival. *Mol. Pharmacol.* **2005**, *68*, 1636–1644. [CrossRef]

129. Okazaki, T.; Jiao, L.; Chang, P.; Evans, D.B.; Abbruzzese, J.L.; Li, D. Single-nucleotide polymorphisms of DNA damage response genes are associated with overall survival in patients with pancreatic cancer. *Clin. Cancer Res.* **2008**, *14*, 2042–2048. [CrossRef]

130. Irlbacher, H.; Franke, J.; Manke, T.; Vingron, M.; Ehrenhofer-Murray, A.E. Control of replication initiation and heterochromatin formation in Saccharomyces cerevisiae by a regulator of meiotic gene expression. *Genes Dev.* **2005**, *19*, 1811–1822. [CrossRef]

131. Weber, J.M.; Irlbacher, H.; Ehrenhofer-Murray, A.E. Control of replication initiation by the Sum1/Rfm1/Hst1 histone deacetylase. *BMC Mol. Biol.* **2008**, *9*, 100. [CrossRef]

132. Knott, S.R.; Peace, J.M.; Ostrow, A.Z.; Gan, Y.; Rex, A.E.; Viggiani, C.J.; Tavare, S.; Aparicio, O.M. Forkhead transcription factors establish origin timing and long-range clustering in S. cerevisiae. *Cell* **2012**, *148*, 99–111. [CrossRef] [PubMed]

133. Wang, J.; Cai, X.; Xia, L.; Zhou, J.; Xin, J.; Liu, M.; Shang, X.; Liu, J.; Li, X.; Chen, Z.; et al. Decreased expression of FOXJ1 is a potential prognostic predictor for progression and poor survival of gastric cancer. *Ann. Surg. Oncol.* **2015**, *22*, 685–692. [CrossRef] [PubMed]

134. Li, J.V.; Chien, C.D.; Garee, J.P.; Xu, J.; Wellstein, A.; Riegel, A.T. Transcriptional repression of AIB1 by FoxG1 leads to apoptosis in breast cancer cells. *Mol. Endocrinol.* **2013**, *27*, 1113–1127. [CrossRef] [PubMed]

135. Jin, J.; Zhou, S.; Li, C.; Xu, R.; Zu, L.; You, J.; Zhang, B. MiR-517a-3p accelerates lung cancer cell proliferation and invasion through inhibiting FOXJ3 expression. *Life Sci.* **2014**, *108*, 48–53. [CrossRef] [PubMed]

136. Ma, W.; Yu, Q.; Jiang, J.; Du, X.; Huang, L.; Zhao, L.; Zhou, Q.I. miR-517a is an independent prognostic marker and contributes to cell migration and invasion in human colorectal cancer. *Oncol. Lett.* **2016**, *11*, 2583–2589. [CrossRef]

137. Liu, Y.; Zhang, L.; Meng, Y.; Huang, L. Benzyl isothiocyanate inhibits breast cancer cell tumorigenesis via repression of the FoxH1-Mediated Wnt/β-catenin pathway. *Int. J. Clin. Exp. Med.* **2015**, *8*, 17601–17611. [PubMed]

138. Jin, Y.; Cao, Q.; Chen, C.; Du, X.; Jin, B.; Pan, J. Tenovin-6-mediated inhibition of SIRT1/2 induces apoptosis in acute lymphoblastic leukemia (ALL) cells and eliminates ALL stem/progenitor cells. *BMC Cancer* **2015**, *15*, 226. [CrossRef]

139. Gong, D.J.; Zhang, J.M.; Yu, M.; Zhuang, B.; Guo, Q.Q. Inhibition of SIRT1 combined with gemcitabine therapy for pancreatic carcinoma. *Clin. Interv. Aging* **2013**, *8*, 889–897. [CrossRef]

140. Balderhaar, H.J.; Ungermann, C. CORVET and HOPS tethering complexes—Coordinators of endosome and lysosome fusion. *J. Cell Sci.* **2013**, *126*, 1307–1316. [CrossRef]

141. Solinger, J.A.; Spang, A. Tethering complexes in the endocytic pathway: CORVET and HOPS. *FEBS J.* **2013**, *280*, 2743–2757. [CrossRef]

142. Laidlaw, K.M.E.; MacDonald, C. Endosomal trafficking of yeast membrane proteins. *Biochem. Soc. Trans.* **2018**, *46*, 1551–1558. [CrossRef] [PubMed]

143. Henne, W.M.; Buchkovich, N.J.; Emr, S.D. The ESCRT pathway. *Dev. Cell* **2011**, *21*, 77–91. [CrossRef] [PubMed]

144. Cohen, M.; Stutz, F.; Belgareh, N.; Haguenauer-Tsapis, R.; Dargemont, C. Ubp3 requires a cofactor, Bre5, to specifically de-ubiquitinate the COPII protein, Sec23. *Nat. Cell Biol.* **2003**, *5*, 661–667. [CrossRef] [PubMed]

145. Schuldiner, M.; Collins, S.R.; Thompson, N.J.; Denic, V.; Bhamidipati, A.; Punna, T.; Ihmels, J.; Andrews, B.; Boone, C.; Greenblatt, J.F.; et al. Exploration of the function and organization of the yeast early secretory pathway through an epistatic miniarray profile. *Cell* **2005**, *123*, 507–519. [CrossRef] [PubMed]

146. Schuldiner, M.; Metz, J.; Schmid, V.; Denic, V.; Rakwalska, M.; Schmitt, H.D.; Schwappach, B.; Weissman, J.S. The GET complex mediates insertion of tail-anchored proteins into the ER membrane. *Cell* **2008**, *134*, 634–645. [CrossRef]

147. Beilharz, T.; Egan, B.; Silver, P.A.; Hofmann, K.; Lithgow, T. Bipartite signals mediate subcellular targeting of tail-anchored membrane proteins in Saccharomyces cerevisiae. *J. Biol. Chem.* **2003**, *278*, 8219–8223. [CrossRef]

148. Ibarrola-Villava, M.; Kumar, R.; Nagore, E.; Benfodda, M.; Guedj, M.; Gazal, S.; Hu, H.H.; Guan, J.; Rachkonda, P.S.; Descamps, V.; et al. Genes involved in the WNT and vesicular trafficking pathways are associated with melanoma predisposition. *Int. J. Cancer* **2015**, *136*, 2109–2119. [CrossRef]

149. Dutta, S.; Roy, S.; Polavaram, N.S.; Baretton, G.B.; Muders, M.H.; Batra, S.; Datta, K. NRP2 transcriptionally regulates its downstream effector WDFY1. *Sci. Rep.* **2016**, *6*, 23588. [CrossRef]

150. Dutta, S.; Roy, S.; Polavaram, N.S.; Stanton, M.J.; Zhang, H.; Bhola, T.; Honscheid, P.; Donohue, T.M., Jr.; Band, H.; Batra, S.K.; et al. Neuropilin-2 Regulates Endosome Maturation and EGFR Trafficking to Support Cancer Cell Pathobiology. *Cancer Res.* **2016**, *76*, 418–428. [CrossRef]

151. Girirajan, S.; Hauck, P.M.; Williams, S.; Vlangos, C.N.; Szomju, B.B.; Solaymani-Kohal, S.; Mosier, P.D.; White, K.L., Jr.; McCoy, K.; Elsea, S.H. Tom1l2 hypomorphic mice exhibit increased incidence of infections and tumors and abnormal immunologic response. *Mamm. Genome* **2008**, *19*, 246–262. [CrossRef]

152. Lachmann, J.; Glaubke, E.; Moore, P.S.; Ungermann, C. The Vps39-like TRAP1 is an effector of Rab5 and likely the missing Vps3 subunit of human CORVET. *Cell. Logist.* **2014**, *4*, e970840. [CrossRef] [PubMed]

153. Chabes, A.; Georgieva, B.; Domkin, V.; Zhao, X.; Rothstein, R.; Thelander, L. Survival of DNA damage in yeast directly depends on increased dNTP levels allowed by relaxed feedback inhibition of ribonucleotide reductase. *Cell* **2003**, *112*, 391–401. [CrossRef]

154. Wu, Y.; Li, X.; Yu, J.; Bjorkholm, M.; Xu, D. ASF1a inhibition induces p53-dependent growth arrest and senescence of cancer cells. *Cell Death Dis.* **2019**, *10*, 76. [CrossRef] [PubMed]

155. Tkach, J.M.; Yimit, A.; Lee, A.Y.; Riffle, M.; Costanzo, M.; Jaschob, D.; Hendry, J.A.; Ou, J.; Moffat, J.; Boone, C.; et al. Dissecting DNA damage response pathways by analysing protein localization and abundance changes during DNA replication stress. *Nat. Cell Biol.* **2012**, *14*, 966–976. [CrossRef] [PubMed]

156. Chong, P.S.; Zhou, J.; Cheong, L.L.; Liu, S.C.; Qian, J.; Guo, T.; Sze, S.K.; Zeng, Q.; Chng, W.J. LEO1 is regulated by PRL-3 and mediates its oncogenic properties in acute myelogenous leukemia. *Cancer Res.* **2014**, *74*, 3043–3053. [CrossRef] [PubMed]

157. Yang, B.; Miao, S.; Zhang, L.N.; Sun, H.B.; Xu, Z.N.; Han, C.S. Correlation of CCNA1 promoter methylation with malignant tumors: A meta-analysis introduction. *BioMed Res. Int.* **2015**, *2015*, 134027. [CrossRef] [PubMed]

158. Hendrick, E.; Peixoto, P.; Blomme, A.; Polese, C.; Matheus, N.; Cimino, J.; Frere, A.; Mouithys-Mickalad, A.; Serteyn, D.; Bettendorff, L.; et al. Metabolic inhibitors accentuate the anti-tumoral effect of HDAC5 inhibition. *Oncogene* **2017**, *36*, 4859–4874. [CrossRef] [PubMed]

159. Wang, X.X.; Wan, R.Z.; Liu, Z.P. Recent advances in the discovery of potent and selective HDAC6 inhibitors. *Eur. J. Med. Chem.* **2018**, *143*, 1406–1418. [CrossRef]

160. Xu, X.; Xie, C.; Edwards, H.; Zhou, H.; Buck, S.A.; Ge, Y. Inhibition of histone deacetylases 1 and 6 enhances cytarabine-induced apoptosis in pediatric acute myeloid leukemia cells. *PLoS ONE* **2011**, *6*, e17138. [CrossRef] [PubMed]

161. Iwahashi, S.; Shimada, M.; Utsunomiya, T.; Morine, Y.; Imura, S.; Ikemoto, T.; Mori, H.; Hanaoka, J.; Sugimoto, K.; Saito, Y. Histone deacetylase inhibitor augments anti-tumor effect of gemcitabine and pegylated interferon-α on pancreatic cancer cells. *Int. J. Clin. Oncol.* **2011**, *16*, 671–678. [CrossRef]

162. Arnold, N.B.; Arkus, N.; Gunn, J.; Korc, M. The histone deacetylase inhibitor suberoylanilide hydroxamic acid induces growth inhibition and enhances gemcitabine-induced cell death in pancreatic cancer. *Clin. Cancer Res.* **2007**, *13*, 18–26. [CrossRef]

163. Cai, M.H.; Xu, X.G.; Yan, S.L.; Sun, Z.; Ying, Y.; Wang, B.K.; Tu, Y.X. Depletion of HDAC1, 7 and 8 by Histone Deacetylase Inhibition Confers Elimination of Pancreatic Cancer Stem Cells in Combination with Gemcitabine. *Sci. Rep.* **2018**, *8*, 1621. [CrossRef]

164. Sung, V.; Richard, N.; Brady, H.; Maier, A.; Kelter, G.; Heise, C. Histone deacetylase inhibitor MGCD0103 synergizes with gemcitabine in human pancreatic cells. *Cancer Sci.* **2011**, *102*, 1201–1207. [CrossRef] [PubMed]

165. Ji, M.; Li, Z.; Lin, Z.; Chen, L. Antitumor activity of the novel HDAC inhibitor CUDC-101 combined with gemcitabine in pancreatic cancer. *Am. J. Cancer Res.* **2018**, *8*, 2402–2418. [PubMed]

166. Song, T.; Yang, L.; Kabra, N.; Chen, L.; Koomen, J.; Haura, E.B.; Chen, J. The NAD+ synthesis enzyme nicotinamide mononucleotide adenylyltransferase (NMNAT1) regulates ribosomal RNA transcription. *J. Biol. Chem.* **2013**, *288*, 20908–20917. [CrossRef]

167. Li, H.; Feng, Z.; Wu, W.; Li, J.; Zhang, J.; Xia, T. SIRT3 regulates cell proliferation and apoptosis related to energy metabolism in non-small cell lung cancer cells through deacetylation of NMNAT2. *Int. J. Oncol.* **2013**, *43*, 1420–1430. [CrossRef]

168. Kim, M.M.; Camelo-Piragua, S.; Schipper, M.; Tao, Y.; Normolle, D.; Junck, L.; Mammoser, A.; Betz, B.L.; Cao, Y.; Kim, C.J.; et al. Gemcitabine Plus Radiation Therapy for High-Grade Glioma: Long-Term Results of a Phase 1 Dose-Escalation Study. *Int. J. Radiat. Oncol. Biol. Phys.* **2016**, *94*, 305–311. [CrossRef] [PubMed]

169. Rao, M.; Song, W.; Jiang, A.; Shyr, Y.; Lev, S.; Greenstein, D.; Brantley-Sieders, D.; Chen, J. VAMP-associated protein B (VAPB) promotes breast tumor growth by modulation of Akt activity. *PLoS ONE* **2012**, *7*, e46281. [CrossRef] [PubMed]

170. Yang, M.C.; Wang, H.C.; Hou, Y.C.; Tung, H.L.; Chiu, T.J.; Shan, Y.S. Blockade of autophagy reduces pancreatic cancer stem cell activity and potentiates the tumoricidal effect of gemcitabine. *Mol. Cancer* **2015**, *14*, 179. [CrossRef]

171. Takahashi, Y.; He, H.; Tang, Z.; Hattori, T.; Liu, Y.; Young, M.M.; Serfass, J.M.; Chen, L.; Gebru, M.; Chen, C.; et al. An autophagy assay reveals the ESCRT-III component CHMP2A as a regulator of phagophore closure. *Nat. Commun.* **2018**, *9*, 2855. [CrossRef]

172. D'Arcangelo, D.; Giampietri, C.; Muscio, M.; Scatozza, F.; Facchiano, F.; Facchiano, A. WIPI1, BAG1, and PEX3 Autophagy-Related Genes Are Relevant Melanoma Markers. *Oxid. Med. Cell. Longev.* **2018**, *2018*, 1471682. [CrossRef] [PubMed]

173. Filimonenko, M.; Stuffers, S.; Raiborg, C.; Yamamoto, A.; Malerod, L.; Fisher, E.M.; Isaacs, A.; Brech, A.; Stenmark, H.; Simonsen, A. Functional multivesicular bodies are required for autophagic clearance of protein aggregates associated with neurodegenerative disease. *J. Cell Biol.* **2007**, *179*, 485–500. [CrossRef] [PubMed]

174. Luo, M.L.; Gong, C.; Chen, C.H.; Hu, H.; Huang, P.; Zheng, M.; Yao, Y.; Wei, S.; Wulf, G.; Lieberman, J.; et al. The Rab2A GTPase promotes breast cancer stem cells and tumorigenesis via Erk signaling activation. *Cell Rep.* **2015**, *11*, 111–124. [CrossRef] [PubMed]

175. Jin, J.; Wu, Y.; Zhou, D.; Sun, Q.; Wang, W. miR448 targets Rab2B and is pivotal in the suppression of pancreatic cancer. *Oncol. Rep.* **2018**, *40*, 1379–1389. [CrossRef] [PubMed]

176. Zhang, Y.; Huang, S.; Li, P.; Chen, Q.; Li, Y.; Zhou, Y.; Wang, L.; Kang, M.; Zhang, B.; Yang, B.; et al. Pancreatic cancer-derived exosomes suppress the production of GIP and GLP-1 from STC-1cells in vitro by down-regulating the PCSK1/3. *Cancer Lett.* **2018**, *431*, 190–200. [CrossRef] [PubMed]

177. Demidyuk, I.V.; Shubin, A.V.; Gasanov, E.V.; Kurinov, A.M.; Demkin, V.V.; Vinogradova, T.V.; Zinovyeva, M.V.; Sass, A.V.; Zborovskaya, I.B.; Kostrov, S.V. Alterations in gene expression of proprotein convertases in human lung cancer have a limited number of scenarios. *PLoS ONE* **2013**, *8*, e55752. [CrossRef] [PubMed]

178. Bajikar, S.S.; Wang, C.C.; Borten, M.A.; Pereira, E.J.; Atkins, K.A.; Janes, K.A. Tumor-Suppressor Inactivation of GDF11 Occurs by Precursor Sequestration in Triple-Negative Breast Cancer. *Dev. Cell* **2017**, *43*, 418–435. [CrossRef] [PubMed]

179. Akada, M.; Crnogorac-Jurcevic, T.; Lattimore, S.; Mahon, P.; Lopes, R.; Sunamura, M.; Matsuno, S.; Lemoine, N.R. Intrinsic chemoresistance to gemcitabine is associated with decreased expression of BNIP3 in pancreatic cancer. *Clin. Cancer Res.* **2005**, *11*, 3094–3101. [CrossRef]

180. Kanki, T.; Wang, K.; Baba, M.; Bartholomew, C.R.; Lynch-Day, M.A.; Du, Z.; Geng, J.; Mao, K.; Yang, Z.; Yen, W.L.; et al. A genomic screen for yeast mutants defective in selective mitochondria autophagy. *Mol. Biol. Cell* **2009**, *20*, 4730–4738. [CrossRef]

181. Johnson, I.R.; Parkinson-Lawrence, E.J.; Keegan, H.; Spillane, C.D.; Barry-O'Crowley, J.; Watson, W.R.; Selemidis, S.; Butler, L.M.; O'Leary, J.J.; Brooks, D.A. Endosomal gene expression: A new indicator for prostate cancer patient prognosis? *Oncotarget* **2015**, *6*, 37919–37929. [CrossRef] [PubMed]

182. Li, F.; Hu, G.; Jiang, Z.; Guo, J.; Wang, K.; Ouyang, K.; Wen, D.; Zhu, M.; Liang, J.; Qin, X.; et al. Identification of NME5 as a contributor to innate resistance to gemcitabine in pancreatic cancer cells. *FEBS J.* **2012**, *279*, 1261–1273. [CrossRef] [PubMed]

183. Matsumoto, A.; Arcaroli, J.; Chen, Y.; Gasparetto, M.; Neumeister, V.; Thompson, D.C.; Singh, S.; Smith, C.; Messersmith, W.; Vasiliou, V. Aldehyde dehydrogenase 1B1: A novel immunohistological marker for colorectal cancer. *Br. J. Cancer* **2017**, *117*, 1537–1543. [CrossRef] [PubMed]

184. Singh, S.; Arcaroli, J.J.; Orlicky, D.J.; Chen, Y.; Messersmith, W.A.; Bagby, S.; Purkey, A.; Quackenbush, K.S.; Thompson, D.C.; Vasiliou, V. Aldehyde Dehydrogenase 1B1 as a Modulator of Pancreatic Adenocarcinoma. *Pancreas* **2016**, *45*, 117–122. [CrossRef]

185. Xu, X.; Chai, S.; Wang, P.; Zhang, C.; Yang, Y.; Yang, Y.; Wang, K. Aldehyde dehydrogenases and cancer stem cells. *Cancer Lett.* **2015**, *369*, 50–57. [CrossRef] [PubMed]

186. Bae, J.S.; Park, S.H.; Jamiyandorj, U.; Kim, K.M.; Noh, S.J.; Kim, J.R.; Park, H.J.; Kwon, K.S.; Jung, S.H.; Park, H.S.; et al. CK2alpha/CSNK2A1 Phosphorylates SIRT6 and Is Involved in the Progression of Breast Carcinoma and Predicts Shorter Survival of Diagnosed Patients. *Am. J. Pathol.* **2016**, *186*, 3297–3315. [CrossRef]

187. Xie, Z.C.; Tang, R.X.; Gao, X.; Xie, Q.N.; Lin, J.Y.; Chen, G.; Li, Z.Y. A meta-analysis and bioinformatics exploration of the diagnostic value and molecular mechanism of miR-193a-5p in lung cancer. *Oncol. Lett.* **2018**, *16*, 4114–4128. [CrossRef] [PubMed]

188. Laramas, M.; Pasquier, D.; Filhol, O.; Ringeisen, F.; Descotes, J.L.; Cochet, C. Nuclear localization of protein kinase CK2 catalytic subunit (CK2alpha) is associated with poor prognostic factors in human prostate cancer. *Eur. J. Cancer* **2007**, *43*, 928–934. [CrossRef]

189. Zou, J.; Luo, H.; Zeng, Q.; Dong, Z.; Wu, D.; Liu, L. Protein kinase CK2alpha is overexpressed in colorectal cancer and modulates cell proliferation and invasion via regulating EMT-related genes. *J. Transl. Med.* **2011**, *9*, 97. [CrossRef]

190. Bae, J.S.; Park, S.H.; Kim, K.M.; Kwon, K.S.; Kim, C.Y.; Lee, H.K.; Park, B.H.; Park, H.S.; Lee, H.; Moon, W.S.; et al. CK2alpha phosphorylates DBC1 and is involved in the progression of gastric carcinoma and predicts poor survival of gastric carcinoma patients. *Int. J. Cancer* **2015**, *136*, 797–809. [CrossRef]

191. Trembley, J.H.; Wang, G.; Unger, G.; Slaton, J.; Ahmed, K. Protein kinase CK2 in health and disease: CK2: A key player in cancer biology. *Cell. Mol. Life Sci.* **2009**, *66*, 1858–1867. [CrossRef]

192. Wang, F.; Chang, J.T.; Kao, C.J.; Huang, R.S. High Expression of miR-532-5p, a Tumor Suppressor, Leads to Better Prognosis in Ovarian Cancer Both In Vivo and In Vitro. *Mol. Cancer Ther.* **2016**, *15*, 1123–1131. [CrossRef] [PubMed]

193. Hanif, I.M.; Hanif, I.M.; Shazib, M.A.; Ahmad, K.A.; Pervaiz, S. Casein Kinase II: An attractive target for anticancer drug design. *Int. J. Biochem. Cell Biol.* **2010**, *42*, 1602–1605. [CrossRef] [PubMed]

194. Gan, Y.; Li, Y.; Li, T.; Shu, G.; Yin, G. CCNA2 acts as a novel biomarker in regulating the growth and apoptosis of colorectal cancer. *Cancer Manag. Res.* **2018**, *10*, 5113–5124. [CrossRef] [PubMed]

195. Gao, T.; Han, Y.; Yu, L.; Ao, S.; Li, Z.; Ji, J. CCNA2 is a prognostic biomarker for ER+ breast cancer and tamoxifen resistance. *PLoS ONE* **2014**, *9*, e91771. [CrossRef] [PubMed]

196. Ding, K.; Li, W.; Zou, Z.; Zou, X.; Wang, C. CCNB1 is a prognostic biomarker for ER+ breast cancer. *Med. Hypotheses* **2014**, *83*, 359–364. [CrossRef] [PubMed]

197. Fang, Y.; Yu, H.; Liang, X.; Xu, J.; Cai, X. Chk1-induced CCNB1 overexpression promotes cell proliferation and tumor growth in human colorectal cancer. *Cancer Biol. Ther.* **2014**, *15*, 1268–1279. [CrossRef] [PubMed]

198. Oji, Y.; Tatsumi, N.; Fukuda, M.; Nakatsuka, S.; Aoyagi, S.; Hirata, E.; Nanchi, I.; Fujiki, F.; Nakajima, H.; Yamamoto, Y.; et al. The translation elongation factor eEF2 is a novel tumorassociated antigen overexpressed in various types of cancers. *Int. J. Oncol.* **2014**, *44*, 1461–1469. [CrossRef]

199. Sato, N.; Maeda, M.; Sugiyama, M.; Ito, S.; Hyodo, T.; Masuda, A.; Tsunoda, N.; Kokuryo, T.; Hamaguchi, M.; Nagino, M.; et al. Inhibition of SNW1 association with spliceosomal proteins promotes apoptosis in breast cancer cells. *Cancer Med.* **2015**, *4*, 268–277. [CrossRef] [PubMed]

200. Koller-Eichhorn, R.; Marquardt, T.; Gail, R.; Wittinghofer, A.; Kostrewa, D.; Kutay, U.; Kambach, C. Human OLA1 defines an ATPase subfamily in the Obg family of GTP-binding proteins. *J. Biol. Chem.* **2007**, *282*, 19928–19937. [CrossRef] [PubMed]

201. Becker, M.; Gzyl, K.E.; Altamirano, A.M.; Vuong, A.; Urban, K.; Wieden, H.J. The 70S ribosome modulates the ATPase activity of Escherichia coli YchF. *RNA Biol.* **2012**, *9*, 1288–1301. [CrossRef]

202. Bai, L.; Yu, Z.; Zhang, J.; Yuan, S.; Liao, C.; Jeyabal, P.V.; Rubio, V.; Chen, H.; Li, Y.; Shi, Z.Z. OLA1 contributes to epithelial-mesenchymal transition in lung cancer by modulating the GSK3beta/snail/E-cadherin signaling. *Oncotarget* **2016**, *7*, 10402–10413. [CrossRef] [PubMed]

203. Cornelison, R.; Dobbin, Z.C.; Katre, A.A.; Jeong, D.H.; Zhang, Y.; Chen, D.; Petrova, Y.; Llaneza, D.C.; Steg, A.D.; Parsons, L.; et al. Targeting RNA-Polymerase I in Both Chemosensitive and Chemoresistant Populations in Epithelial Ovarian Cancer. *Clin. Cancer Res.* **2017**, *23*, 6529–6540. [CrossRef] [PubMed]

204. Lee, H.C.; Wang, H.; Baladandayuthapani, V.; Lin, H.; He, J.; Jones, R.J.; Kuiatse, I.; Gu, D.; Wang, Z.; Ma, W.; et al. RNA Polymerase I Inhibition with CX-5461 as a Novel Therapeutic Strategy to Target MYC in Multiple Myeloma. *Br. J. Haematol.* **2017**, *177*, 80–94. [CrossRef] [PubMed]

205. Rossetti, S.; Wierzbicki, A.J.; Sacchi, N. Undermining ribosomal RNA transcription in both the nucleolus and mitochondrion: An offbeat approach to target MYC-driven cancer. *Oncotarget* **2018**, *9*, 5016–5031. [CrossRef] [PubMed]

206. Linden, M.; Segersten, U.; Runeson, M.; Wester, K.; Busch, C.; Pettersson, U.; Lind, S.B.; Malmstrom, P.U. Tumour expression of bladder cancer-associated urinary proteins. *BJU Int.* **2013**, *112*, 407–415. [CrossRef] [PubMed]

207. Bullock, N.; Oltean, S. The many faces of SRPK1. *J. Pathol.* **2017**, *241*, 437–440. [CrossRef] [PubMed]

208. Chen, Y.; Meng, D.; Wang, H.; Sun, R.; Wang, D.; Wang, S.; Fan, J.; Zhao, Y.; Wang, J.; Yang, S.; et al. VAMP8 facilitates cellular proliferation and temozolomide resistance in human glioma cells. *Neuro Oncol.* **2015**, *17*, 407–418. [CrossRef] [PubMed]

209. Yuan, M.; Liao, J.; Luo, J.; Cui, M.; Jin, F. Significance of Vesicle-Associated Membrane Protein 8 Expression in Predicting Survival in Breast Cancer. *J. Breast Cancer* **2018**, *21*, 399–405. [CrossRef] [PubMed]

210. Grunnet, M.; Calatayud, D.; Schultz, N.A.; Hasselby, J.P.; Mau-Sorensen, M.; Brunner, N.; Stenvang, J. TOP1 gene copy numbers are increased in cancers of the bile duct and pancreas. *Scand. J. Gastroenterol.* **2015**, *50*, 485–494. [CrossRef] [PubMed]

211. Sun, L.; Xu, X.; Chen, Y.; Zhou, Y.; Tan, R.; Qiu, H.; Jin, L.; Zhang, W.; Fan, R.; Hong, W.; et al. Rab34 regulates adhesion, migration, and invasion of breast cancer cells. *Oncogene* **2018**, *37*, 3698–3714. [CrossRef] [PubMed]

212. Wu, J.; Lu, Y.; Qin, A.; Qiao, Z.; Jiang, X. Overexpression of RAB34 correlates with poor prognosis and tumor progression in hepatocellular carcinoma. *Oncol. Rep.* **2017**, *38*, 2967–2974. [CrossRef] [PubMed]

213. Wang, H.J.; Gao, Y.; Chen, L.; Li, Y.L.; Jiang, C.L. RAB34 was a progression- and prognosis-associated biomarker in gliomas. *Tumour Biol.* **2015**, *36*, 1573–1578. [CrossRef] [PubMed]

214. Artero-Castro, A.; Castellvi, J.; Garcia, A.; Hernandez, J.; Ramon y Cajal, S.; Lleonart, M.E. Expression of the ribosomal proteins Rplp0, Rplp1, and Rplp2 in gynecologic tumors. *Hum. Pathol.* **2011**, *42*, 194–203. [CrossRef] [PubMed]

215. Sendoel, A.; Dunn, J.G.; Rodriguez, E.H.; Naik, S.; Gomez, N.C.; Hurwitz, B.; Levorse, J.; Dill, B.D.; Schramek, D.; Molina, H.; et al. Translation from unconventional 5′ start sites drives tumour initiation. *Nature* **2017**, *541*, 494–499. [CrossRef] [PubMed]

216. Neklesa, T.K.; Davis, R.W. A genome-wide screen for regulators of TORC1 in response to amino acid starvation reveals a conserved Npr2/3 complex. *PLoS Genet.* **2009**, *5*, e1000515. [CrossRef] [PubMed]

217. Wu, X.; Tu, B.P. Selective regulation of autophagy by the Iml1-Npr2-Npr3 complex in the absence of nitrogen starvation. *Mol. Biol. Cell* **2011**, *22*, 4124–4133. [CrossRef] [PubMed]

218. Smardon, A.M.; Tarsio, M.; Kane, P.M. The RAVE complex is essential for stable assembly of the yeast V-ATPase. *J. Biol. Chem.* **2002**, *277*, 13831–13839. [CrossRef] [PubMed]

219. Seol, J.H.; Shevchenko, A.; Shevchenko, A.; Deshaies, R.J. Skp1 forms multiple protein complexes, including RAVE, a regulator of V-ATPase assembly. *Nat. Cell Biol.* **2001**, *3*, 384–391. [CrossRef] [PubMed]

220. Nakamura, N.; Matsuura, A.; Wada, Y.; Ohsumi, Y. Acidification of vacuoles is required for autophagic degradation in the yeast, Saccharomyces cerevisiae. *J. Biochem.* **1997**, *121*, 338–344. [CrossRef] [PubMed]

221. Yang, Z.; Geng, J.; Yen, W.L.; Wang, K.; Klionsky, D.J. Positive or negative roles of different cyclin-dependent kinase Pho85-cyclin complexes orchestrate induction of autophagy in Saccharomyces cerevisiae. *Mol. Cell* **2010**, *38*, 250–264. [CrossRef] [PubMed]

222. Wollert, T.; Wunder, C.; Lippincott-Schwartz, J.; Hurley, J.H. Membrane scission by the ESCRT-III complex. *Nature* **2009**, *458*, 172–177. [CrossRef] [PubMed]

223. Richter, C.M.; West, M.; Odorizzi, G. Doa4 function in ILV budding is restricted through its interaction with the Vps20 subunit of ESCRT-III. *J. Cell Sci.* **2013**, *126*, 1881–1890. [CrossRef] [PubMed]

224. Mukubou, H.; Tsujimura, T.; Sasaki, R.; Ku, Y. The role of autophagy in the treatment of pancreatic cancer with gemcitabine and ionizing radiation. *Int. J. Oncol.* **2010**, *37*, 821–828. [PubMed]

225. Hashimoto, D.; Blauer, M.; Hirota, M.; Ikonen, N.H.; Sand, J.; Laukkarinen, J. Autophagy is needed for the growth of pancreatic adenocarcinoma and has a cytoprotective effect against anticancer drugs. *Eur. J. Cancer* **2014**, *50*, 1382–1390. [CrossRef] [PubMed]

226. Chen, M.; He, M.; Song, Y.; Chen, L.; Xiao, P.; Wan, X.; Dai, F.; Shen, P. The cytoprotective role of gemcitabine-induced autophagy associated with apoptosis inhibition in triple-negative MDA-MB-231 breast cancer cells. *Int. J. Mol. Med.* **2014**, *34*, 276–282. [CrossRef] [PubMed]

227. Beilharz, T.H.; Harrison, P.F.; Miles, D.M.; See, M.M.; Le, U.M.; Kalanon, M.; Curtis, M.J.; Hasan, Q.; Saksouk, J.; Margaritis, T.; et al. Coordination of Cell Cycle Progression and Mitotic Spindle Assembly Involves Histone H3 Lysine 4 Methylation by Set1/COMPASS. *Genetics* **2017**, *205*, 185–199. [CrossRef]

228. Miller, T.; Krogan, N.J.; Dover, J.; Erdjument-Bromage, H.; Tempst, P.; Johnston, M.; Greenblatt, J.F.; Shilatifard, A. COMPASS: A complex of proteins associated with a trithorax-related SET domain protein. *Proc. Natl. Acad. Sci. USA* **2001**, *98*, 12902–12907. [CrossRef] [PubMed]

229. Shilatifard, A. The COMPASS family of histone H3K4 methylases: Mechanisms of regulation in development and disease pathogenesis. *Annu. Rev. Biochem.* **2012**, *81*, 65–95. [CrossRef] [PubMed]

230. Greer, E.L.; Shi, Y. Histone methylation: A dynamic mark in health, disease and inheritance. *Nat. Rev. Genet.* **2012**, *13*, 343–357. [CrossRef]

231. Dehe, P.M.; Dichtl, B.; Schaft, D.; Roguev, A.; Pamblanco, M.; Lebrun, R.; Rodriguez-Gil, A.; Mkandawire, M.; Landsberg, K.; Shevchenko, A.; et al. Protein interactions within the Set1 complex and their roles in the regulation of histone 3 lysine 4 methylation. *J. Biol. Chem.* **2006**, *281*, 35404–35412. [CrossRef] [PubMed]

232. Alvarado, A.G.; Thiagarajan, P.S.; Mulkearns-Hubert, E.E.; Silver, D.J.; Hale, J.S.; Alban, T.J.; Turaga, S.M.; Jarrar, A.; Reizes, O.; Longworth, M.S.; et al. Glioblastoma Cancer Stem Cells Evade Innate Immune Suppression of Self-Renewal through Reduced TLR4 Expression. *Cell Stem Cell* **2017**, *20*, 450–461. [CrossRef] [PubMed]

233. Lu, C.; Yang, D.; Sabbatini, M.E.; Colby, A.H.; Grinstaff, M.W.; Oberlies, N.H.; Pearce, C.; Liu, K. Contrasting roles of H3K4me3 and H3K9me3 in regulation of apoptosis and gemcitabine resistance in human pancreatic cancer cells. *BMC Cancer* **2018**, *18*, 149. [CrossRef] [PubMed]

234. Li, D.; Sun, H.; Sun, W.J.; Bao, H.B.; Si, S.H.; Fan, J.L.; Lin, P.; Cui, R.J.; Pan, Y.J.; Wen, S.M.; et al. Role of RbBP5 and H3K4me3 in the vicinity of Snail transcription start site during epithelial-mesenchymal transition in prostate cancer cell. *Oncotarget* **2016**, *7*, 65553–65567. [CrossRef] [PubMed]

235. Zhou, H.; Bao, J.; Zhu, X.; Dai, G.; Jiang, X.; Jiao, X.; Sheng, H.; Huang, J.; Yu, H. Retinoblastoma Binding Protein 5 Correlates with the Progression in Hepatocellular Carcinoma. *BioMed Res. Int.* **2018**, *2018*, 1073432. [CrossRef]

236. Telles, E.; Seto, E. Modulation of cell cycle regulators by HDACs. *Front. Biosci. (Sch. Ed.)* **2012**, *4*, 831–839.

237. Seto, E.; Yoshida, M. Erasers of histone acetylation: The histone deacetylase enzymes. *Cold Spring Harb. Perspect. Biol.* **2014**, *6*, a018713. [CrossRef]

238. Wu, J.; Carmen, A.A.; Kobayashi, R.; Suka, N.; Grunstein, M. HDA2 and HDA3 are related proteins that interact with and are essential for the activity of the yeast histone deacetylase HDA1. *Proc. Natl. Acad. Sci. USA* **2001**, *98*, 4391–4396. [CrossRef] [PubMed]

239. Alic, N.; Higgins, V.J.; Dawes, I.W. Identification of a Saccharomyces cerevisiae gene that is required for G1 arrest in response to the lipid oxidation product linoleic acid hydroperoxide. *Mol. Biol. Cell* **2001**, *12*, 1801–1810. [CrossRef]

240. Alic, N.; Higgins, V.J.; Pichova, A.; Breitenbach, M.; Dawes, I.W. Lipid hydroperoxides activate the mitogen-activated protein kinase Mpk1p in Saccharomyces cerevisiae. *J. Biol. Chem.* **2003**, *278*, 41849–41855. [CrossRef]

241. Addinall, S.G.; Downey, M.; Yu, M.; Zubko, M.K.; Dewar, J.; Leake, A.; Hallinan, J.; Shaw, O.; James, K.; Wilkinson, D.J.; et al. A genomewide suppressor and enhancer analysis of cdc13-1 reveals varied cellular processes influencing telomere capping in Saccharomyces cerevisiae. *Genetics* **2008**, *180*, 2251–2266. [CrossRef]

242. van der Veen, A.G.; Ploegh, H.L. Ubiquitin-like proteins. *Annu. Rev. Biochem.* **2012**, *81*, 323–357. [CrossRef] [PubMed]

243. Judes, A.; Bruch, A.; Klassen, R.; Helm, M.; Schaffrath, R. Sulfur transfer and activation by ubiquitin-like modifier system Uba4*Urm1 link protein urmylation and tRNA thiolation in yeast. *Microb. Cell* **2016**, *3*, 554–564. [CrossRef] [PubMed]

244. Nakai, Y.; Nakai, M.; Hayashi, H. Thio-modification of yeast cytosolic tRNA requires a ubiquitin-related system that resembles bacterial sulfur transfer systems. *J. Biol. Chem.* **2008**, *283*, 27469–27476. [CrossRef] [PubMed]

245. Noma, A.; Sakaguchi, Y.; Suzuki, T. Mechanistic characterization of the sulfur-relay system for eukaryotic 2-thiouridine biogenesis at tRNA wobble positions. *Nucleic Acids Res.* **2009**, *37*, 1335–1352. [CrossRef] [PubMed]

246. Hawer, H.; Hammermeister, A.; Ravichandran, K.E.; Glatt, S.; Schaffrath, R.; Klassen, R. Roles of Elongator Dependent tRNA Modification Pathways in Neurodegeneration and Cancer. *Genes* **2018**, *10*, 19. [CrossRef] [PubMed]

247. Rapino, F.; Delaunay, S.; Rambow, F.; Zhou, Z.; Tharun, L.; De Tullio, P.; Sin, O.; Shostak, K.; Schmitz, S.; Piepers, J.; et al. Codon-specific translation reprogramming promotes resistance to targeted therapy. *Nature* **2018**, *558*, 605–609. [CrossRef] [PubMed]

248. Plunkett, W.; Huang, P.; Searcy, C.E.; Gandhi, V. Gemcitabine: Preclinical pharmacology and mechanisms of action. *Semin Oncol.* **1996**, *23*, 3–15. [PubMed]

249. Wong, A.; Soo, R.A.; Yong, W.P.; Innocenti, F. Clinical pharmacology and pharmacogenetics of gemcitabine. *Drug Metab. Rev.* **2009**, *41*, 77–88. [CrossRef]

250. Krishnan, P.; Fu, Q.; Lam, W.; Liou, J.Y.; Dutschman, G.; Cheng, Y.C. Phosphorylation of pyrimidine deoxynucleoside analog diphosphates: Selective phosphorylation of L-nucleoside analog diphosphates by 3-phosphoglycerate kinase. *J. Biol. Chem.* **2002**, *277*, 5453–5459. [CrossRef]

251. Flentie, K.; Gonzalez, C.; Kocher, B.; Wang, Y.; Zhu, H.; Marasa, J.; Piwnica-Worms, D. Nucleoside Diphosphate Kinase-3 (NME3) Enhances TLR5-Induced NFkappaB Activation. *Mol. Cancer Res.* **2018**, *16*, 986–999. [CrossRef]

252. O'Kane, G.M.; Connor, A.A.; Gallinger, S. Characterization, Detection, and Treatment Approaches for Homologous Recombination Deficiency in Cancer. *Trends Mol. Med.* **2017**, *23*, 1121–1137. [CrossRef] [PubMed]

253. Jackson, J.C.; Lopes, J.M. The yeast UME6 gene is required for both negative and positive transcriptional regulation of phospholipid biosynthetic gene expression. *Nucleic Acids Res.* **1996**, *24*, 1322–1329. [CrossRef] [PubMed]

254. Bae-Lee, M.S.; Carman, G.M. Phosphatidylserine synthesis in Saccharomyces cerevisiae. Purification and characterization of membrane-associated phosphatidylserine synthase. *J. Biol. Chem.* **1984**, *259*, 10857–10862.

255. Madeo, F.; Frohlich, E.; Frohlich, K.U. A yeast mutant showing diagnostic markers of early and late apoptosis. *J. Cell Biol.* **1997**, *139*, 729–734. [CrossRef] [PubMed]

256. Modrak, D.E.; Cardillo, T.M.; Newsome, G.A.; Goldenberg, D.M.; Gold, D.V. Synergistic interaction between sphingomyelin and gemcitabine potentiates ceramide-mediated apoptosis in pancreatic cancer. *Cancer Res.* **2004**, *64*, 8405–8410. [CrossRef]

257. Modrak, D.E.; Leon, E.; Goldenberg, D.M.; Gold, D.V. Ceramide regulates gemcitabine-induced senescence and apoptosis in human pancreatic cancer cell lines. *Mol. Cancer Res.* **2009**, *7*, 890–896. [CrossRef]

258. Frohlich, F.; Petit, C.; Kory, N.; Christiano, R.; Hannibal-Bach, H.K.; Graham, M.; Liu, X.; Ejsing, C.S.; Farese, R.V.; Walther, T.C. The GARP complex is required for cellular sphingolipid homeostasis. *Elife* **2015**, *4*, e08712. [CrossRef]

259. Hua, Z.; Fatheddin, P.; Graham, T.R. An essential subfamily of Drs2p-related P-type ATPases is required for protein trafficking between Golgi complex and endosomal/vacuolar system. *Mol. Biol. Cell* **2002**, *13*, 3162–3177. [CrossRef]

260. Pomorski, T.; Lombardi, R.; Riezman, H.; Devaux, P.F.; van Meer, G.; Holthuis, J.C. Drs2p-related P-type ATPases Dnf1p and Dnf2p are required for phospholipid translocation across the yeast plasma membrane and serve a role in endocytosis. *Mol. Biol. Cell* **2003**, *14*, 1240–1254. [CrossRef]

261. Nakano, K.; Yamamoto, T.; Kishimoto, T.; Noji, T.; Tanaka, K. Protein kinases Fpk1p and Fpk2p are novel regulators of phospholipid asymmetry. *Mol. Biol. Cell* **2008**, *19*, 1783–1797. [CrossRef]

262. Bastide, A.; David, A. The ribosome, (slow) beating heart of cancer (stem) cell. *Oncogenesis* **2018**, *7*, 34. [CrossRef]

263. Manfrini, N.; Gobbini, E.; Baldo, V.; Trovesi, C.; Lucchini, G.; Longhese, M.P. G(1)/S and G(2)/M cyclin-dependent kinase activities commit cells to death in the absence of the S-phase checkpoint. *Mol. Cell. Biol.* **2012**, *32*, 4971–4985. [CrossRef] [PubMed]

264. Hu, X.; Lu, Z.; Yu, S.; Reilly, J.; Liu, F.; Jia, D.; Qin, Y.; Han, S.; Liu, X.; Qu, Z.; et al. CERKL regulates autophagy via the NAD-dependent deacetylase SIRT1. *Autophagy* **2019**, *15*, 453–465. [CrossRef] [PubMed]

265. Sun, F.; Xiong, Y.; Zhou, X.H.; Li, Q.; Xiao, L.; Long, P.; Li, L.J.; Cai, M.Y.; Wei, Y.X.; Ma, Y.L.; et al. Acylglycerol kinase is over-expressed in early-stage cervical squamous cell cancer and predicts poor prognosis. *Tumour Biol.* **2016**, *37*, 6729–6736. [CrossRef] [PubMed]

266. Liu, N.; Wang, Z.; Cheng, Y.; Zhang, P.; Wang, X.; Yang, H.; Liu, H.; Zhang, Y.; Tu, Y. Acylglycerol kinase functions as an oncogene and an unfavorable prognostic marker of human gliomas. *Hum. Pathol.* **2016**, *58*, 105–112. [CrossRef] [PubMed]

267. Cui, Y.; Lin, C.; Wu, Z.; Liu, A.; Zhang, X.; Zhu, J.; Wu, G.; Wu, J.; Li, M.; Li, J.; et al. AGK enhances angiogenesis and inhibits apoptosis via activation of the NF-kappaB signaling pathway in hepatocellular carcinoma. *Oncotarget* **2014**, *5*, 12057–12069. [CrossRef] [PubMed]

268. Wang, X.; Lin, C.; Zhao, X.; Liu, A.; Zhu, J.; Li, X.; Song, L. Acylglycerol kinase promotes cell proliferation and tumorigenicity in breast cancer via suppression of the FOXO1 transcription factor. *Mol. Cancer* **2014**, *13*, 106. [CrossRef]

269. Kang, H.; Tsygankov, D.; Lew, D.J. Sensing a bud in the yeast morphogenesis checkpoint: A role for Elm1. *Mol. Biol. Cell* **2016**, *27*, 1764–1775. [CrossRef] [PubMed]

270. Choi, E.J.; Yoo, N.J.; Kim, M.S.; An, C.H.; Lee, S.H. Putative Tumor Suppressor Genes EGR1 and BRSK1 Are Mutated in Gastric and Colorectal Cancers. *Oncology* **2016**, *91*, 289–294. [CrossRef]

271. Wang, H.; Liu, X.B.; Chen, J.H.; Wang, Q.Q.; Chen, J.P.; Xu, J.F.; Sheng, C.Y.; Ni, Q.C. Decreased expression and prognostic role of cytoplasmic BRSK1 in human breast carcinoma: Correlation with Jab1 stability and PI3K/Akt pathway. *Exp. Mol. Pathol.* **2014**, *97*, 191–201. [CrossRef]

272. Saiyin, H.; Na, N.; Han, X.; Fang, Y.; Wu, Y.; Lou, W.; Yang, X. BRSK2 induced by nutrient deprivation promotes Akt activity in pancreatic cancer via downregulation of mTOR activity. *Oncotarget* **2017**, *8*, 44669–44681. [CrossRef] [PubMed]

273. Ye, Y.; Gu, B.; Wang, Y.; Shen, S.; Huang, W. E2F1-mediated MNX1-AS1-miR-218-5p-SEC61A1 feedback loop contributes to the progression of colon adenocarcinoma. *J. Cell. Biochem.* **2019**, *120*, 6145–6153. [CrossRef]

274. Phan, N.N.; Wang, C.Y.; Chen, C.F.; Sun, Z.; Lai, M.D.; Lin, Y.C. Voltage-gated calcium channels: Novel targets for cancer therapy. *Oncol. Lett.* **2017**, *14*, 2059–2074. [CrossRef] [PubMed]

275. Liu, K.T.; Yeh, I.J.; Chou, S.K.; Yen, M.C.; Kuo, P.L. Regulatory mechanism of fatty acidCoA metabolic enzymes under endoplasmic reticulum stress in lung cancer. *Oncol. Rep.* **2018**, *40*, 2674–2682. [CrossRef] [PubMed]

276. Furuta, J.; Nobeyama, Y.; Umebayashi, Y.; Otsuka, F.; Kikuchi, K.; Ushijima, T. Silencing of Peroxiredoxin 2 and aberrant methylation of 33 CpG islands in putative promoter regions in human malignant melanomas. *Cancer Res.* **2006**, *66*, 6080–6086. [CrossRef] [PubMed]

277. Gao, Y.; Wang, W.; Cao, J.; Wang, F.; Geng, Y.; Cao, J.; Xu, X.; Zhou, J.; Liu, P.; Zhang, S. Upregulation of AUF1 is involved in the proliferation of esophageal squamous cell carcinoma through GCH1. *Int. J. Oncol.* **2016**, *49*, 2001–2010. [CrossRef]

278. Mocino-Rodriguez, M.D.; Santillan-Benitez, J.G.; Dozal-Dominguez, D.S.; Hernandez-Navarro, M.D.; Flores-Merino, M.V.; Sandoval-Cabrera, A.; Garcia Vazquez, F.J. Expression of AdipoR1 and AdipoR2 Receptors as Leptin-Breast Cancer Regulation Mechanisms. *Dis. Markers* **2017**, *2017*, 4862016. [CrossRef] [PubMed]

279. Wang, L.; Collings, C.K.; Zhao, Z.; Cozzolino, K.A.; Ma, Q.; Liang, K.; Marshall, S.A.; Sze, C.C.; Hashizume, R.; Savas, J.N.; et al. A cytoplasmic COMPASS is necessary for cell survival and triple-negative breast cancer pathogenesis by regulating metabolism. *Genes Dev.* **2017**, *31*, 2056–2066. [CrossRef]

280. Ross, J.B.; Huh, D.; Noble, L.B.; Tavazoie, S.F. Identification of molecular determinants of primary and metastatic tumour re-initiation in breast cancer. *Nat. Cell Biol.* **2015**, *17*, 651–664. [CrossRef]

281. Bhise, N.S.; Chauhan, L.; Shin, M.; Cao, X.; Pounds, S.; Lamba, V.; Lamba, J.K. MicroRNA-mRNA Pairs Associated with Outcome in AML: From In Vitro Cell-Based Studies to AML Patients. *Front. Pharmacol.* **2015**, *6*, 324. [CrossRef]

282. Tenreiro, S.; Outeiro, T.F. Simple is good: Yeast models of neurodegeneration. *FEMS Yeast Res.* **2010**, *10*, 970–979. [CrossRef] [PubMed]

283. Billant, O.; Blondel, M.; Voisset, C. p53, p63 and p73 in the wonderland of S. cerevisiae. *Oncotarget* **2017**, *8*, 57855–57869. [CrossRef] [PubMed]

284. Rodriguez-Escudero, I.; Roelants, F.M.; Thorner, J.; Nombela, C.; Molina, M.; Cid, V.J. Reconstitution of the mammalian PI3K/PTEN/Akt pathway in yeast. *Biochem. J.* **2005**, *390*, 613–623. [CrossRef] [PubMed]

285. Hamza, A.; Tammpere, E.; Kofoed, M.; Keong, C.; Chiang, J.; Giaever, G.; Nislow, C.; Hieter, P. Complementation of Yeast Genes with Human Genes as an Experimental Platform for Functional Testing of Human Genetic Variants. *Genetics* **2015**, *201*, 1263–1274. [CrossRef] [PubMed]

286. Sun, S.; Yang, F.; Tan, G.; Costanzo, M.; Oughtred, R.; Hirschman, J.; Theesfeld, C.L.; Bansal, P.; Sahni, N.; Yi, S.; et al. An extended set of yeast-based functional assays accurately identifies human disease mutations. *Genome Res.* **2016**, *26*, 670–680. [CrossRef] [PubMed]

287. Kachroo, A.H.; Laurent, J.M.; Yellman, C.M.; Meyer, A.G.; Wilke, C.O.; Marcotte, E.M. Evolution. Systematic humanization of yeast genes reveals conserved functions and genetic modularity. *Science* **2015**, *348*, 921–925. [CrossRef]

288. Tardiff, D.F.; Khurana, V.; Chung, C.Y.; Lindquist, S. From yeast to patient neurons and back again: Powerful new discovery platform. *Mov. Disord.* **2014**, *29*, 1231–1240. [CrossRef]

289. Veit, G.; Oliver, K.; Apaja, P.M.; Perdomo, D.; Bidaud-Meynard, A.; Lin, S.T.; Guo, J.; Icyuz, M.; Sorscher, E.J.; Hartman, J.L., IV; et al. Ribosomal Stalk Protein Silencing Partially Corrects the DeltaF508-CFTR Functional Expression Defect. *PLoS Biol.* **2016**, *14*, e1002462. [CrossRef]

290. Costanzo, M.; Kuzmin, E.; van Leeuwen, J.; Mair, B.; Moffat, J.; Boone, C.; Andrews, B. Global Genetic Networks and the Genotype-to-Phenotype Relationship. *Cell* **2019**, *177*, 85–100. [CrossRef]

291. Ferreira, M.A.; Gamazon, E.R.; Al-Ejeh, F.; Aittomaki, K.; Andrulis, I.L.; Anton-Culver, H.; Arason, A.; Arndt, V.; Aronson, K.J.; Arun, B.K.; et al. Genome-wide association and transcriptome studies identify target genes and risk loci for breast cancer. *Nat. Commun.* **2019**, *10*, 1741. [CrossRef]

292. Breslow, D.K.; Cameron, D.M.; Collins, S.R.; Schuldiner, M.; Stewart-Ornstein, J.; Newman, H.W.; Braun, S.; Madhani, H.D.; Krogan, N.J.; Weissman, J.S. A comprehensive strategy enabling high-resolution functional analysis of the yeast genome. *Nat. Methods* **2008**, *5*, 711–718. [CrossRef] [PubMed]